الجمهورية الجزائرية الديمقراطية الشعبية

People's Democratic Republic of Algeria

Ministry of Higher Education and Scientific Research

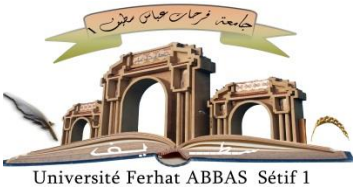

UNIVERSITY FERHAT ABBAS - SETIF 1

FACULTY OF TECHNOLOGY

THESIS

Presented at the Department of Electronics

To obtain the diploma of

DOCTORATE

Domain: Sciences and Technologies

Specialty: Electronic Option: Electronic Instrumentation

By

MAY Abdelouahad

THEME

Contribution to the predictive control of multilevel and quasi-Z-source type inverters dedicated to the energy management of a photovoltaic installation connected to the electrical grid

Defended on 03/07/2024 in front of the Jury:

Abdelhalim MAYOUF	Professor	Univ. Ferhat Abbas Setif 1	President
Fateh KRIM	Professor	Univ. Ferhat Abbas Sétif 1	Thesis director
Hamza FEROURA	MCB	Univ. Ferhat Abbas Sétif 1	Co-Director
Nourredine AMARDJIA	Professor	Univ. Ferhat Abbas Sétif 1	Examiner
Abdellah KOUZOU	Professor	Univ. Ziane Achour Djelfa	Examiner

الجمهورية الجزائرية الديمقراطية الشعبية

République Algérienne Démocratique et Populaire

Ministère de L'Enseignement Supérieur et de la Recherche Scientifique

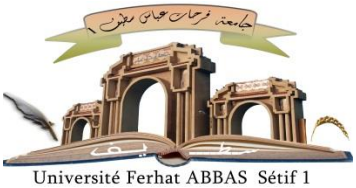

UNIVERSITÉ FERHAT ABBAS - SETIF1

FACULTÉ DE TECHNOLOGIE

THÈSE

Présentée au Département de Électronique

Pour l'obtention du diplôme de

DOCTORAT

Domaine : Sciences et Technologies

Filière: Électronique Option: Instrumentation Électronique

Par

MAY Abdelouahad

THÈME

Contribution à la commande prédictive d'onduleurs de type multiniveaux et quasi-Z-source dédiés à la gestion d'énergie d'une installation photovoltaïque connectée au réseau électrique

Soutenue le 03/07/2024 devant le Jury:

Abdelhalim MAYOUF	Professeur	Univ. Ferhat Abbas Sétif 1	Président
Fateh KRIM	Professeur	Univ. Ferhat Abbas Sétif 1	Directeur de thèse
Hamza FEROURA	MCB	Univ. Ferhat Abbas Sétif 1	Co-Directeur
Nourredine AMARDJIA	Professeur	Univ. Ferhat Abbas Sétif 1	Examinateur
Abdellah KOUZOU	Professeur	Univ. Ziane Achour Djelfa	Examinateur

First and above all, I praise the almighty ALLAH for granting me the capability to proceed successfully. This thesis would not have been possible without the support of several individuals who in one way or another contributed their valuable assistance in the completion of this work.

I would like to express my utmost gratitude and thanks to my academic Thesis director, Pr. Fateh KRIM, and Co-Director, Dr. Hamza FEROURA, who have advised, guided and supported me throughout this research work.

I would like to express my thanks to the examiners committee. Special thanks to all the members of our laboratory group (LEPCI), and to all my colleagues.

Dedicated

To my parents;
To my brothers;
To my grandmother;
And to my friends.

Abdelouahad MAY

Contents

List of Figures

List of Tables

List of abbreviations

DG	Distributed Generation
PV	Photovoltaic
VSIs	Voltage Source Inverters
qZSIs	quasi-Z-Source Inverters
D-S	Dual-Stage
S-S	Single-Stage
AC	Alternating Current
DC	Direct Current
ZSIs	Impedance Source Inverters
SG	Smart Grids
RES	Renewable Energy Sources
ICTs	Information and Communication Technologies
EMI	Electromagnetic Interference
CHB	Cascaded H-Bridge
NPC	Neutral-Point-Clamped
FC	Flying Capacitor
PUC	Packed-U-Cell
MLI	Multilevel Inverters
MVSIs	Multi-level VSIs
MPPT	Maximum Power Point Tracking
ZSN	Z-Source Impedance Network
ST	Shoot-Through
NST	Non- Shoot-Through
QZSN	quasi-Z-Source Network
ISN	Impedance Source Network
CSIs	Current Source Inverters
P&O	Perturb and observe
IncCon	Incremental Conductance
P	Proportional

PI	Proportional Integral
PID	Proportional Integral Derivative
PR	Proportional Resonant
LQG	Linear Quadratic Gaussian
PC	Predictive Controllers
THD	Total Harmonic Distortion
MPC	Model Predictive Control
SMC	Sliding Mode Controllers
FFL	Full Feedback Linearization
PFL	Partial Feedback Linearization
HC	Hysteresis Controllers
NN	Neural Network
RC	Repetitive Controllers
PIS	Plug-In Scheme
IM	Internal Model
FLC	Fuzzy Logic Controllers
PWM	Pulse Width Modulation
SBC	Simple Boost Control
MBC	Maximum Boost Control
MCBC	Maximum Constant Boost Control
SPWM	Sinusoidal Pulse Width Modulation
SVM	Space Vector Modulation
FCS-MPC	Finite Control Set Model Predictive Control
7L-PUC	7 level packed U cells
HIL	Hardware in the loop
M^2PC	Modulated Model Predictive Control
CM^2PC	Conventional Modulated Model Predictive Control

List of symbols

a, b, c	Natural frame components
α, β	Stationary reference frame components
m	Modulation index
G_{max}	Maximum qZS inverter gain
d_{max}	Maximum shoot-through duty cycle
b_{max}	Maximum boost factor
I_{PV}	Photovoltaic array current
I_{SC}	Photovoltaic array short-circuit current
V_{PV}	Photovoltaic array voltage
P_{PV}	Photovoltaic array power
I_{DC}	DC link current
V_{OC}	Photovoltaic array open-circuit voltage
V_1	DC link voltage in dual-stage
I_1	DC link current in dual-stage
I_{ref}	Reference current
T_S	Sampling time
g	Cost function
k_1, k_2	Weighting factors
ΔI	IncCon step-size
S	Converter power switches
S_a to S_c'	Packed-U-cell inverter power switches
V_{inv}	Output packed-U-cell voltage
I_S	Grid current
V_S	Grid voltage
P	Active power
P_{dc}	DC-side power
P_{ac}	AC-side active power
P_o	Average power value
P_r	Double-frequency ripple power

V_{ref}	Reference voltage
V	Grid RMS voltage
I	Grid RMS current
I^*	Reference RMS grid current
ω	Grid angular pulsation
φ	Grid voltage vector angle
ΔV_1	Peak-to-peak capacitor voltage variation
f	Grid frequency
f_s	Sampling frequency
C_1, C_2	DC capacitor
L_1, L_2	Converter Inductors
D	Soot-through duty-cycle

General Introduction

Governments are setting renewable energy targets and implementing policies that indirectly promote the uptake of renewables, including climate change policies, economic and green recovery plans, fossil fuel phase-outs and targets for net zero greenhouse gas emissions. Such policies can impact the economy on both the demand and supply sides. Recent events such as the Russian Federation's invasion of Ukraine and rising inflation have led policy makers to prioritise energy security, resulting in comprehensive policies such as the RePowerEU package and the Inflation Reduction Act. These measures create more favourable market conditions for renewables, driving innovation, reducing costs and emissions, providing economic opportunities and enhancing global energy security.

Renewable energy targets, coupled with legislation and committed funding for implementation, illustrate the level of ambition that countries have to accelerate the energy transition. By the end of 2022, 128 countries had in place economy-wide targets for renewable energy, although only 31 countries had targets for 100% renewables, most of them for the year 2050.

In 2022, total electricity generation worldwide increased 2.3% to reach 29,165 terawatt-hours (TWh), a growth rate close to pre-COVID levels and below the 6.2% rebound of 2021. Renewable energy sources contributed 92% of the increase, while the rest was covered mainly by nuclear, fossil gas and coal. Electricity generation from nuclear power declined 0.7% and from oil fell 4.4%. By comparison, in 2021 the increase in electricity generation was covered mainly by coal, fossil gas, and nuclear power sources (a combined 64%), whereas renewables (excluding hydropower) accounted for only 32% of this growth. In 2022, the world's total power generation capacity (from all sources) grew 4.1%, similar to the growth in 2021. The energy transition towards renewables has focused mainly on a handful of technologies in the power sector. Wind and solar power accounted for 23.9% of the total installed generation capacity in 2022, 2.4 percentage points above 2021 levels. The installed capacity of solar power reached 1,185 GW and wind power 906 GW.

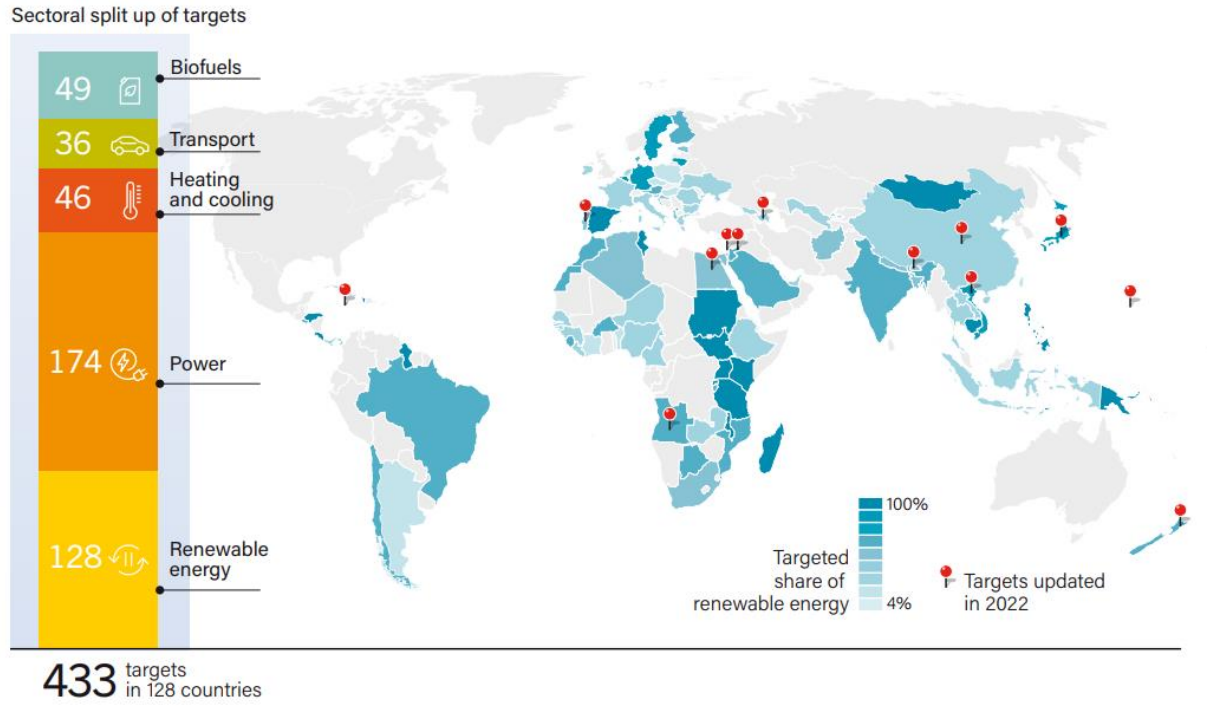

Figure 1.1: Countries with Economy-wide Renewable Energy Targets, by Sector and Targeted Share, 2022.

Overall, renewable energy has demonstrated resilience despite the rise in renewable power prices in major global markets due to supply chain challenges, construction delays, higher costs of raw materials, parts, and labour, as well as inflation, higher interest rates and interconnection delays.

Solar PV accounted for 70% of the total capacity additions of renewable power (348 GW) in 2022, followed by wind power 77 GW (22%) and hydropower 22 GW (6.3%). Availability of sun energy around the earth and the developments in solar technology had made a solar energy system a reliable source of energy today.

Regarding power electronic converters to interface Photovoltaic (PV) arrays to the grid. The Voltage Source Inverter (VSI) is the most used topology to date. However, this topology has some limitations when it comes to PV applications. The VSI topology has buck (step-down) characteristics; therefore, to step up the low voltage output from the PV array, an extra power electronic converter is required; this is known as the Dual-Stage (D-S) topology. The Quasi-Z-Source Inverter (qZSI) is a new type of inverter. It is different from the conventional VSI. The main feature is that the impedance network consists of inductors, capacitors, and switches/diodes, and it is employed in the circuit to boost or buck the voltage, it is a circuit to combine the DC-DC boost converter and inverter, using a Single-Stage (S-S) power conversion system.

Though researchers have studied VSI, and qZSI for different applications, there still exist many points that could be investigated and improved. Motivated by the huge demand for solar energy and immediate need for improvements in PV systems, the research reported in this thesis intends to add to the existing knowledge on PV system applications of VSI, and qZSI and make quality contributions to the field.

The main objectives of the research can be summarized as follows:

- To achieve a complete survey on VSIs, and qZSI, in terms of working principle, modeling, design, and existing modulation and control techniques.
- To develop model predictive control strategies for voltage control of VSI and qZSI that could be used to grid-connected. The developed techniques should ensure fast and accurate voltage and frequency control and should also pass the robustness tests.
- To develop new control strategies for dual-stage multi-level PV grid connected VSI. The developed strategies should be capable of extracting maximum power from the PV arrays at all insolation levels, and injecting a clean sinusoidal current into the power grid in accordance with grid codes.

To achieve the aforementioned objectives and facilitate the presentation of results derived in the course of this research, the thesis is organized as follows:

Chapter 1 Provides a literature survey on distributed generation systems in the first part. Then, an overview of inverter topologies is presented. In the next section of the chapter, the existing inverters modulation techniques for VSI and qZSI.

Chapter 2 presents a literature study on control strategies for VSI, then qZSI, with a comparison of the strategies for both topologies.

Chapter 3 This chapter proposes a novel control strategy for a dual-stage grid-tied PV system based on a high-gain DC-DC converter and a 7-level packed U cells (7L-PUC) inverter. The proposed control strategy is based on Finite-Control-Set Model Predictive Control (FCS-MPC) and a novel model for controlling the DC-link voltage by considering system losses. This chapter presents simulation and experimental results that demonstrate the high effectiveness of the proposed control strategy in terms of power quality, response time, and accuracy under changing weather conditions. The proposed system is feasible and can enhance the power quality of grid-tied PV systems.

Chapter 4 This chapter proposes a novel grid-tied qZSI PV control system, combining Modulated Model Predictive Control (M^2PC) and Fuzzy Logic Control (FLC) techniques. The proposed control system is compared to Conventional M^2PC (CM^2PC) to assess their

performance. The proposed control system exhibits rapid and accurate tracking of maximum power and can autonomously inject current into the grid. Comprehensive simulation and comparative analysis are conducted to verify the effectiveness of the proposed system, demonstrating the robust performance of the implemented control techniques in regulating grid-connected PV systems.

A general conclusion is given at the end of this dissertation to take stock of the contributions of this work and presents perspectives and the issues that remain to be resolved and developed.

Chapter 1: Literature Survey of Inverters

1.1 Introduction

The escalating depletion of fossil-based energy reservoirs, coupled with the imperative to curtail CO2 emissions, has catalyzed a shift towards harnessing a greater proportion of clean energy from renewable sources. This has spurred heightened interest in Distributed Generation (DG) as an alternative to conventional electrical distribution systems, promising enhanced performance and energy management.

This chapter provides a succinct overview of DG trends, with a particular emphasis on systems driven by renewable sources like photovoltaic (PV) and wind. The discourse zeros in on photovoltaic energy, elucidating the intricacies of electricity generation and presenting potential grid integration configurations. The configurations are broadly categorized into single-stage and dual-stage. In the dual-stage setup, the generator-side converter focuses on extracting maximum power, while the grid-side converter is tasked with injecting the resultant power in a suitable form. Conversely, the single-stage configuration consolidates both control objectives within the inverter.

The chapter further delves into a classification and description of prevalent inverter topologies employed for interfacing PV systems. The exploration concludes with literature reviews centered on the Impedance Source Inverter (ZSI).

1.2 Distributed generation systems

The current power grids can be conceptualized as hierarchical systems, with power plants situated at the apex and loads at the base, creating a unidirectional flow of electrical power. This system is managed with limited information regarding the interactions between sources and terminal points. This structure has notable drawbacks, including[1]:

- System Sensitivity: The system is susceptible to voltage and frequency instabilities, as well as power security issues arising from load variations and dynamic network reconfigurations.
- Risk of Failures and Blackouts: There's an increased risk of failures and blackouts, leading to reduced system efficiency.
- Unsuitability for Renewable Energy Integration: The existing grid structure is ill-suited for the seamless integration of renewable energy sources.

Over the past decade, the electrical energy market has undergone significant changes marked by rising demand for energy and two notable innovations: the rapid growth and widespread adoption of Renewable Energy Sources (RESs) and the subsequent development of Distributed Generation (DG) systems and Smart Grids (SGs)[1-4].

DG fundamentally involves generating energy in close proximity to its point of consumption. Instead of relying solely on large centralized power plants (coal, nuclear, hydroelectric, etc.) that produce massive amounts of energy transmitted over an extensive network, DG involves smaller power plants generating a more moderate amount of energy located nearer to the homes and businesses that directly consume it. This shift in approach is closely tied to the advancements in RESs and the evolution toward smarter and more decentralized energy grids[1].

The evolution of future electrical systems is expected to be driven by a set of crucial parameters, reflecting the changing landscape of power requirements[1, 2]:

- High Power Capability: Electricity's role as the primary power source is growing, demanding a substantial increase in power capability. This trend is anticipated to persist for decades, with resilience to external perturbations like economic or political crises.
- High Power Quality and Reliability: Ensuring electricity availability with minimal latency, stable voltage and frequency, and low harmonic distortion is essential for meeting the demands of users.
- High Efficiency: Minimizing electricity wastage during production, transportation, and distribution processes is imperative. Both the grid and loads should be managed to achieve optimal system efficiency.
- High Flexibility: Future power systems should be highly configurable, facilitating seamless integration among diverse power sources. Dynamic changes in loads and power sources should not compromise system performance and power quality.

- Low Environmental Impact: There is a need for a progressive shift towards renewable energy sources to replace traditional polluting sources, aligning with sustainability goals.

The realization of these requirements calls for a substantial revision of existing power systems, marked by the introduction of new functionalities and systems, commonly referred to as the Distributed Generation (DG) and Smart Grid (SG) revolution. This transformation necessitates [1-3]:

- Full Exploitation of Renewables: Leveraging the full potential of renewable energy sources.
- Technological Enhancements and Energy Storage: Widespread adoption of energy storage systems and technological advancements.
- ICT Integration: Massive incorporation of Information and Communication Technologies (ICTs).
- Self-Healing Systems: Implementation of high-granularity self-healing mechanisms and resilience against undesired situations such as blackouts or natural disasters.
- Consumer Participation: Active participation of consumers in the electricity market.
- Innovative Products and Markets: Introduction of new products, services, and markets to adapt to evolving needs.

This comprehensive approach acknowledges the need for technological innovation, advanced functionalities, and dynamic operational strategies to shape the next generation of power systems.

1.2.1 Distributed generators

As mentioned earlier, it is imperative for the engineering community to intensify its focus on researching Renewable Energy Sources (RESs). Several forms of renewable energy resources are currently viable for integration into the power grid, with the top four being wind, solar photovoltaic, hydroelectric, and geothermal. In this section, the discussion will exclusively center around the photovoltaic generator as it aligns with the primary focus of this research.

1.2.1.1 Photovoltaic generators

Photovoltaic (PV) cells serve as direct current (DC) generators, employing semiconductor technology to convert sunlight energy into electricity. Silicon, specifically, is

widely used as the semiconductor material in PV cells. These cells feature a junction composed of n- and p-doped silicon. Here's a brief overview of the operation of PV cells[5, 6]:

- Material and Junction: PV cells use silicon, and their structure includes a junction with n- and p-doped silicon. This junction is crucial for the conversion process.
- Conversion Process: When sunlight, composed of photons, strikes the junction, the energy within these photons is converted into electric power.
- Voltage and Current Output: The voltage produced by PV cells is influenced by intrinsic cell characteristics, the number of cascaded cells, and their temperature. On the other hand, the available current is dependent on cell characteristics, the number of parallel strings (a string is a group of cascaded cells), and sunlight irradiation.
- Panel Configuration: With current technology, PV cells are arranged in panels.

To power standard loads that operate on alternating current (AC), solar panels are interconnected either in series, parallel or a combination of both to achieve the required voltage and current levels. This combined output is then used to supply an inverter. Additionally, photovoltaic (PV) sources can be integrated into the distribution grid using an appropriate conversion chain. Broadly PV systems are characterized as stand-alone systems and grid-connected systems as shown in Figure 1.1. Grid-connected PV systems: are designed to be capable of injecting sinusoidal current into the public grid. In contrast, a stand-alone PV system, as the name suggests, is designed to operate independently of the public grid.

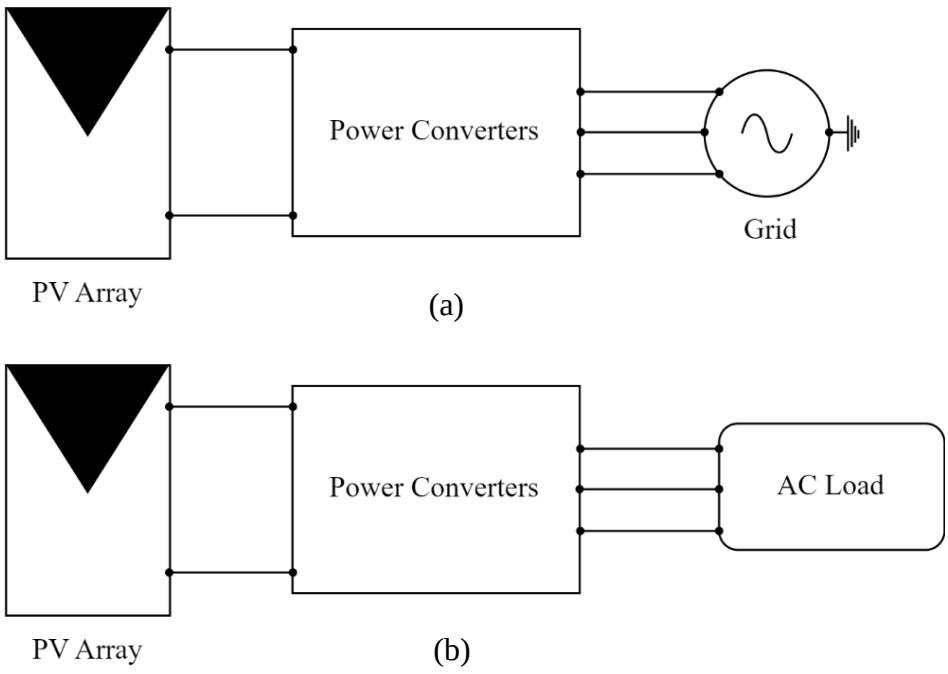

Figure 1.1: PV systems: a) connected to the grid, b) Stand-alone.

1.3 Configurations for a PV system connected to the grid

There are generally two configurations for a PV system connected to the grid: Single-Stage (S-S) and Dual-Stage(D-S), as shown in Figure 1.2. It's worth noting that the choice between single and Dual-Stage configurations depends on various factors, including the specific requirements of the application, efficiency considerations, and control objectives.

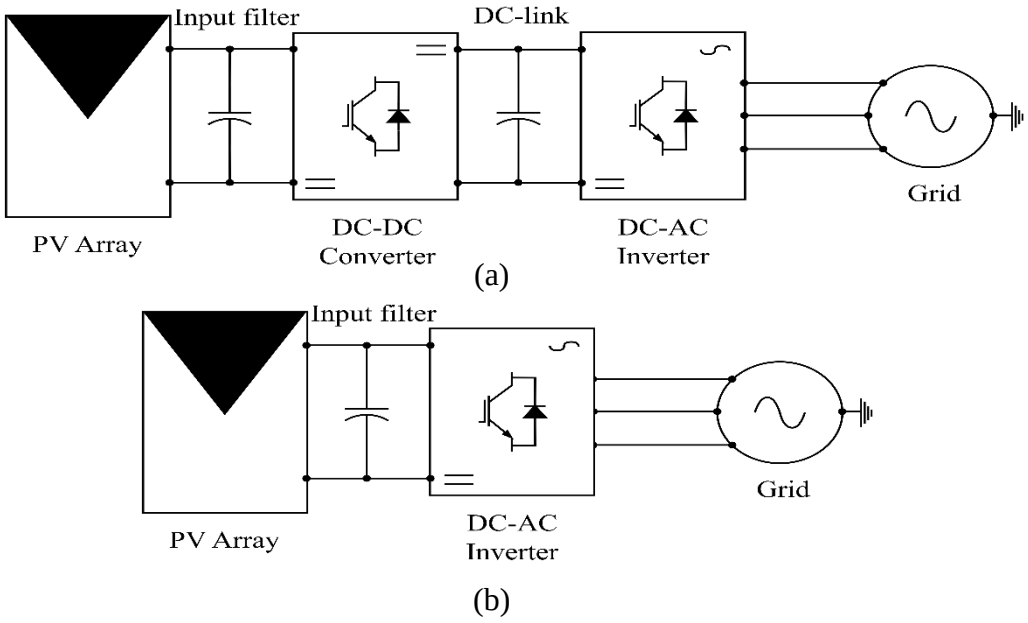

Figure 1.2: Schematic diagram of photovoltaic grid-connected system configurations: (a) Dual-stage (b) Single-stage.

1.3.1 Dual Stage Configuration

D-S in the context of grid-tied PV systems refers to a configuration where a DC-DC converter is placed between the PV array and the inverter. This additional converter helps regulate the DC voltage of the PV panels and assists in maximizing power output. In D-S systems, the DC-DC converter handles tasks like DC voltage regulation and Maximum Power Point Tracking (MPPT), while the inverter converts this power into high-quality AC signal for grid connection. One of the advantages of dual-stage PV inverters is that they support single/three-phase connections because they are based on a two-stage structure [7].

1.3.1.1 DC-DC Converter

Enhancing DC-DC converters, play a pivotal role in grid-connected PV systems by facilitating the efficient integration of solar power into the electrical grid. These converters perform various critical functions within such systems. DC-DC converters regulate voltage levels between the PV array and the inverter. They ensure that the voltage produced by the solar panels matches the requirements of the grid, facilitating smooth and safe power transmission.

1.3.1.1.A Buck Converter

The DC–DC buck converter, shown in Figure 1.3, steps down the output voltage level to be less when compared with the input voltage level [8, 9]. Therefore, this converter topology can be employed for integrating the greater module voltages to the lower loads or lower battery voltages. There are various solar PV applications used along with the DC–DC buck converters, are employed in the standalone solar PV pumping systems that are enabled to use the water supply in rural areas [10], solar battery charger [11, 12], grid-connected MPPT tracking [13], and the off-grid PV systems [14].

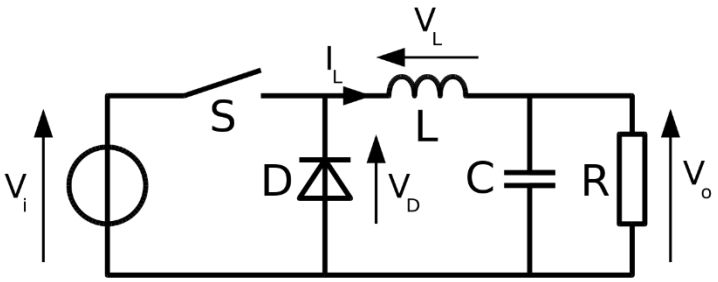

Figure 1.3: Buck converter scheme.

1.3.1.1.B Boost converter

Boost converters in Figure 1.4 are a type of DC-DC switching converter that efficiently increase (step-up) the input voltage to a higher output voltage. By storing energy in an inductor during the switch-on phase and releasing it to the load during the switch-off phase, this voltage conversion is made possible. Power electronics applications requiring a greater output voltage than the input source, in particular, depend on boost converters.

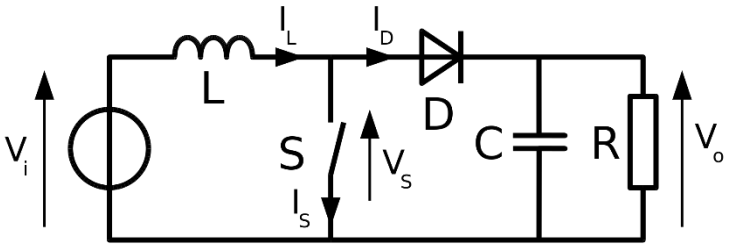

Figure 1.4: Boost converter scheme.

1.3.1.1.C Buck–Boost Converter

The buck–boost converter in Figure 1.5 is formed by integrating basic buck and boost converter topology and that can be used in various applications as standalone/grid-connected PV systems and motor drives. The current research on the buck–boost converter is still under progress for solar PV applications. To enhance the voltage gain, many researchers across the

world are developing various non-isolated DC–DC converter topologies namely Cuk, SEPIC, and Luo converters that are constructed relying on the buck–boost topology.

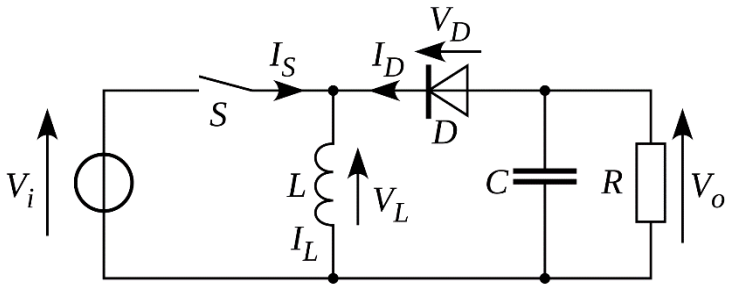

Figure 1.5: Buck-Boost converter scheme.

1.3.1.2 Voltage Source Inverters

Power inverters, essential for converting Direct Current (DC) to Alternating Current (AC), are traditionally categorized as voltage source inverters (VSIs), with distinct characteristics outlined in Figure 1.6. The fundamental structure of a three-phase two-level voltage source inverter (VSI) is depicted in Figure 1.6. It comprises a DC source, input capacitor, three-phase legs, output filter, and a three-phase load. Each leg includes two power transistors with an antiparallel diode in series. VSIs are versatile, generating variable frequency and amplitude sinusoidal waveforms, making them applicable in diverse systems like AC motor drivers, active power filters, photovoltaic (PV) systems, and wind power systems[15, 16].

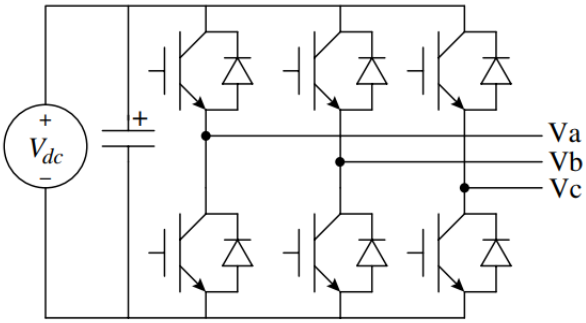

Figure 1.6: Three-phase two-level VSI.

1.3.1.2.A Multi-level VSIs

Multi-level VSIs (MVSIs) have been shown to mitigate the harmonic content and THD of the output current by generating a staircase output voltage waveform that closely approximates a sinusoidal shape [17, 18]. Additionally, in comparison to two-level VSIs, multi-level variants offer advantages such as lower switching stresses, decreased switching frequency, reduced switching losses, lower dv/dt, and minimized Electromagnetic Interference (EMI). Furthermore, they can attain high voltage levels, rendering them suitable for applications demanding elevated voltage levels.

1.3.1.2.A.1 Cascaded H-Bridge

Figure 1.7 illustrates a five-level Cascaded H-Bridge (CHB) inverter, where each bridge can provide three levels of voltages. The number of voltage levels can be expressed as $2m + 1$, with 'm' representing the number of bridges. A significant advantage of this topology is the absence of additional capacitors and diodes. Consequently, the CHB inverter can achieve the same voltage levels with fewer components. Furthermore, the CHB topology is easily modularized as each bridge requires a separate DC source. However, it's important to note that the number of separate DC sources increases proportionally with the rise in voltage levels, and each source necessitates real power conversion.

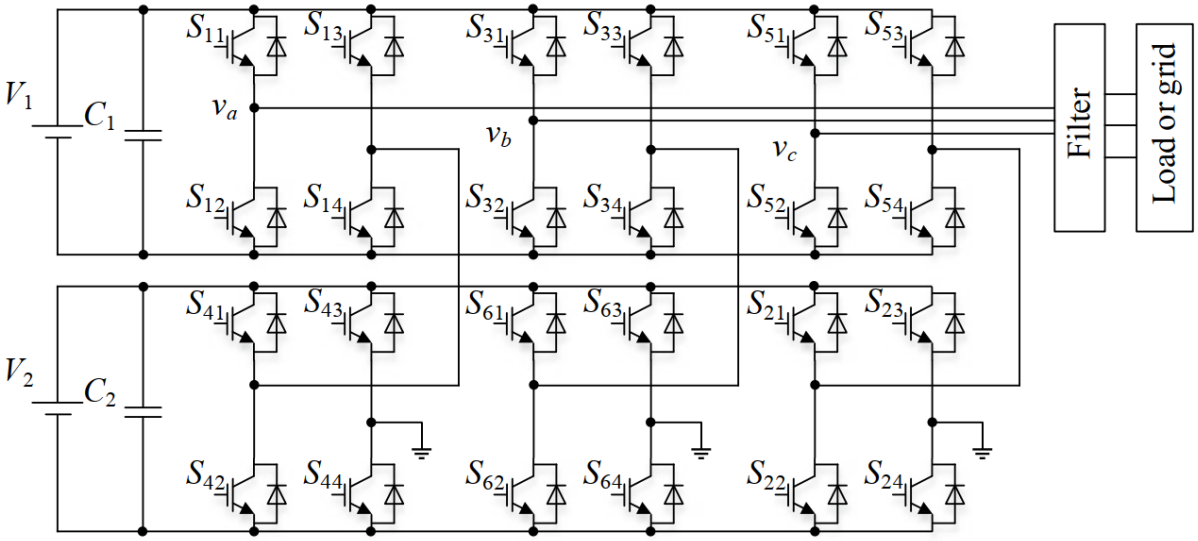

Figure 1.7: Five-level cascaded H-bridge inverter.

1.3.1.2.A.2 Neutral-Point-Clamped

The configuration of the three-level Neutral-Point-Clamped (NPC) inverter is depicted in Figure 1.8. It introduces six diodes, six power transistor modules, and one capacitor to the basic two-level voltage source inverter. Notably, the power transistors in the NPC inverter do not experience the full voltage of the DC source, as the capacitors divide the source into two parts. This feature allows for a reduction in the power rating of the devices. Moreover, the NPC inverter exhibits high efficiency and doesn't require additional filters to mitigate harmonics. An important capability of the NPC inverter is the control of reactive power flow [19]. However, modularizing the NPC topology is challenging, and a higher number of diodes is needed for increased voltage levels.

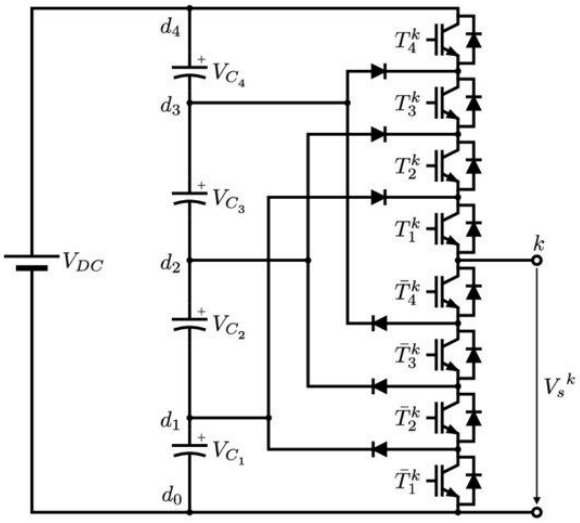

Figure 1.8: Five-level Neutral-Point-Clamped inverter.

1.3.1.2.A.3 Flying Capacitor

The Flying Capacitor (FC) converter, the third prominent multilevel converter, is depicted in Figure 1.9 with its representative three-level phase-leg. By regulating the isolated capacitor C_1 at half the DC-link voltage, this converter can generate three distinct output voltage levels: $V_{dc}/2$, 0, and $-V_{dc}/2$. Assuming that the voltage rating of the capacitors matches that of the active semiconductor switches, an n-level FC converter can be designed with $(n-1)\times(n-2)/2$ clamping capacitors per phase-leg, in addition to $(n-1)$ DC-link capacitors. This presents a drawback as the system size significantly increases with the number of output voltage levels.

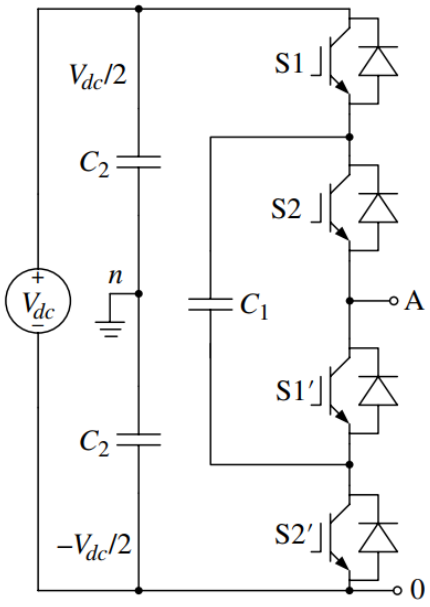

Figure 1.9: Three-level FC inverter.

However, this increase poses fewer technical challenges compared to the diode-clamped topology. With an appropriate phase-shifted modulation scheme, the capacitor voltages of the FC inverter naturally self-balance. Consequently, a higher-level FC inverter can be implemented more easily, although it is unlikely to surpass the cascaded multilevel inverter.

1.3.1.2.A.4 Packed-U-Cells

The Packed-U-Cells (PUC) inverter stands out as a promising contender in the realm of single-DC-source Multi-level Inverters (MLI), is depicted in Figure 1.10 with its representative five-level. Its unique features position it as a competitive choice across various applications. Noteworthy advantages include minimal impact on the power grid, the flexibility to scale up to higher output levels without extending the DC bus, a diverse range of controllable actions, augmented filter bandwidth through switching state redundancy, improved reliability and cost-effectiveness through fewer active components, and an enhanced ride-through capability facilitated by existing storage capacitors [4].

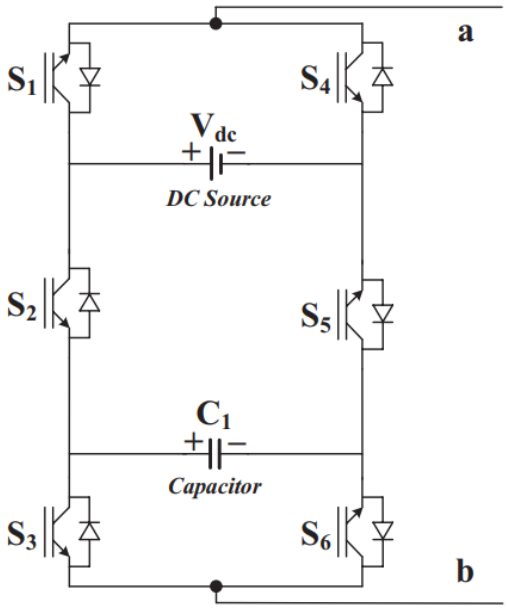

Figure 1.10: Five-level PUC inverter.

1.3.1.2.B Comparison of MLIs topologies

Some comparisons should be made to evaluate the distinctiveness of the topology. The selected topologies include CHB, NPC, FC, and PUC [17]. The idea of selecting those topologies was that they are the most popular ones and are manufactured by industries. Moreover, except for CHB, they can be single-DC-source topologies. Additionally, all of them generate a 5-level voltage waveform at the output. Too many topologies have been reported as

multiple-DC-source, which are not interesting for the industries anymore. The comparison summary has been listed in Table 1.1.

Table 1.1: Results of comparison between MLIs topologies.

Topology	level	DC Source	Capacitor	Switch	Diode	Component to level ratio	Voltage Balancing
CHB	5	2	0	8	0	2	External Regulator
NPC	5	1	4	8	6	3	External Regulator
FC	5	1	2	8	0	2.2	Redundant States
PUC	5	1	1	6	0	1.6	Redundant States

The above table can be analyzed by each column. The higher the number of levels, the lower THD, and the smaller the size of the filter and manufactured product. The next column is the number of isolated DC sources that means a bulky transformer plus a diode bridge or PV panel or batteries. Their prices are much more than switches so CHB is eliminated in the comparison process. Considering the next three columns, PUC has lower number of components among other topologies of NPC, and FC. Moreover, by defining the component to level ratio, it is still distinguishing that the PUC structure generates more voltage levels while using less components.

1.3.2 Single-Stage Configuration

S-S in the context of grid-tied PV systems refers to a configuration where PV panels are directly connected to a grid-tied inverter (DC/AC converter) without the presence of a DC-DC converter between the PV array and the inverter. In S-S systems, the grid-tied inverter is responsible for tasks like MPPT and ensuring high efficiency while connecting the DC output of the PV array to the grid as usable AC power. This setup offers a simple topology and cost-effectiveness but may require efficient control design to extract the maximum available power from the PV array and transfer it to the grid. All of these advantages can be provided by Impedance Source Inverter (ZSI) topologies.

1.3.2.1 Impedance Source Inverters

Traditional VSIs face limitations in working exclusively in buck (step-down) or boost (step-up) modes, respectively. Issues such as dead times for VSIs introduce compromises in output waveform quality. Additionally, the growing demand for renewable energy requires a wider voltage gain range, challenging traditional inverters. While two-stage inverters with a DC–DC converter have been proposed, they increase system complexity and size.

To tackle these challenges, S-S ZSIs, capable of both bucking and boosting voltages without requiring dead times or overlap delays, have been introduced. These inverters find applications in PV power generation, wind power generation, electric vehicles, and more.

One of the earliest impedance source inverters is the ZSI. The ZSI can adjust its DC-link voltage by varying the Shoot-Through (ST) time of the same phase leg. This makes the ZSI less susceptible to inadvertent short circuits and waveform distortions caused by dead times and overlap delays.

The topology of a one-phase ZSI consists of a DC source, impedance network (comprising inductors L_1 and L_2, and capacitors C_1 and C_2 in an X shape), an H-bridge, output filter, and AC load, as shown in Figure 1.11. The impedance network plays a crucial role, endowing the ZSI with the inherent features of impedance source inverters. By incorporating the impedance network into the input source and inverter bridge of a traditional three-phase source inverter, a three-phase impedance source inverter is created. Moreover, the impedance network can be applied to AC–DC, AC–AC, and DC–DC power conversion, showcasing its versatility in similar functionalities. Hence, the impedance network emerges as a pivotal component in impedance source inverters and converters [20].

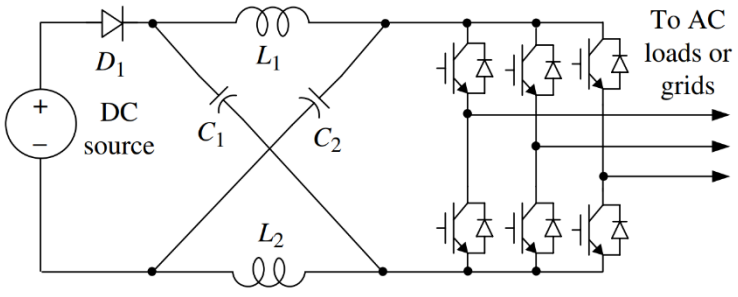

Figure 1.11: Three-phase Z-source inverter.

1.3.2.2 Quasi-Z-source Inverter

The ZSI, introduced three decades ago, boasts a unique circuit enabling it to boost the input voltage. Widely employed as a single-stage inverter, particularly in renewable energy conversion systems, it leverages the Z-source impedance network (ZSN) features. The inverter

achieves control in both Shoot-through (ST) and Non-Shoot-Through (NST) states, providing operational flexibility. Despite its proficiency in simultaneous boosting and inversion, the ZSI faces challenges, notably a discontinuous input current. This limitation prompted the development of an alternative topology known as the quasi-Z-source network (QZSN) in 2008. The QZSN addresses the discontinuity issue, ensuring a continuous DC input current [21, 22].

The ZSI topology is presented as an innovative alternative to traditional VSI. Acting as a buffer between the source and the inverter bridge, the Impedance Source Network (ISN) is introduced to mitigate certain challenges. However, the conventional ZSN is acknowledged for having drawbacks, including drawing a discontinuous input current and being unsuitable for very low input DC voltages.

In response to the limitations of the conventional ZSN, the qZSI is proposed as a modification aimed at enhancing performance and overcoming existing issues. Two variations of the qZSI are outlined in Figure 1.12(a) and (b), illustrating its potential improvements. Various parameters, such as Vin (input DC voltage or PV voltage), Vdc (boost voltage from the Z-source impedance), VC (voltage across the Z-source capacitor), Do (duty ratio during the shoot-through interval), and B (boost factor of the impedance network), play crucial roles in defining the characteristics and behaviors of the qZSI.

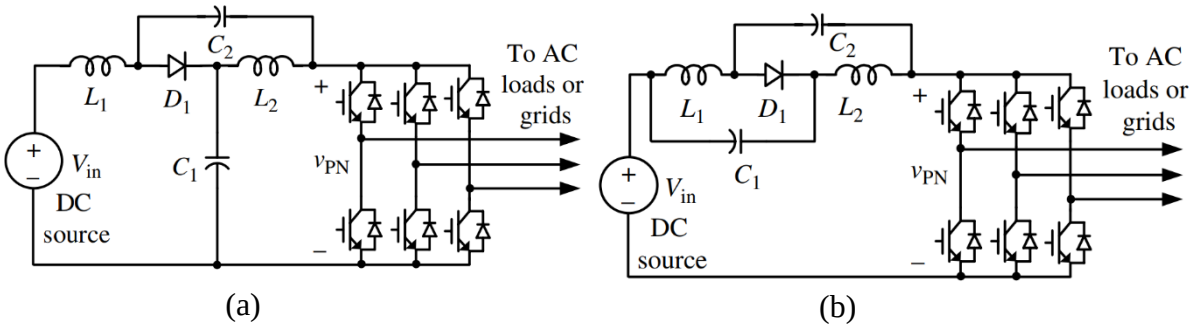

Figure 1.12: Topologies of qZSI: (a) qZSI with continuous input current, (b) qZSI with discontinuous input current.

1.3.2.3 Comparison of ZSI and qZSI

Several modifications and improvements have been proposed in the original ZSI to overcome the drawbacks of the traditional ZSI and improve its performance. Some succeeded in increasing the boosting capability, and others reduced the capacitor voltage and the start-up inrush current. Thus, each ISNs derived from the ZSI has advantages and disadvantages in solving the problems of the original configuration, so the user may not be able to select the appropriate network in practice quickly and accurately. Table 1.2 summaries the differences

between the ZSI and qZSI of components and characteristics, respectively. In contrast, Table 1.3 compares topologies in terms of advantages and disadvantages.

Table 1.2: Comparison of the configuration of ZSI and qZSI.

Name	D	C	L	Integrated winding	Continuous I_{in}	Inruch I_{in}	Common earthing
ZSI	1	2	2	-	No	Yes	No
qZSI	1	2	2	-	Yes	No	Yes

Table 1.3: Comparison of the optimization results of ZSI and qZSI.

Name	Advantages	Disadvantages
ZSI	• Bypassing VSI and CSI problems. • Operating both switches in the same phase and at the same time does not cause any damage. • Suitable for PV applications.	• Discontinuous input current. • Hight inrush current. • Hight capacitor voltage requires a large capacity. • ST duty ratio was less than 0.5.
qZSI	• Continuous input current. • Capacitors' ratings are decreased. • Current stress in lower than ZSI. • Suitable for PV applications.	• ST duty ratio was less than 0.5. • Not suitable for very low input DC source.

1.4 Conclusion

In this chapter, a brief analysis and description of DG systems are achieved, and it has been reported that conventional power grids present many drawbacks. Therefore, DGs should have more interest in the coming years. PV generators' operation principle and their grid interfacing configuration were investigated, where the dual and single stages were discussed in detail. A classification and description of the most common inverter topologies are reported in

the third section of this chapter, and a comparison between them is carried out. Finally, a literature review on single-stage grid PV system ZSIs-based systems.

References

[1] H. Abu-Rub, M. Malinowski, and K. Al-Haddad, *Power electronics for renewable energy systems, transportation and industrial applications*. John Wiley & Sons, 2014.

[2] F. Blaabjerg and D. M. Ionel, "Renewable energy devices and systems–state-of-the-art technology, research and development, challenges and future trends," *Electric Power Components and Systems,* vol. 43, no. 12, pp. 1319-1328, 2015.

[3] A. Anzalchi and A. Sarwat, "Overview of technical specifications for grid-connected photovoltaic systems," *Energy conversion and management,* vol. 152, pp. 312-327, 2017.

[4] A. May, F. Krim, H. Feroura, and A. Belaout, "Power Quality Enhancement of Grid-Tied 7L-PUC Inverter-Based PV System Using a Novel DC-Link Controller," *Arabian Journal for Science and Engineering,* vol. 48, no. 11, pp. 15305-15319, 2023.

[5] F. A. Silva, "Advanced DC\/AC inverters: applications in renewable energy (Luo, FL and Ye, H.; 2013)[book news]," *IEEE Industrial Electronics Magazine,* vol. 7, no. 4, pp. 68-69, 2013.

[6] R. Teodorescu, M. Liserre, and P. Rodriguez, *Grid converters for photovoltaic and wind power systems*. John Wiley & Sons, 2011.

[7] E. Kabalcı, "Review on novel single-phase grid-connected solar inverters: Circuits and control methods," *Solar Energy,* vol. 198, pp. 247-274, 2020.

[8] F. Yusivar, M. Farabi, R. Suryadiningrat, W. Ananduta, and Y. Syaifudin, "Buck-converter photovoltaic simulator," *International Journal of Power Electronics and Drive Systems,* vol. 1, no. 2, p. 156, 2011.

[9] M. H. Rashid, *Power electronics handbook*. Butterworth-heinemann, 2017.

[10] N. Mohan, T. M. Undeland, and W. P. Robbins, *Power electronics: converters, applications, and design*. John wiley & sons, 2003.

[11] A. Jayakrishnan *et al.*, "Are lead-free relaxor ferroelectric materials the most promising candidates for energy storage capacitors?," *Progress in Materials Science,* vol. 132, p. 101046, 2023.

[12] C. G. Villegas-Mier, J. Rodriguez-Resendiz, J. M. Álvarez-Alvarado, H. Rodriguez-Resendiz, A. M. Herrera-Navarro, and O. Rodríguez-Abreo, "Artificial neural networks in MPPT algorithms for optimization of photovoltaic power systems: A review," *Micromachines,* vol. 12, no. 10, p. 1260, 2021.

[13] K. V. G. Raghavendra *et al.*, "A comprehensive review of DC–DC converter topologies and modulation strategies with recent advances in solar photovoltaic systems," *electronics*, vol. 9, no. 1, p. 31, 2019.

[14] D. Verma, S. Nema, A. Shandilya, and S. K. Dash, "Maximum power point tracking (MPPT) techniques: Recapitulation in solar photovoltaic systems," *Renewable and Sustainable Energy Reviews*, vol. 54, pp. 1018-1034, 2016.

[15] K. Jayanth, V. Boddapati, and R. Geetha, "Comparative study between three-leg and four-leg current-source inverter for solar PV application," in *2018 International Conference on Power, Instrumentation, Control and Computing (PICC)*, 2018: IEEE, pp. 1-6.

[16] I. Pharne and Y. Bhosale, "A review on multilevel inverter topology," in *2013 International Conference on Power, Energy and Control (ICPEC)*, 2013: IEEE, pp. 700-703.

[17] L. P. Suresh, "A brief review on multi level inverter topologies," in *2016 international conference on circuit, power and computing technologies (ICCPCT)*, 2016: IEEE, pp. 1-6.

[18] S. Alatai *et al.*, "A Review on State-of-the-Art Power Converters: Bidirectional, Resonant, Multilevel Converters and Their Derivatives," *Applied Sciences*, vol. 11, no. 21, p. 10172, 2021.

[19] A. Bughneda, M. Salem, A. Richelli, D. Ishak, and S. Alatai, "Review of multilevel inverters for PV energy system applications," *Energies*, vol. 14, no. 6, p. 1585, 2021.

[20] N. Subhani, R. Kannan, A. Mahmud, and F. Blaabjerg, "Z-source inverter topologies with switched Z-impedance networks: A review," *IET Power Electronics*, vol. 14, no. 4, pp. 727-750, 2021.

[21] I. Jamal, M. F. Elmorshedy, S. M. Dabour, E. M. Rashad, W. Xu, and D. J. Almakhles, "A comprehensive review of grid-connected PV systems based on impedance source inverter," *IEEE Access*, vol. 10, pp. 89101-89123, 2022.

[22] S. Vadi, R. Bayindir, and E. Hossain, "A review of control methods on suppression of 2ω ripple for single-phase quasi-Z-source inverter," *IEEE Access*, vol. 8, pp. 42055-42070, 2020.

Chapter 2: Literature survey on control strategies

2.1 Introduction

The purpose of the inverter in a DG system is to convert the raw power generated into a form compatible with the local distribution grid, in order to allow the power to be used by standard appliances or to be fed back into the utility grid. Therefore, suitable inverter modulation techniques and control strategies are of high importance to satisfy all the control objectives of the DG system [1].

This chapter provides an overview of control algorithms designed to track the maximum power point of a PV array and introduces control strategies for grid-connected PV systems, including predictive control, intelligent Control, fuzzy logic control, etc. The discussion focuses on leading control methods, elucidating all structural diagrams. Control methods are broadly classified into several categories, distinguishing between linear and nonlinear control. Unlike VSIs and Current Source Inverters (CSI) which employ similar control methods, qZSI requires specific control methods tailored to its unique voltage boost and buck characteristics. Additionally, the chapter describes and compares qZSI control methods.

2.2 Maximum Power Point Tracking Algorithms

The MPPT unit is a power conversion system equipped with a suitable control algorithm designed to extract the maximum power from a PV array. This optimization involves regulating either the current drawn from the PV array or the voltage across it to operate at or near the MPP. Various MPPT algorithms have been proposed in the literature, each varying in complexity, accuracy, efficiency, and implementation difficulty, all aiming to maximize the energy

utilization efficiency of PV arrays. According to their popularity, they can be classified as follows:

2.2.1 Fractional open-circuit voltage method

The almost linear relationship between V_{MPP} and the open-circuit voltage of a PV generator, under varying levels of sunlight and temperature, has given rise to the fractional V_{OC} method, where the relationship between V_{MPP} and V_{OC} is nearly linear.

$$V_{MPP} = K_1 \times V_{OC} \quad (2.1)$$

When K_1 is a proportionality constant, it depends on the characteristics of the photovoltaic generator used. It usually needs to be calculated in advance by empirically determining V_{MPP} and V_{OC} for the specific PV field at different irradiance and temperature levels. The values of the K_1 factor would be between 0.71 and 0.7.

2.2.2 Fractional short-circuit current method

The fractional short-circuit current results from the fact that, under varying atmospheric conditions, I_{MPP} is approximately linearly related to I_{SC} of a photovoltaic generator.

$$I_{MPP} = K_2 \times I_{SC} \quad (2.2)$$

Where K_2 is a constant of proportionality. As with the fractional V_{OC} technique, K_2 must be determined based on the photovoltaic generator used. The value of the constant K_2 is generally found to be between 0.78 and 0.92. Measuring I_{SC} during operation is problematic. An additional switch usually needs to be added to the power converter to periodically short-circuit the PV generator so that I_{SC} can be measured using a current senso.

2.2.3 Perturb and observe algorithm

This is the most commonly used algorithm for MPP tracking. It is based on voltage perturbation and observing *dP*/*dt*. The sign of the *dP*/*dt* derivative indicates whether the voltage is too high or too low compared to the MPP voltage. Consequently, this voltage can be decreased or increased until the MPP is reached, resulting in a zero derivative. Since this algorithm is based on perturbation, there will always be oscillations even when the MPP is reached. In Figure 2.1, the flowchart of the Perturb and observe (P&O) algorithm is presented.

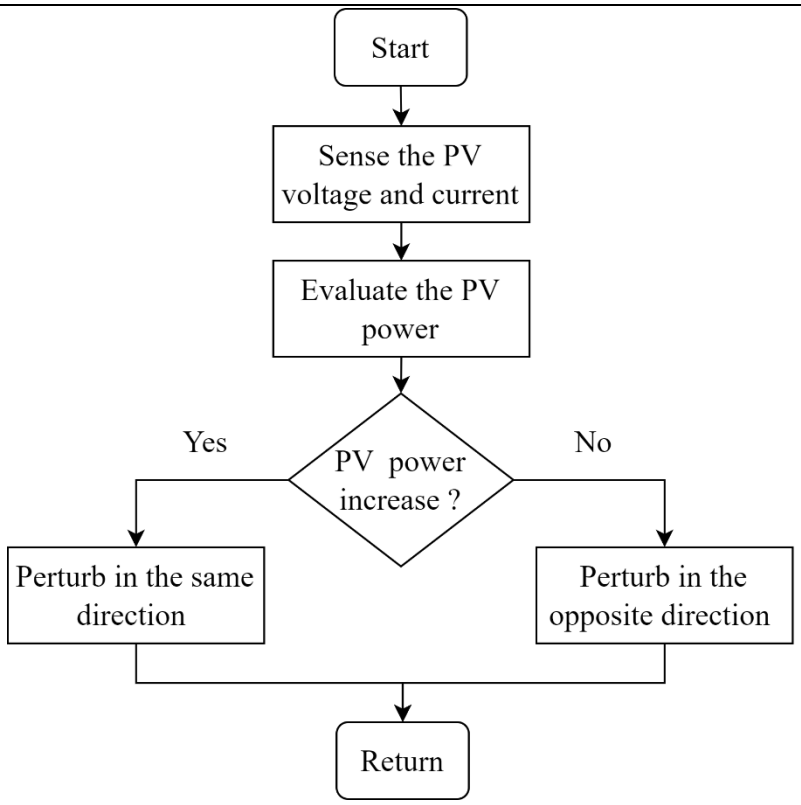

Figure 2.1: Flowchart of the P&O algorithm.

2.2.4 Incremental conductance algorithm

The Incremental Conductance (IncCon) algorithm is similar to the P&O method and has been proposed to improve tracking accuracy and dynamic performance in rapidly changing atmospheric conditions. The IncCon algorithm is derived from the P_{PV}-V_{PV} curve of the photovoltaic generator, as shown in Figure 2.2, where the slope of the curve is positive on the left side of the MPP, negative on the right side of the MPP, and zero at the MPP. The slope of the power-voltage curve can be expressed as follows:

$$\begin{cases} \dfrac{dP_{PV}}{dV_{PV}} = \dfrac{dI_{PV}V_{PV}}{dV_{PV}} = I_{PV} + V_{PV}\dfrac{dI_{PV}}{dV_{PV}} \\ \dfrac{1}{V_{PV}}\dfrac{dP_{PV}}{dV_{PV}} = \dfrac{I_{PV}}{V_{PV}} + \dfrac{dI_{PV}}{dV_{PV}} \end{cases} \quad (2.3)$$

Therefore, the basic equations of this method are:

$$\frac{dI_{PV}}{dV_{PV}} = -\frac{I_{PV}}{V_{PV}} \quad \text{At the MPP} \quad (2.4)$$

$$\frac{dI_{PV}}{dV_{PV}} > -\frac{I_{PV}}{V_{PV}} \quad \text{To the left of the MPP} \quad (2.5)$$

$$\frac{dI_{PV}}{dV_{PV}} < -\frac{I_{PV}}{V_{PV}} \quad \text{To the right of the MPP} \quad (2.6)$$

Where:

$\frac{dI_{PV}}{dV_{PV}}$: Is the incremental conductance.

$\frac{I_{PV}}{V_{PV}}$: Is the conductance.

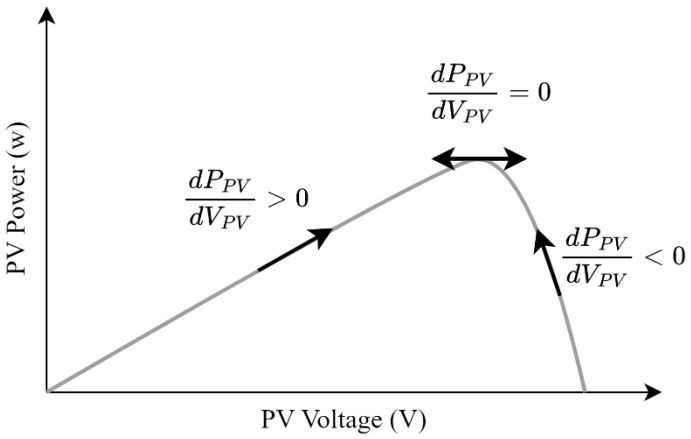

Figure 2.2: Basic idea of the IncCon algorithm on a curve (P_{PV}-V_{PV}) of a photovoltaic generator.

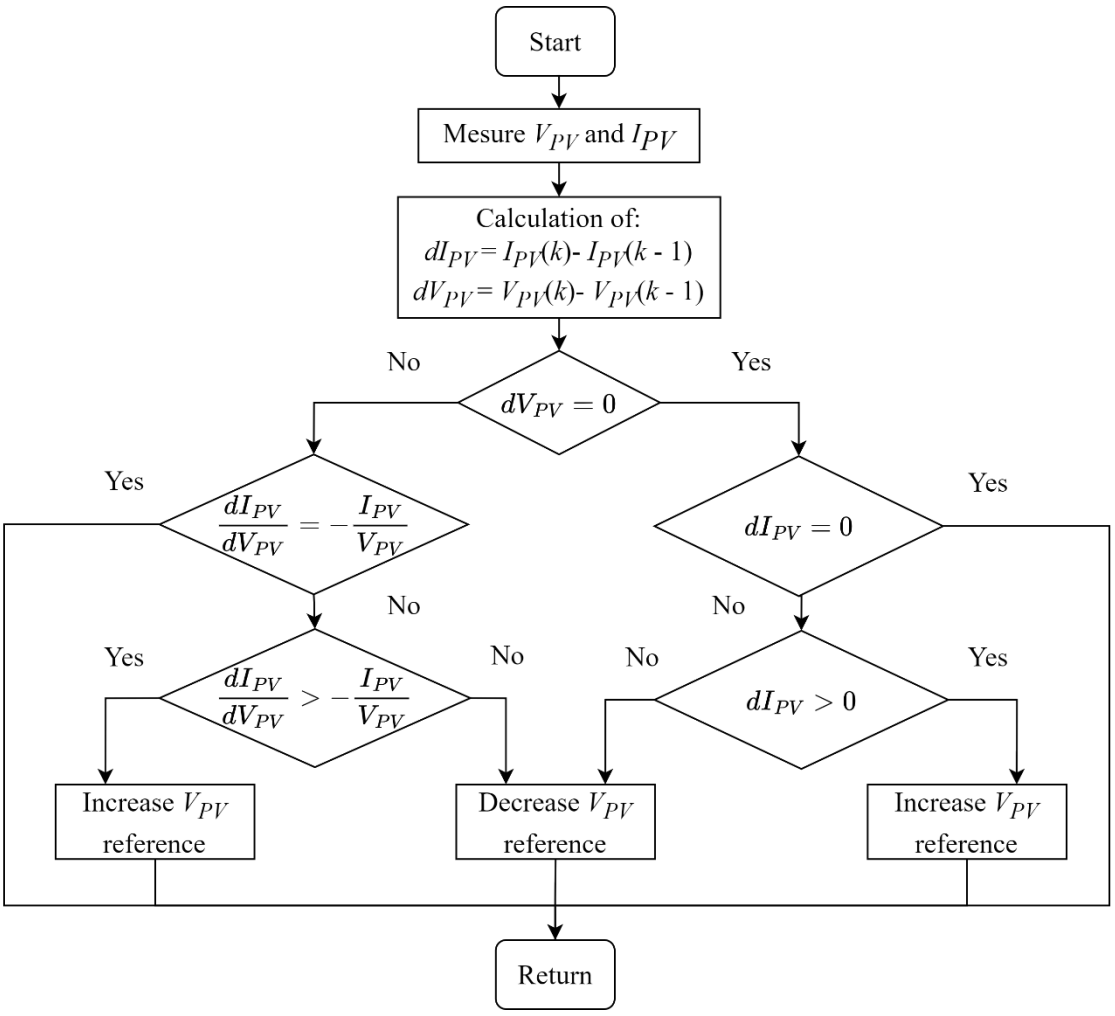

Figure 2.3: Flowchart of the IncCon algorithm.

The derivative of the current with respect to the derivative of voltage can be estimated as the difference between the actual values and the previous instant values in that iteration process. Therefore, by comparing the conductance I_{PV}/V_{PV} to the incremental conductance dI_{PV}/dV_{PV} as shown in Figure 2.3, the algorithm can track the MPP and stay there until a change of dI_{PV} or dV_{PV} occurs as a result of a change in atmospheric condition.

2.3 Control Strategies for Grid-Connected PV Systems

A PV system, being power-electronics-based, relies heavily on effective control mechanisms to ensure its stable and smooth operation within the power system. Without a robust and appropriate controller for the inverter, there's a risk of grid instability and disturbances. Controllers for PV systems are categorized based on grid behavior and operating conditions into various types, including linear, predictive, robust, non-linear, adaptive, and intelligent controllers as shown in Figure 2.4. The selection of the controller type depends on the specific requirements and characteristics of the grid and the PV system in question.

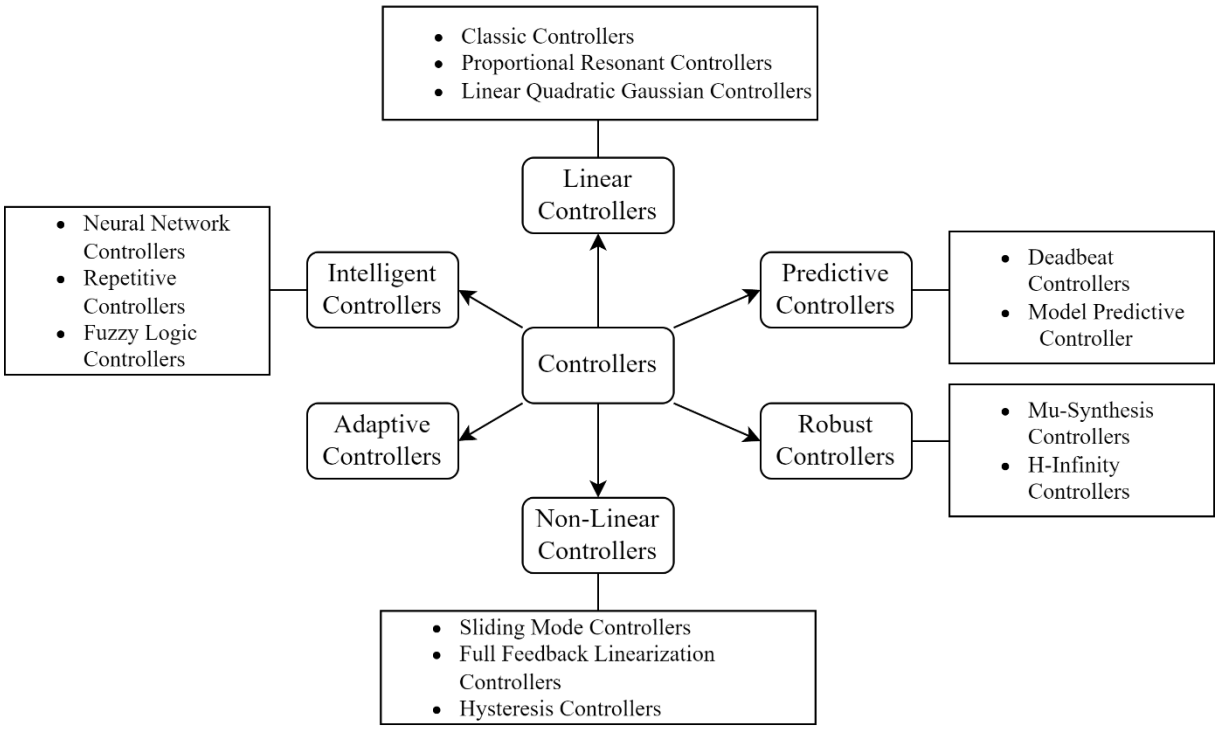

Figure 2.4: Different types of control strategies.

2.3.1 Linear Controllers

These controllers are designed on the foundation of the dynamics and features of the linear systems. A concept of classical feedback control is used while designing these types of controllers. They are further divided into three types and are described below.

2.3.1.1 Classic Controllers

The family of classic controllers includes Proportional (P), Proportional Integral (PI), Proportional Integral Derivative (PID), and Proportional Derivative (PD) controllers. Moreover, these controllers are considered as the foundation of a linear system. Among all the controller types, these controllers are more frequently and commonly used in grid-connected PV power plants and in many other commercial and industrial applications due to its easy implementation, realization, and simple structure.

2.3.1.2 Proportional Resonant (PR) Controllers

The popularity of PR controllers has increased over the last few years in grid-tied PV systems. PI and PR controllers have very much in common but there are two main differences between them. The first one is that the PI and PR controllers are operating in different reference frames. A PI controller efficiently tracks the DC signals in the *dq* reference frame, while a PR controller allows the tracking of a sinusoidal signal in *αβ* reference frame. Whereas, the second difference is that the integration part in PR controller is different from PI controller. In PR controller, only those frequencies are integrated that are close to the resonant frequency. As a result, no phase shift and stationary magnitude errors are involved [2]. A generalized control structure of PR is presented in Figure 2.5(a).

2.3.1.3 Linear Quadratic Gaussian (LQG) Controllers

LQG controller is formed by the combination of Kalman filter and LQ regulator. An LQG controller presented in Figure 2.5(b) shows that the controllers are designed and computed separately, according to the separation principle. An LQG controller performs its operation and functionality very smoothly in both time-variant and invariant systems [3].

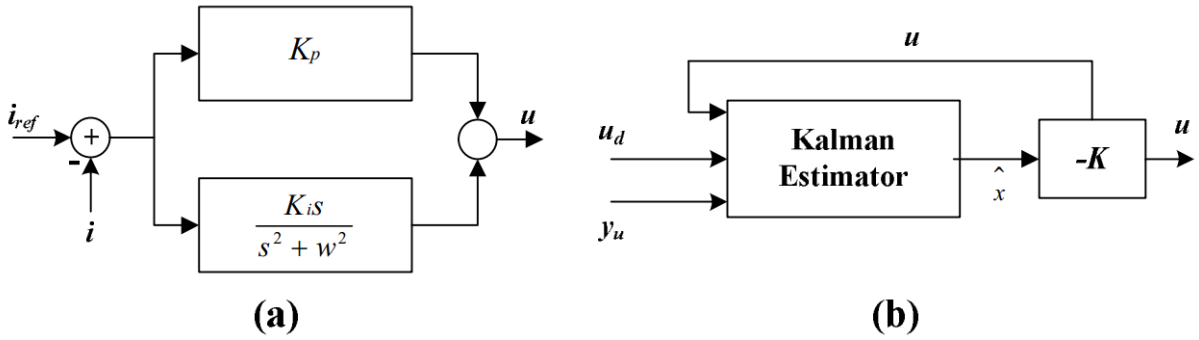

Figure 2.5: Block diagram of controllers (a) proportional resonant (PR); (b) linear quadratic.

2.3.2 Robust Controllers

Robust controllers are designed on the basis of a control theory that is related to uncertainties of the system. The end goal of robust controllers is to achieve stability and robust

performance even in the occurrence of incomplete modeling errors. This controller guarantees the stable performance of the close loop, in both single and multi-variable systems. A control configuration of the robust control scheme is sketched and presented in Figure 2.6 [4].

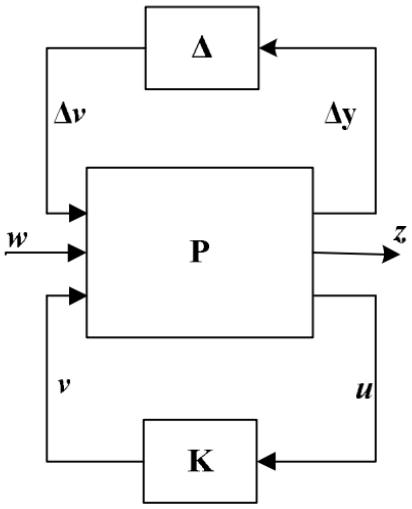

Figure 2.6: Block diagram robust controllers.

2.3.2.1 Mu-Synthesis Controllers

This approach is used to consider the consequences of uncertainties (unstructured and structured) on the system performance. In this approach, the concept of a controller design is dependent on a singular value that may be either a structured or an un-structured valve.

2.3.2.2 H-Infinity (Hœ) Controllers

The expression Hœ control originates from the term mathematical space on which the optimization takes place: Hœ is considered as a space of matrix-valued functions that are investigative and confined in the open right-half of the complex plane. In this type of control system, first of all, the control problem is formulated and then mathematical optimization is implemented i.e., selection of the best element according to criterion from the set of obtainable alternatives [5-7] . H-infinity control techniques are generally pertinent for the multivariable systems. The impact of a perturbation can be reduced by using H-infinity control techniques in a closed loop system subject to the problem formulation. The impact can be measured either in terms of performance or stabilization of the system. However, modeling of the system should be well-defined for implementation of these control techniques. Moreover, H-infinity control techniques have another discrepancy of high computational complications. In case of non-linear systems limitations, the control system cannot handle them well and response time also increases [8].

2.3.3 Predictive Controllers (PC)

Predictive controllers are commenced as a propitious control technique for electronics inverters. The system model is considered critically and then the imminent behavior of the control variables is predicted conferring to the specified criterion. It is an uncomplicated technique and can handle multivariable systems efficiently. Moreover, it can handle the system with several limitations or non-linearities. It is generally preferred due to its prompt static as well as dynamic response and ability to handle stable errors. However, its computational analysis is complex as compared to classical controllers [4]. It is further categorized into Deadbeat control and Model Predictive control. A block presentation of PC is shown in Figure 2.7, where for every switching state the system characteristics are predicted by grid current i(k) and switching states s(k).

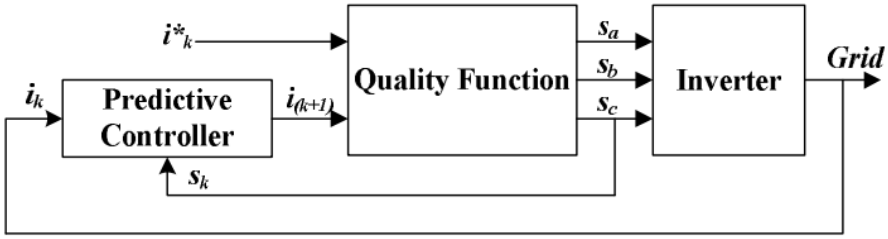

Figure 2.7: Block diagram of predictive controllers.

2.3.3.1 Deadbeat Controllers

The deadbeat control technique is the most authentic, competent, and attractive technique in terms of low Total Harmonic Distortion (THD) value, frequency as well as rapid transient response. Differential equations are derived and discretized in this type of control system for controlling the dynamic behavior of the system. The control signal is predicted for the new sampling period for attaining the reference value. Its effective dynamic performance and high bandwidth simplify the current control for this type of controller. Error compensation is a specialty of a deadbeat controller. However, its major discrepancy is its sensitivity for network parameters and accurate mathematical filter modeling [9]. The deadbeat controller structure is presented in Figure 2.8.

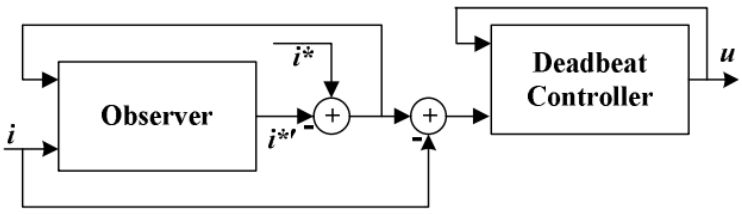

Figure 2.8: Block diagram of deadbeat controllers.

2.3.3.2 Model Predictive Controller (MPC)

As the name depicts, a model of the system is used to predict the behavior of the system in the Model Predictive Control (MPC) technique. A cost function criterion is defined in this type of control system, which can be minimized for optimal control actions. The controller adapts the optimal switching states according to the cost function criterion. Forecast errors can be lessened for current tracking implementation. Moreover, system limitations and non-linearities, as well as multiple inputs and output systems, are handled well by MPC. A generalized configuration of MPC is presented in Figure 2.9 [10-13].

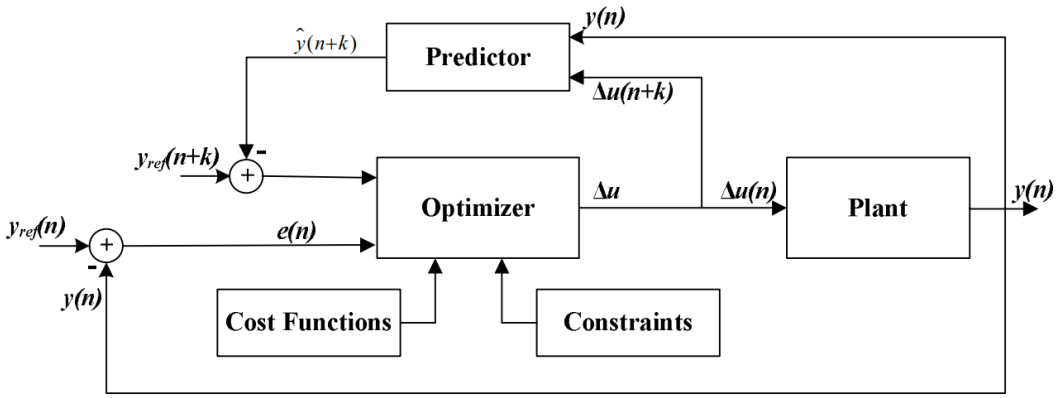

Figure 2.9: Block diagram of MPC

2.3.4 Non-Linear Controllers

The non-linear controllers have high dynamic response and their performance and operation are astonishing as compared to linear controllers. However, the realization and design of these controllers are complicated. The non-linear controllers are subdivided into sliding mode, partial feedback linearization, and hysteresis gaussian controllers.

2.3.4.1 Sliding Mode Controllers (SMC)

The SMC is considered to be an advanced power control technique for the power converters. It fits into the family of adaptive control and variable structure control [14, 15]. This controller is more robust and capable of removing the stable error as compared to the classical controllers. However, some drawbacks in implementing a SMC are difficulty in finding a suitable sliding surface and limitation of sampling rate that degrades the performance of SMC will be degraded. Whenever tracking a variable reference, the chattering phenomenon is another drawback of SMC technique. As a result, overall system efficacy is reduced [16-18].

2.3.4.2 Partial or Full Feedback Linearization (PFL or FFL) Controllers

In the PFL method, the non-linearities that are associated with the system are canceled because of the transformation of the non-linear system into a partial or complete linear system.

If the system having non-linearities are partially transformed into linear system, then it is known as PFL and if it is completely transformed then it is called as an FFL controller. Moreover, the system nonlinearities are canceled by establishing the non-linear terms within the system therefore they are not bound to a specific operating point [19-22].

2.3.4.3 Hysteresis Controllers (HC)

HC is considered as a nonlinear method [4, 23-25]. The hysteresis controllers are used to track the error between the referred and measured currents. Therefore, the gating signals are generated on the basis of this reference tracking. Hysteresis bandwidth is adjusted for error removal in reference tracking. This is an uncomplicated concept and has been used since analog control platforms were intensively used. This technique does not require a modulator; therefore, the switching frequency of an inverter is dependent on the hysteresis bandwidth operating conditions and filter parameters [26]. A generalized structure of HC is sketched and presented in Figure 2.10.

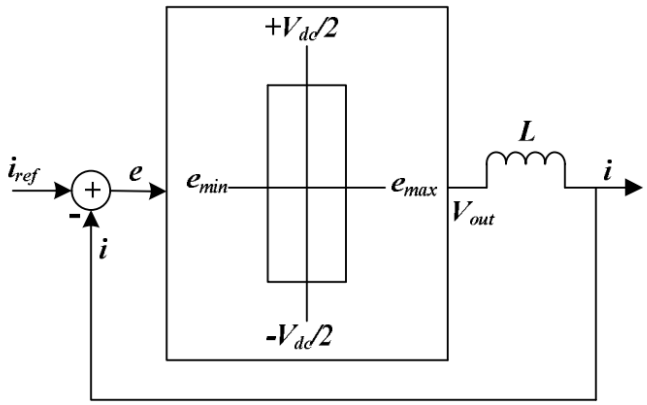

Figure 2.10: Block diagram of HC.

2.3.5 Adaptive Controllers

An adaptive controller is designed to have the ability of self-tuning, i.e., to regulate itself spontaneously according to variations in the system parameters. It does not require initial conditions, system parameters or limitations for its implementation due to its ability to modify the control law according to system requirements. Recursive least squares and Gradient descent are two most commonly known technique for parameters estimation in adaptive controllers [27]. A generalized diagram of the adaptive controller is presented in Figure 2.11.

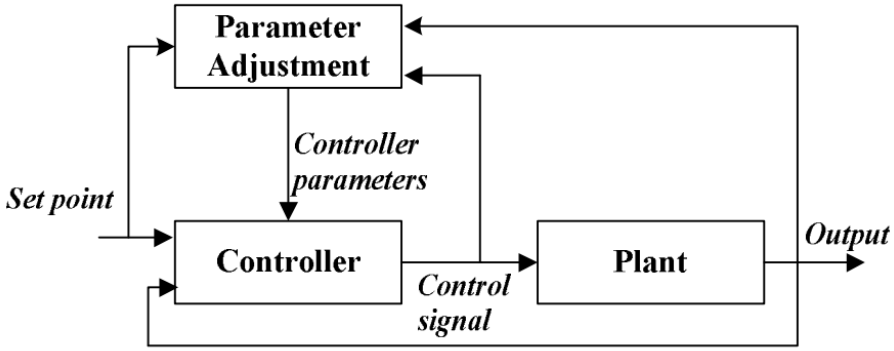

Figure 2.11: Block diagram of Adaptive Controllers

2.3.6 Intelligent Controllers

Automation is obtained by the intelligent controllers through the replication of biological intelligence. Moreover, these controllers do not require the system mathematical modeling and have the potential to approximate the non-linearities. The intelligent controllers are classified into three types. These are the following:

2.3.6.1 Neural Network (NN) Controllers

The concept of designing an NN controller is based on the human nervous system. It is a connection of many artificial neurons that is simulated by the biological brain system. When an NN approach is used in a control system it can be trained either online or offline. NN can achieve high fault tolerance and has a potential to approximate the function mapping [28]. Moreover, NN controllers require very less system modeling; therefore, they are frequently adopted in many practical and industrial applications [29].

2.3.6.2 Repetitive Controllers (RC)

The Plug-In Scheme (PIS) and Internal Model (IM) principle are the basic concepts of repetitive control (RC). RC uses an IMP which is in correspondence to the model of a periodic signal. In order to derive this model, trigonometric Fourier series expansion is used. If the model of reference is fed into the closed loop path, optimal reference tracking can be obtained. Moreover, it is found robust disturbances and has the ability to reject them. RC mostly deals with periodic signals. Closed loop behavior of the system and Magnitude response of the IM are the core factors used for analyzing the performance of the repetitive controller in case of frequency variation or any other uncertainty in the system. Both these factors indicate the performance sagging in case of variation or uncertainty in the reference signal. In presence of a periodic disturbance, RC intends to attain zero tracking error when a periodic or a constant command is referred to it. RC has an ability to locate an error, a time-period before and fine-

tunes the next command according to the feedback control system for eliminating the observed error. However, it lacks the ability to handle physical noise [5, 30-33]. The general structure of a repetitive controller is shown in Figure 2.12.

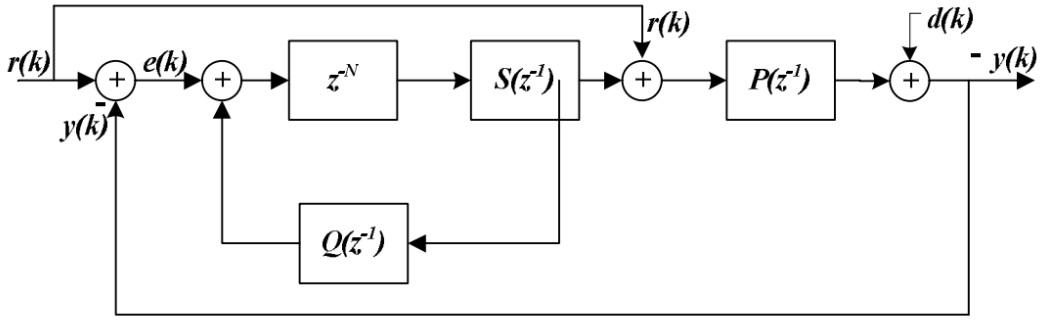

Figure 2.12: Block diagram of RC.

2.3.6.3 Fuzzy Logic Controllers (FLC)

This control technique belongs to the family of intelligent control systems. This controller design is dependent on the awareness, knowledge, skills and experience of the converter designer in terms of functions involvement. Due to non-linear nature of the power converters, the system can be stabilized in case of parameters variation even if the exact model of the converter is unknown. FLC are also categorized as non-linear controllers and probably the best controllers amongst the repetitive controllers [4, 33-35]. However, strong assumptions and adequate experience are required in the fuzzification of this controller. As it is dependent on the system input and draw conclusions according to the set of rules assigned to them during the process of their modeling and designing. Block diagram of a fuzzy logic control is shown in Figure 2.13.

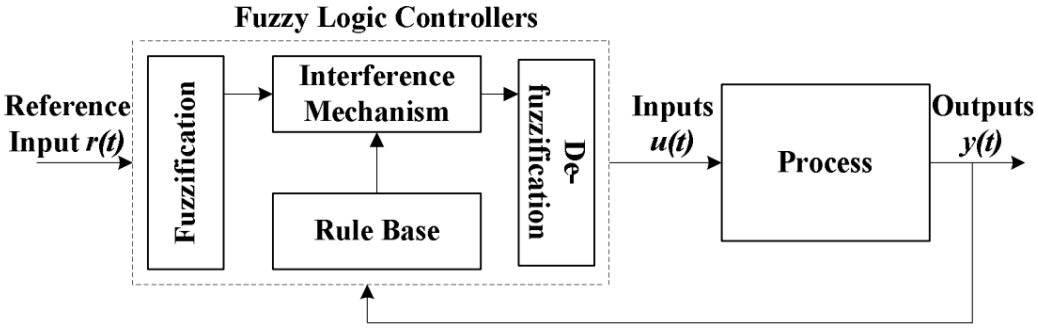

Figure 2.13: Block diagram of FLC.

2.4 Control Strategies for qZSI

2.4.1 Pulse Width Modulation Techniques

2.4.1.1 Sinusoidal Pulse Width Modulation

There are three conventional carrier-based Pulse Width Modulation (PWM) methods for the qZSI: Simple Boost Control (SBC) [36], Maximum Boost Control (MBC) [37], and Maximum Constant Boost Control (MCBC) [38]. These methods introduce shoot-through states by applying distinct shoot-through references to the traditional carrier-based Sinusoidal Pulse Width Modulation (SPWM). In the sketch maps of SBC and MBC depicted in Figure 2.14, when the carrier is greater than the upper shoot-through reference (v_p) and the upper envelope of the three-phase modulating waves (v_a*, v_b*, v_c*), or lower than the lower shoot-through reference (v_n) and the lower envelope of modulating waves, the three bridge legs conduct together, resulting in a shoot-through state. In between these conditions, the switches behave similarly to traditional carrier-based SPWM. However, the different shoot-through references lead to variations in boost capability, voltage gain, and stress on the inverter power switches.

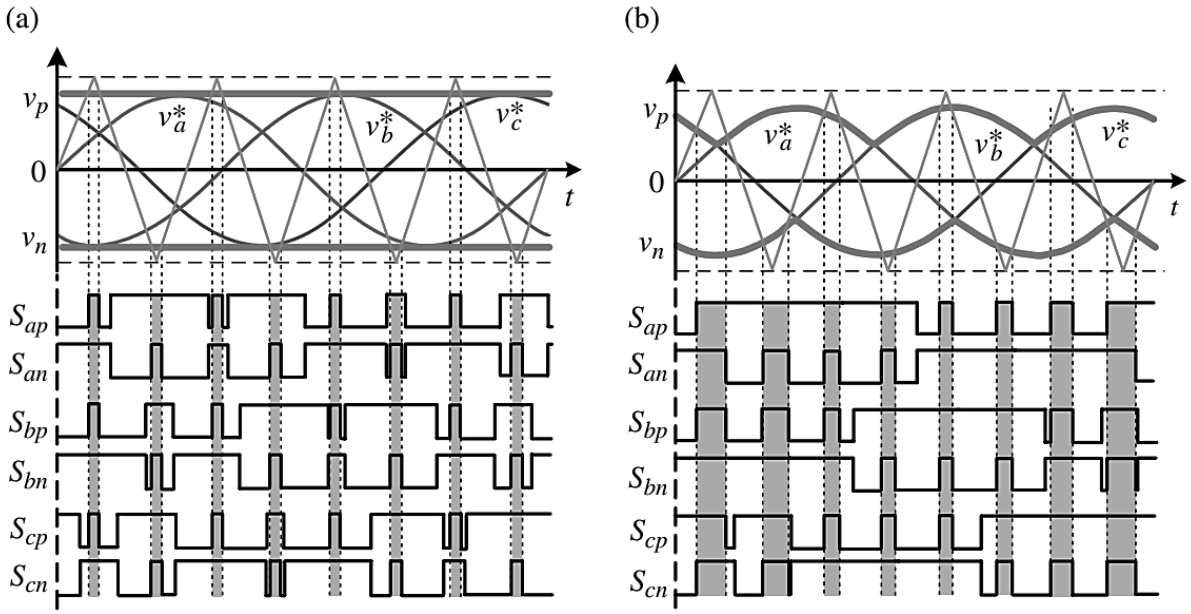

Figure 2.14: Modulation methods of (a) simple boost control and (b) maximum boost control for the three-phase two-level qZSI.

2.4.1.1.A Simple Boost Control

In the SBC method, the shoot-through reference is represented by a straight line, as illustrated in Figure 2.14(a), which is equal to or greater than the upper envelope of the modulating waves or equal to or lower than the lower envelope of the modulating waves. With this configuration, the maximum shoot-through duty ratio (d_{max}) is ($1 - m$), and it decreases as

the modulation index (m) increases. Moreover, when M reaches one, indicating that the inverter is operating as a traditional VSI, the shoot-through duty ratio becomes zero.

In the Simple Boost method [36], two straight lines, equal to or greater than the peak value of the three-phase references, are utilized to introduce the shoot-through duty ratio. Consequently, the shoot-through time per switching cycle remains constant, resulting in a constant boost factor. However, the achievable shoot-through duty ratio diminishes with an increase in the modulation index (m). Hence, the d_{max} is constrained to $(1 - m)$. When m reaches its maximum value, the shoot-through duty ratio becomes zero, and the inverter operates akin to a traditional VSI. In this scenario, the DC inductor current and capacitor voltage exhibit no ripple associated with the output frequency.

2.4.1.1.B Maximum Boost Control

In the MBC method illustrated in Figure 2.14(b), the shoot-through reference is precisely equal to the upper or lower envelope of the modulating waves. Unlike the SBC, where only a portion of the zero states is replaced by shoot-through states, the MBC replaces all traditional zero states with shoot-through states. This results in achieving the maximum zero-state duty ratio (d_{max}) per switching cycle, specifically $(1\text{-}3\sqrt{3}m/2\pi)$, introducing a low-frequency ripple into the quasi-Z-source capacitor voltage and inductor current [37].

However, it's important to note that the shoot-through duty ratio in MBC varies at six times the output frequency, contributing to low-frequency ripple in the quasi-Z-source capacitor voltage and inductor current. This ripple becomes more pronounced and necessitates higher requirements for the Z-network components when the output frequency is very low. Therefore, MBC is better suited for application fields with a fixed or comparatively high output frequency, where the impact of the low-frequency ripple is less significant.

2.4.1.1.C Maximum Constant Boost Control

The MCBC, as depicted in Figure 2.15, is implemented with slight modifications to the shoot-through references of the MBC. The key advantage of MCBC is maintaining a constant shoot-through duty ratio per switching cycle. This method strikes a balance between SBC and MBC, offering a higher voltage gain for the qZSI compared to SBC without introducing low-frequency ripples in the voltage and current across the impedance components [38]. In MCBC, the inverter transitions to a shoot-through zero state when the carrier triangle wave exceeds the upper shoot-through envelope or falls below the lower shoot-through envelope. While this results in slightly higher voltage stress on the devices compared to the maximum control method, and a slightly smaller voltage gain than maximum boost control, it significantly reduces voltage stress compared to simple control. Importantly, MCBC maintains a constant

shoot-through duty ratio without introducing low-frequency ripple associated with the output frequency [38]. As a consequence, the inductor and capacitor requirements for the Z-network are substantially reduced. Table 2.1 shows a comparison of the conventional carrier-based PWM methods. Note that m denotes the inverter modulation index, G_{max} is the maximum inverter gain, and $\hat{v}_{dc}/v_{in}$ represents the voltage stress on the inverter switches.

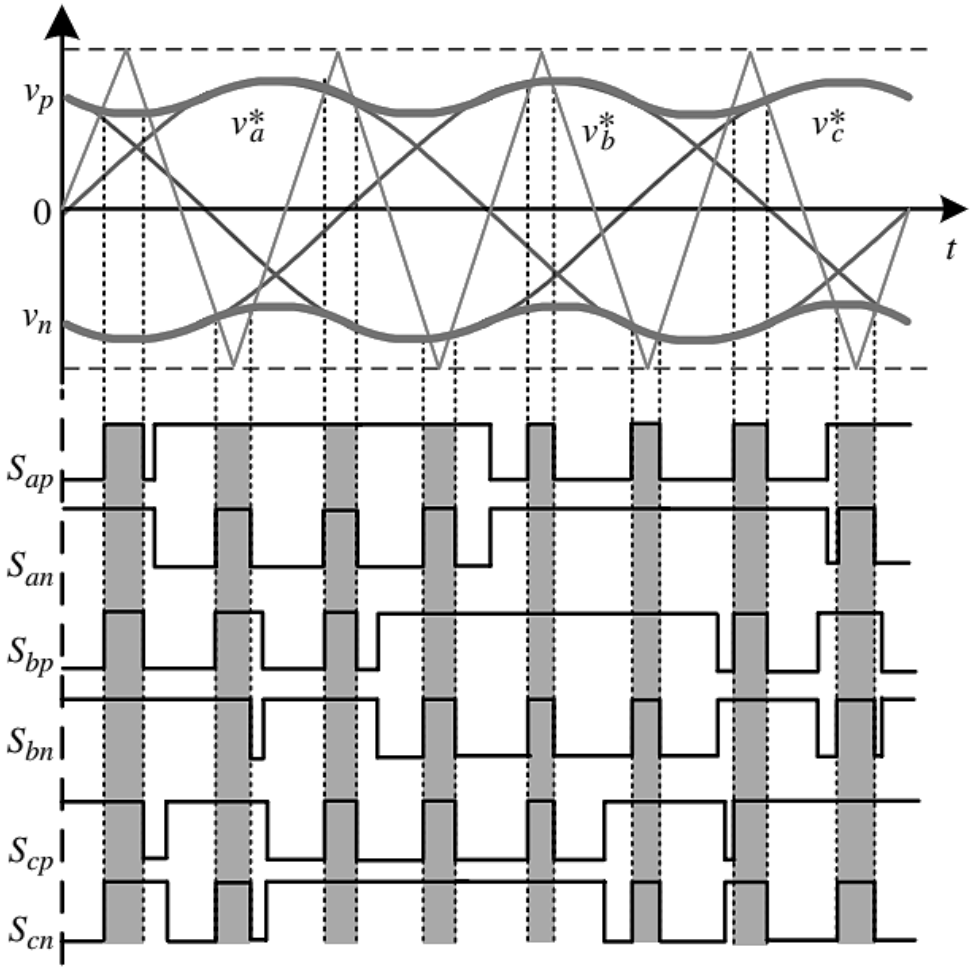

Figure 2.15: Maximum constant boost control of the qZSI.

2.4.2 Space Vector Modulations

Driven by its merits like reduced current harmonics, complete DC-link voltage utilization, and high modulation index, Space Vector Modulation (SVM) has found application in impedance source inverters [39-42]. When employing SVM in qZSIs, the shoot-through time is evenly distributed into multiple parts per the sampling interval. The literature suggests four primary ZSVM techniques:

The first technique is known as ZSVM with six insertions (ZSVM6). In this approach, the shoot-through vector is evenly divided into six parts within one sampling interval and inserted into the transition moment of switching states, as depicted in Figure 2.16(a). Consequently, only one phase-leg is short-circuited in a single switching cycle, with each

inverter leg having two shoot-through states in each cycle. Compared to traditional ZSVM, this method eliminates additional switching transitions, requires no dead time in phase legs, and maintains an invariant action time of effective vectors. These characteristics result in switching losses identical to those of conventional VSIs and increased reliability.

In the second technique, ZSVM with four insertions (SVPWM4), the shoot-through time is also divided into six parts in one sampling interval, as in ZSVM6. However, it modifies only four switching signals, as shown in Figure 2.16(b). The third method is called ZSVM with two insertions (SVPWM2). This modulation method divides the desired total shoot-through time into four parts and modifies only two switching signals, as illustrated in Figure 2.16(c).

Table 2.1: Comparison of different conventional carrier-based PWM techniques for the qZSI.

	SBC	MBC	MCBC
Maximum shoot-through duty cycle d_{max}	$1-m$	$1-\frac{3\sqrt{3}}{2\pi}m$	$1-\frac{\sqrt{3}}{2}m$
Maximum boost factor b_{max}	$\frac{1}{2m-1}$	$\frac{\pi}{3\sqrt{3}m-\pi}$	$\frac{1}{\sqrt{3}m-1}$
Maximum gain G_{max}	$\frac{m}{2m-1}$	$\frac{\pi m}{3\sqrt{3}m-\pi}$	$\frac{m}{\sqrt{3}m-1}$
Voltage stress $\hat{v}_{dc}/v_{in}$	$2G_{\max}-1$	$\frac{3\sqrt{3}G_{\max}}{\pi}-1$	$\sqrt{3}G_{\max}-1$

Finally, the ZSVM with single insertion (SVPWM1) is proposed. In comparison with traditional and previous ZSVM methods, this technique modifies only one control signal — either the upper switch of the minimum timing control signal or the lower switch of the maximum control signal. Figure 2.16(d) illustrates the switching pattern for changing the upper switch control signal.Figure 2.16: SVMs for the qZSI: switching time sequences of (a) ZSVM6, (b) ZSVM4, (c) ZSVM2, (d) ZSVM1-I.

Table *2.2* provides a comparative analysis of various ZSVM methods based on criteria such as the maximum boost factor, overall inverter gain, and voltage stress. This summary aims to offer insights into the performance of different modulation techniques.

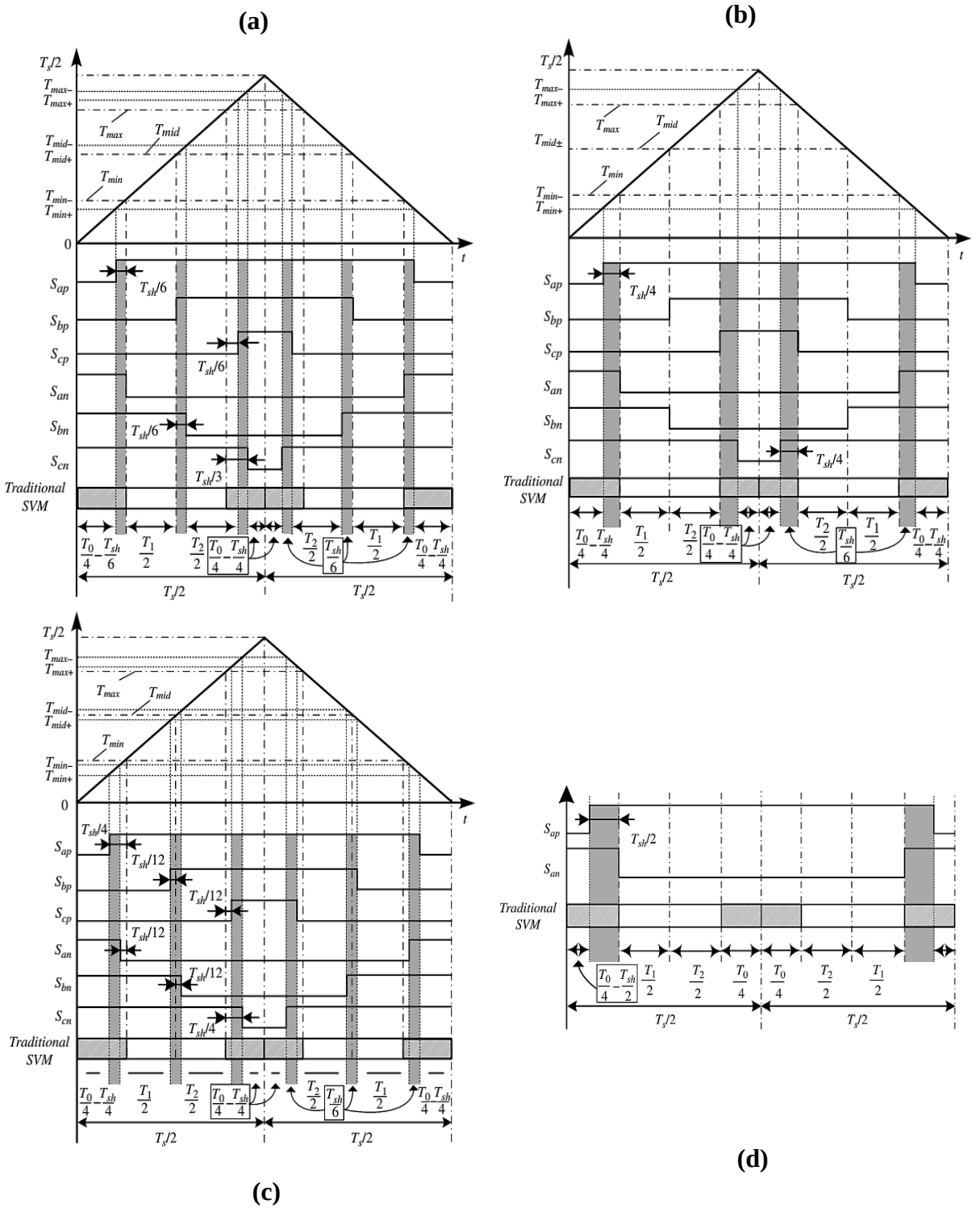

Figure 2.16: SVMs for the qZSI: switching time sequences of (a) ZSVM6, (b) ZSVM4, (c) ZSVM2, (d) ZSVM1-I.

Table 2.2: Comparison of different ZSVM techniques for the qZSI.

	ZSVM6/2	ZSVM4	ZSVM1
Maximum shoot-through duty cycle d_{max}	$1-\frac{3\sqrt{3}}{2\pi}m$	$\frac{3}{4}\left(1-\frac{3\sqrt{3}}{2\pi}m\right)$	$\frac{1}{2}\left(1-\frac{3\sqrt{3}}{2\pi}m\right)$
Maximum boost factor b_{max}	$\frac{\pi}{3\sqrt{3}m-\pi}$	$\frac{4\pi}{9\sqrt{3}m-2\pi}$	$\frac{2\pi}{3\sqrt{3}m}$
Maximum gain G_{max}	$\frac{\pi m}{3\sqrt{3}m-\pi}$	$\frac{4\pi m}{9\sqrt{3}m-2\pi}$	$\frac{2\pi}{3\sqrt{3}}$
Voltage stress $\hat{v}_{dc}/v_{in}$	$\frac{3\sqrt{3}G_{\max}}{\pi}-1$	$\frac{9\sqrt{3}G_{\max}}{2\pi}-2$	$\frac{2\pi}{3\sqrt{3}m}$

2.5 Conclusion

In summary, the chapter highlights the critical role of inverters in DG systems and emphasizes the importance of selecting suitable control algorithms and strategies to achieve optimal performance. It provides an overview of various control methods tailored for tracking the maximum power point of a PV array. Various control methods of grid-connected PV systems are reviewed, which include a specific focus on advanced control techniques such as MPC, Intelligent Controllers, and FLC. A detailed comparison of control methods across various stages is presented, emphasizing the distinction between linear and nonlinear control. It also reveals that VSI and qZSI can be controlled using the same methods, whereas qZSI requires specific control approaches tailored to its unique voltage boosting and reduction characteristics. This research enhances understanding of the challenges and opportunities in developing control strategies for energy conversion systems. These strategies aim to meet the needs of local energy networks and seamlessly integrate with the public grid.

References

[1] L. A. Barros, A. P. Martins, and J. G. Pinto, "A comprehensive review on modular multilevel converters, submodule topologies, and modulation techniques," *Energies*, vol. 15, no. 3, p. 1078, 2022.

[2] K.-J. Lee, B.-G. Park, R.-Y. Kim, and D.-S. Hyun, "Robust predictive current controller based on a disturbance estimator in a three-phase grid-connected inverter," *IEEE transactions on power electronics,* vol. 27, no. 1, pp. 276-283, 2011.

[3] M. Azab, "High performance decoupled active and reactive power control for three-phase grid-tied inverters using model predictive control," *Protection and Control of Modern Power Systems,* vol. 6, pp. 1-19, 2021.

[4] S. Tahir, J. Wang, M. H. Baloch, and G. S. Kaloi, "Digital control techniques based on voltage source inverters in renewable energy applications: A review," *Electronics,* vol. 7, no. 2, p. 18, 2018.

[5] T. Hornik and Q.-C. Zhong, "A Current-Control Strategy for Voltage-Source Inverters in Microgrids Based on $ H^{\infty} $ and Repetitive Control," *IEEE Transactions on Power Electronics,* vol. 26, no. 3, pp. 943-952, 2010.

[6] S. Yang, Q. Lei, F. Z. Peng, and Z. Qian, "A robust control scheme for grid-connected voltage-source inverters," *IEEE transactions on Industrial Electronics,* vol. 58, no. 1, pp. 202-212, 2010.

[7] Q.-C. Zhong and T. Hornik, "Cascaded current–voltage control to improve the power quality for a grid-connected inverter with a local load," *IEEE Transactions on Industrial Electronics,* vol. 60, no. 4, pp. 1344-1355, 2012.

[8] G. Zames, "Feedback and optimal sensitivity: Model reference transformations, multiplicative seminorms, and approximate inverses," *IEEE Transactions on automatic control,* vol. 26, no. 2, pp. 301-320, 1981.

[9] P. Mattavelli, G. Spiazzi, and P. Tenti, "Predictive digital control of power factor preregulators with input voltage estimation using disturbance observers," *IEEE Transactions on Power Electronics,* vol. 20, no. 1, pp. 140-147, 2005.

[10] M. Trabelsi, K. A. Ghazi, N. Al-Emadi, and L. Ben-Brahim, "An original controller design for a grid connected PV system," in *IECON 2012-38th Annual Conference on IEEE Industrial Electronics Society*, 2012: IEEE, pp. 924-929.

[11] P. Falkowski and A. Sikorski, "Finite control set model predictive control for grid-connected AC–DC converters with LCL filter," *IEEE Transactions on Industrial Electronics,* vol. 65, no. 4, pp. 2844-2852, 2017.

[12] C. Xia, T. Liu, T. Shi, and Z. Song, "A simplified finite-control-set model-predictive control for power converters," *IEEE Transactions on Industrial Informatics,* vol. 10, no. 2, pp. 991-1002, 2013.

[13] V. Yaramasu, M. Rivera, B. Wu, and J. Rodriguez, "Model predictive current control of two-level four-leg inverters—Part I: Concept, algorithm, and simulation analysis," *IEEE transactions on power electronics,* vol. 28, no. 7, pp. 3459-3468, 2012.

[14] N. Kumar, T. K. Saha, and J. Dey, "Sliding-mode control of PWM dual inverter-based grid-connected PV system: Modeling and performance analysis," *IEEE Journal of Emerging and Selected Topics in Power Electronics*, vol. 4, no. 2, pp. 435-444, 2015.

[15] H.-G. Jeong, W.-S. Kim, K.-B. Lee, B.-C. Jeong, and S.-H. Song, "A sliding-mode approach to control the active and reactive powers for a DFIG in wind turbines," in *2008 IEEE Power Electronics Specialists Conference*, 2008: IEEE, pp. 120-125.

[16] H. Özbay, S. Öncü, and M. Kesler, "SMC-DPC based active and reactive power control of grid-tied three phase inverter for PV systems," *International Journal of Hydrogen Energy*, vol. 42, no. 28, pp. 17713-17722, 2017.

[17] J. Fei and Y. Zhu, "Adaptive fuzzy sliding control of single-phase PV grid-connected inverter," *Plos one*, vol. 12, no. 8, p. e0182916, 2017.

[18] Y. Zhu and J. Fei, "Adaptive global fast terminal sliding mode control of grid-connected photovoltaic system using fuzzy neural network approach," *IEEE access*, vol. 5, pp. 9476-9484, 2017.

[19] A. O. Zué and A. Chandra, "State feedback linearization control of a grid connected photovoltaic interface with MPPT," in *2009 IEEE Electrical Power & Energy Conference (EPEC)*, 2009: IEEE, pp. 1-6.

[20] D. Lalili, A. Mellit, N. Lourci, B. Medjahed, and E. Berkouk, "Input output feedback linearization control and variable step size MPPT algorithm of a grid-connected photovoltaic inverter," *Renewable energy*, vol. 36, no. 12, pp. 3282-3291, 2011.

[21] M. A. W. Begh *et al.*, "Design of state-feedback controller for a single-phase grid-connected Siwakoti-H inverter with LCL filter," in *PCIM Europe 2019; International Exhibition and Conference for Power Electronics, Intelligent Motion, Renewable Energy and Energy Management*, 2019: VDE, pp. 1-8.

[22] M. Mahmud, H. Pota, and M. Hossain, "Nonlinear controller design for single-phase grid-connected photovoltaic systems using partial feedback linearization," in *2012 2nd Australian Control Conference*, 2012: IEEE, pp. 30-35.

[23] C. Jaen, J. Pou, R. Pindado, V. Sala, and J. Zaragoza, "A linear-quadratic regulator with integral action applied to pwm dc-dc converters," in *IECON 2006-32nd Annual Conference on IEEE Industrial Electronics*, 2006: IEEE, pp. 2280-2285.

[24] A. Shukla, A. Ghosh, and A. Joshi, "Hysteresis modulation of multilevel inverters," *IEEE transactions on power electronics*, vol. 26, no. 5, pp. 1396-1409, 2010.

[25] N. Prabhakar and M. K. Mishra, "Dynamic hysteresis current control to minimize switching for three-phase four-leg VSI topology to compensate nonlinear load," *IEEE Transactions on Power Electronics*, vol. 25, no. 8, pp. 1935-1942, 2009.

[26] F. Wu, F. Feng, L. Luo, J. Duan, and L. Sun, "Sampling period online adjusting-based hysteresis current control without band with constant switching frequency," *IEEE Transactions on Industrial Electronics,* vol. 62, no. 1, pp. 270-277, 2014.

[27] T. D. Do, V. Q. Leu, Y.-S. Choi, H. H. Choi, and J.-W. Jung, "An adaptive voltage control strategy of three-phase inverter for stand-alone distributed generation systems," *IEEE Transactions on industrial Electronics,* vol. 60, no. 12, pp. 5660-5672, 2012.

[28] F. Blaabjerg, R. Teodorescu, M. Liserre, and A. V. Timbus, "Overview of control and grid synchronization for distributed power generation systems," *IEEE Transactions on industrial electronics,* vol. 53, no. 5, pp. 1398-1409, 2006.

[29] W.-M. Lin and C.-M. Hong, "A new Elman neural network-based control algorithm for adjustable-pitch variable-speed wind-energy conversion systems," *IEEE transactions on power electronics,* vol. 26, no. 2, pp. 473-481, 2010.

[30] G. Escobar, A. A. Valdez, J. Leyva-Ramos, and P. Mattavelli, "Repetitive-based controller for a UPS inverter to compensate unbalance and harmonic distortion," *IEEE Transactions on industrial Electronics,* vol. 54, no. 1, pp. 504-510, 2007.

[31] M. H. Baloch, J. Wang, and G. S. Kaloi, "A review of the state of the art control techniques for wind energy conversion system," *International Journal of Renewable Energy Research (IJRER),* vol. 6, no. 4, pp. 1276-1295, 2016.

[32] A. M. Bouzid, J. M. Guerrero, A. Cheriti, M. Bouhamida, P. Sicard, and M. Benghanem, "A survey on control of electric power distributed generation systems for microgrid applications," *Renewable and Sustainable Energy Reviews,* vol. 44, pp. 751-766, 2015.

[33] Q. Guo, J. Wang, and H. Ma, "Frequency adaptive repetitive controller for grid-connected inverter with an all-pass infinite impulse response (IIR) filter," in *2014 IEEE 23rd International Symposium on Industrial Electronics (ISIE),* 2014: IEEE, pp. 491-496.

[34] M. Hannan, J. A. Ali, A. Mohamed, and A. Hussain, "Optimization techniques to enhance the performance of induction motor drives: A review," *Renewable and Sustainable Energy Reviews,* vol. 81, pp. 1611-1626, 2018.

[35] S. Gdaim, A. Mtibaa, and M. F. Mimouni, "Design and experimental implementation of DTC of an induction machine based on fuzzy logic control on FPGA," *IEEE transactions on fuzzy systems,* vol. 23, no. 3, pp. 644-655, 2014.

[36] F. Z. Peng, "Z-source inverter," *IEEE Transactions on industry applications,* vol. 39, no. 2, pp. 504-510, 2003.

[37] F. Z. Peng, M. Shen, and Z. Qian, "Maximum boost control of the Z-source inverter," *IEEE Transactions on power electronics,* vol. 20, no. 4, pp. 833-838, 2005.

[38] M. Shen, J. Wang, A. Joseph, F. Z. Peng, L. M. Tolbert, and D. J. Adams, "Maximum constant boost control of the Z-source inverter," in *Conference Record of the 2004 IEEE Industry Applications Conference, 2004. 39th IAS Annual Meeting.*, 2004, vol. 1: IEEE.

[39] Y. Li, J. Anderson, F. Z. Peng, and D. Liu, "Quasi-Z-source inverter for photovoltaic power generation systems," in *2009 Twenty-Fourth Annual IEEE Applied Power Electronics Conference and Exposition*, 2009: IEEE, pp. 918-924.

[40] J.-W. Jung and A. Keyhani, "Control of a fuel cell based Z-source converter," *IEEE Transactions on Energy Conversion,* vol. 22, no. 2, pp. 467-476, 2007.

[41] Y. Liu, H. Abu-Rub, B. Ge, and F. Peng, "Analysis of space vector modulations for three-phase Z-Source/quasi-Z-source inverter," in *IECON 2012-38th Annual Conference on IEEE Industrial Electronics Society*, 2012: IEEE, pp. 5268-5273.

[42] Y. Liu, B. Ge, H. Abu-Rub, and F. Z. Peng, "Overview of space vector modulations for three-phase Z-source/quasi-Z-source inverters," *IEEE Transactions on Power Electronics,* vol. 29, no. 4, pp. 2098-2108, 2013.

Chapter 3: Dual-Stage Grid-Connected Photovoltaic-Based PUC

3.1 Introduction

This chapter presents a novel grid-tied two-stage inverter topology aimed at addressing the challenges associated with conventional control strategies and achieving high-performance power conversion from PV sources. The proposed topology comprises a high-gain DC-DC converter [1] and a 7 level packed U cells (7L-PUC) inverter interconnected with the grid. Both components are meticulously controlled by the Finite Control Set Model Predictive Control (FCS-MPC) strategy, which offers enhanced dynamic response and grid synchronization capabilities.

To harness the maximum power output from the PV array, we employ an IncCon based MPPT algorithm. Despite its simplicity, the IncCon algorithm exhibits commendable performance in tracking the maximum power point under varying environmental conditions. The IncCon algorithm is responsible for generating the photocurrent reference, which is then adjusted using the FCS-MPC strategy for high-gain DC-DC converter control, ensuring optimal power transfer from the PV array to the inverter.

One of the key contributions of this chapter lies in addressing the challenges associated with controlling the DC-link voltage in multistage inverter systems. Conventional control strategies often fail to maintain stable DC-link voltage, leading to suboptimal performance and potential grid instability [2, 3]. To overcome this limitation, we propose a novel DC-link control scheme that leverages the active power equation derived from the PV panels and the power injected into the grid. This approach not only ensures high dynamic performance but also

facilitates precise DC-link voltage regulation, maintaining it at a reference voltage exceeding the peak value of the grid current.

The efficacy of the proposed topology and control strategies is validated through comprehensive simulation studies and real-time implementation results. By analyzing the simulation and experimental data, we demonstrate the superior performance of the proposed system in terms of power conversion efficiency, grid synchronization, and DC-link voltage regulation. Moreover, we discuss the practical implications and potential applications of the proposed approach in real-time grid-tied PV systems.

3.2 System describing and modeling

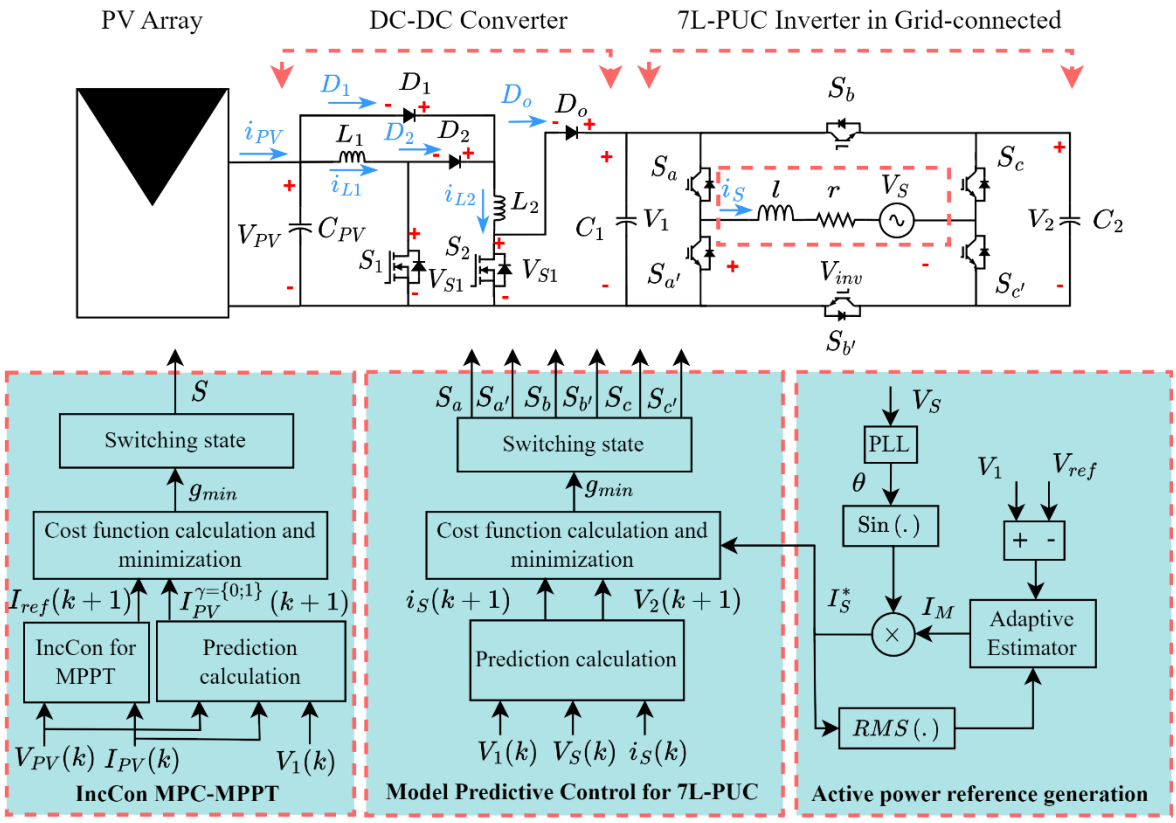

Figure 3.1: Proposed power electronic interface system overview.

3.2.1 DC-DC converter with high gain

The high-gain DC-DC converter proposed in [1] was used in this study, because it has a high boost ratio with relatively low voltage stress on its diodes and switches compared to other similar topologies. As shown in Figure 3.1, the converter is composed of two power switches, three diodes, an output capacitor and two inductors. The converter has two operating intervals depending on the state of the switches (γ = 0 or 1), as shown in Figure 3.2.

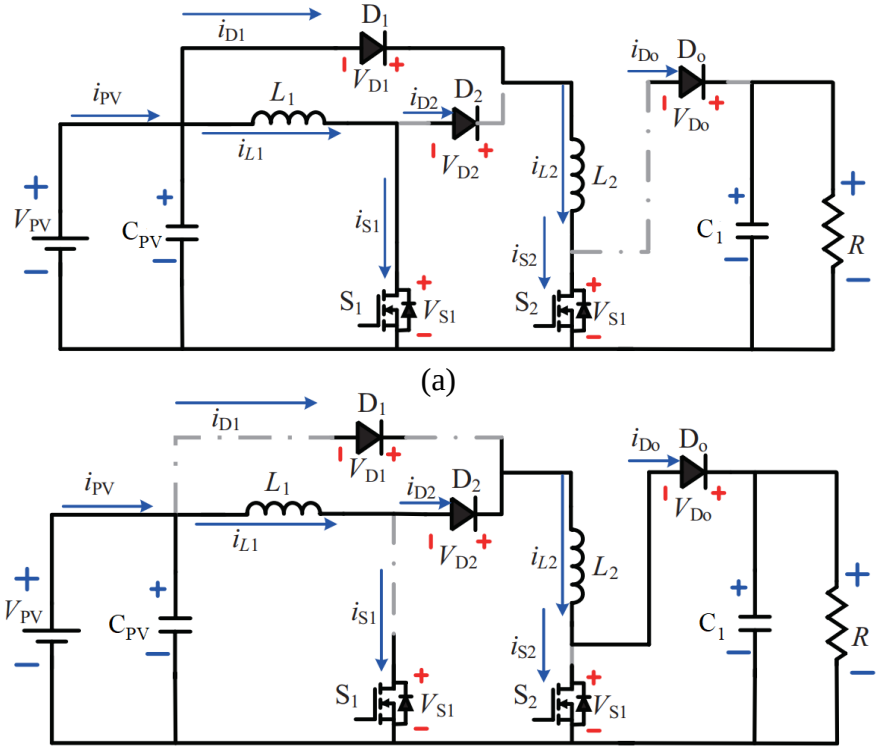

Figure 3.2: Operation analysis of the high DC-DC converter: (a) two switches ON, (b) two switches OFF.

- **Switch ON (γ =1):** When triggered by a high pulse signal, both switches are activated. As illustrated in Figure 3.2 (a), once the switches are turned on, diodes D_2 and D_o are blocked. Therefore, inductances L_1 and L_2 are charged from the DC source. The equations 3.1) describing this operating interval are given as follows:

$$\begin{cases} V_{L1}(t) = V_{PV} \\ I_{PV} = C_{PV}\dfrac{dV_{PV}}{dt} + 2I_{L1} \\ V_{L2}(t) = V_{PV} \\ C_1\dfrac{dV_1}{dt} = I_{C1} = -V_1/R \end{cases} \qquad 3.1)$$

- **Switch OFF (γ =0):** Both switches are triggered with a low pulse signal, and consequently, they are turned off. As seen in Figure 3.2 (b), once the switches are open, diodes D_2 and D_o become conductive to provide a path for inductance currents, and diode D_1 is then blocked. Therefore, inductances L_1 and L_2 return their energy in series to the output capacitor. The equations (3.2) describing this operating interval are as follows:

$$\begin{cases} V_{L1}(t) = V_{L2}(t) = \left(\frac{V_{PV} - V_O}{2}\right) \\ I_{PV} = C_{PV}\frac{dV_{PV}}{dt} + I_{L1} \\ C_1\frac{dV_1}{dt} = I_{C1} = I_{L1} - V_1/R \end{cases} \quad (3.2)$$

3.2.2 MPC-MPPT algorithm

The adopted control algorithm, known as MPC-MPPT, is based on the fusion of the predictive and MPPT controls. This command was based on a limited number of linear models. Each pattern corresponds to a specific switching state. Each switching state was pre C_1 dicted using FCS-MPC, and the state with the lowest error was generated and applied to the circuit after the minimization process using the cost function [4, 5].

Owing to the operation in the continuous conduction mode for the converter, there are only two operating intervals. Therefore, using the Euler forward approximation, a predictive model for the DC-DC boost converter proposed in [1] is constructed, and ${I_{PV}}^1(k+1)$ (for state γ = 1) and ${I_{PV}}^0(k+1)$ (for state γ = 0) can be stated by Eqs. (3.3) and (3.4) respectively (where T_s is the sampling time).

$${I_{PV}}^1(k+1) = {I_{PV}}^1(k) + \frac{2T_S}{L}V_{PV}(k) \quad (3.3)$$

$${I_{PV}}^0(k+1) = {I_{PV}}^0(k) + \frac{T_S}{2L}(V_{PV}(k) - V_1) \quad (3.4)$$

While V_1 is the DC-link voltage, I_{PV} and V_{PV} are the PV panel current and voltage, respectively.

The final phase of the MPC command involves optimizing potential future states and choosing the state that produces the minimum error. The optimization is performed using the cost function described by Eq. (3.5):

$$g^{\gamma=\{0,1\}} = \left|I_{ref} - I_{PV}^{\gamma}\right| \quad (3.5)$$

Where g and I_{ref} are the cost function and reference current, respectively. The incremental conductance algorithm employed in the MPC algorithm, produces I_{ref}, as shown in Figure 3.3, where Δ*I* in the figure represents the fixed size of the perturbation step.

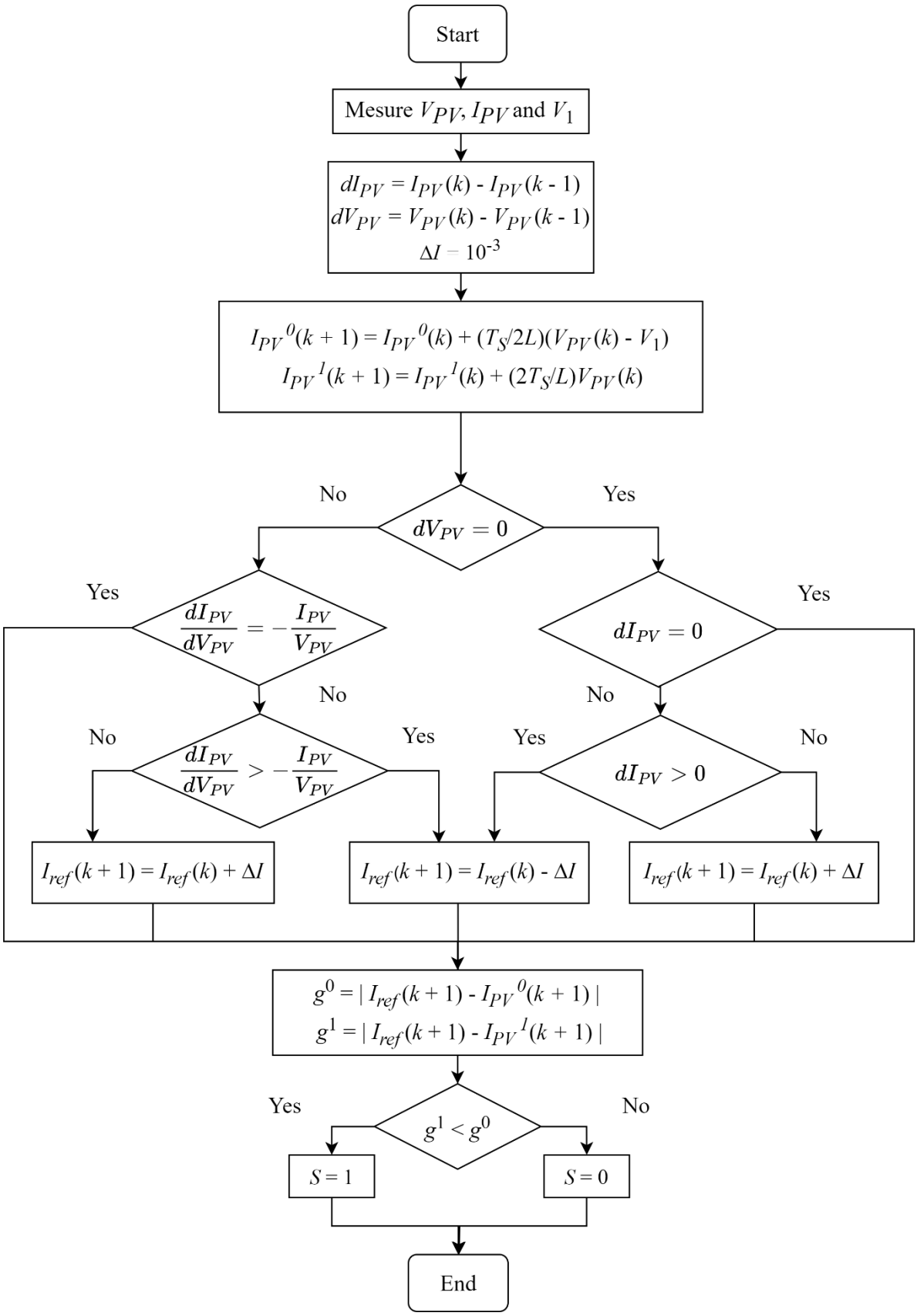

Figure 3.3: Flowchart of MPC-MPPT control.

3.2.3 Grid-tied PUC inverter

With grid-tied PV systems, more money can be saved when the PV system equipment is cheaper with higher efficiency and lower installation cost. As a result, these systems are typically less expensive and easier to install [6]. The latter converters depend on inverters to control the current and voltage supplied by the DC-DC converters, which are in turn supplied by the PV panels. Al-Haddad introduced the PUC inverter in 2011 [7] and Vahedi developed it in 2015 [4, 7]. It can be utilized as a three-phase or single-phase inverter. Figure 3.1 show the general layout of a grid-tied PUC inverter, where the PUC is connected to the grid by a line filter (inductor (l) with parametric resistance (r)).

The 7L- PUC is composed of a DC voltage source, capacitor and six power switches: S_a, S_b, S_c, S_a', S_b' and S_c'. The switches S_x and S_x' (x= a, b, c) are complementary, and the source of DC voltage is V_1 and another DC source is V_2 (capacitor). Third of the difference between V_1 and V_2 is used to create seven output voltage levels. Therefore, the waveform of the output voltage V_{inv} is created of the voltage levels of 0, E, 2E, and 3E if V_1=3V_2=3E. Table 3.1 lists the different switching states and V_{inv} values.

Table 3.1: 7L-PUC inverter switching states.

States	Sa	Sb	Sc	V_{inv}	Value (V_{inv})
1	0	0	0	0	0
2	0	0	1	$-V_2$	-E
3	0	1	0	V_2-V_1	-2E
4	0	1	1	$-V_1$	-3E
5	1	0	0	V_1	+3E
6	1	0	1	V_1-V_2	+2E
7	1	1	0	V_2	+E
8	1	1	1	0	0

3.2.4 Model predictive control of 7L-PUC

For the PUC topology, many control techniques have been applied to it, including MPC control technique. Due to its simplicity and ease of use, FCS-MPC is among the most promising control techniques, and can accurately track and respond quickly and dynamically [8-10]. MPC measures the variable x(k) and uses predictive control to determine the future value x (k + 1) for each potential switching state. After that, the predicted value x (k + 1) and reference value

x*(k + 1) are used to determine the cost function. The best switching state is ultimately selected for the cost function's minimum value, and this leads to an increase in the energy quality and efficiency of the system [7]. MPC is based on the measurements and equations of the system model. Capacitor voltage V_2 and grid current I_S are the two variables that need to be under control in 7L-PUC. The flowchart for the MPC applied to the 7L-PUC inverter is shown in Algorithm, as illustrated in Figure 3.1, the capacitor voltage and the grid currant are measured for each sample time k.

The voltage vector generated by the inverter is calculated using equation (3.6).

$$V_{inv} = (Sa - Sb)V_1 + (Sb - Sc)V_2 \tag{3.6}$$

Concerning the capacitor voltage,

$$i_2 = C_2 \times \frac{dV_2}{dt} = -(Sb - Sc) \times i_S \tag{3.7}$$

Using these values and forward Euler approximation, the equations $V_2(k+1)$ and $I_S(k+1)$ were predicted as

$$V_2(k+1) = V_2(k) - \frac{T_s(Sb - Sc)}{C_2} I_S(k) \tag{3.8}$$

$$I_S(k+1) = \left(1 - \frac{rT_s}{l}\right) I_S(k) + \frac{T_s}{l}(V_{inv}(k) - V_S) \tag{3.9}$$

The cost function is expressed as follows:

$$g = k_1(I_S(k+1) - I_S^*(k+1))^2 + k_2(V_2(k+1) - V_2^*(k+1))^2 \tag{3.10}$$

Where T_s denotes the sampling time. k_1, k_2 are the weighting factors, which are set experimentally and are given in Table 3.3, $I_S(k+1)$, $I_S^*(k+1)$ are the future behavior of the grid current and reference respectively, $V_2(k+1)$, $V_2^*(k+1)$ are the future behavior and reference capacitor voltage, respectively.

Algorithm 1: Adopted FCS-MPC Algorithm

1 :function ModelPredictiveControl () Sampling time at $\boldsymbol{T_s}$,Input $\boldsymbol{V_1(k)}$, $\boldsymbol{I_S(k)}$, $\boldsymbol{V_2(k)}$, $\boldsymbol{V_S(k)}$.

g_min ⇐ ∞, j_min ⇐ 0

2: *Loop-1:* Computation of predictive control and cost function

for j = 0, . . . , 7:

I_S Predictive model:

$\boldsymbol{I_S(k+1)(j)}$ ⇐ Compute from (3.9)

V_2 Predictive model:

$\boldsymbol{V_2(k+1)(j)}$ ⇐ Compute from (3.8)

Compute *g(j)***from (3.10)**

3: *Loop-2:* Minimize the cost function

if $\boldsymbol{g(j)} \leq g_$min, *then*

$g_$min ⇐ $\boldsymbol{g(j)}$, $j_$min ⇐ j

end if

end for

4: *Switching state*

Return Si (Switching state that corresponds to *j*)

end function

3.3 Reference current generation

Figure 3.1 shown a typical block diagram of the reference current generation. To control the 7L-PUC, simultaneous control of multiple quantities is required. In general, V_1, V_2, and I_S are controlled for a PUC inverter. V_1 voltage control is separated from the cost function, to provide a simpler predictive controller and to facilitate the tuning of the weighting function. In this study, we proposed a control for voltage V_1, which is based on the active power equation provided by the PV panels and the active power injected into the grid.

When a DC-link controller is applied, the DC-link voltage response is divided into two states: the transient and steady-state responses. Two parameters feature the transient state: the settling time and overshoot with the required value, whereas the steady-state phase is featured by only one parameter, namely, the steady-state error. These three parameters must be minimized to ensure the speed and efficiency of the DC-link controller.

For the first stage (at the DC-DC converter and PV panel set), the active power can be expressed by Eqs. (3.11) and (3.12), depending on whether the losses are negligible.

$$P_{dc_{ideal}} = I_{PV}V_{PV} = I_1V_1 \tag{3.11}$$

$$P_{dc_{real}} = P_{dc_{ideal}} - P_{loss} = I_{PV}V_{PV} - P_{loss} \tag{3.12}$$

Where $P_{dcideal}$, P_{dcreal} and P_{loss} represent ideal power, real power and losses respectively.

The expressions of the current and grid voltage are given by Eqs. (3.13):

$$\begin{cases} I_S(t) = I\sqrt{2}\,sin(wt-\varphi) \\ V_S(t) = V\sqrt{2}sin(wt) \end{cases} \quad (3.13)$$

Where φ is the phase angle, while V and I are the RMS values of grid voltage and current, respectively.

For the second stage, at the PUC7 inverter output, the instantaneous power $P_{ac}(t)$ can be expressed in terms of grid voltage and current, as in Eq. (3.14).

$$P_{ac}(t) = IVcos(\varphi) + IVcos(2wt-\varphi) \quad (3.14)$$

As shown in (3.14), $P_{ac}(t)$ is composed of the average value P_o, Eq. (3.15), and double-frequency ripple power P_r, Eq. (3.16),

$$P_o = IVcos(\varphi) \quad (3.15)$$

$$P_r = IVcos(2wt-\varphi) \quad (3.16)$$

When power factor is 1, meaning there is no phase shift, this instantaneous power could be written as in Eq. (3.17):

$$P_{ac}(t) = IV + IVcos(2wt) = P_o + P_o cos(2wt) \quad (3.17)$$

The average value of the instantaneous power P_o is equal to the power P_{dc},

$$\begin{cases} P_o = P_{dc} \\ I_{PV}V_{PV} = IV \end{cases} \quad (3.18)$$

The purpose of the DC-link controller is to estimate the reference grid current and stabilize the DC-link voltage V_1 at the reference voltage value V_{ref}. In this paper, we propose deducing the RMS value of the grid current from Eqs. (3.12) and (3.18), to stabilize the voltage V_1 at V_{ref} and then reduce the tracking error. Eq. (3.12), can be rewritten as Eq. (3.19)

$$\frac{P_{dc_{real}}}{V} = \frac{P_{dc_{ideal}} - P_{loss}}{V} \quad (3.19)$$

Then Eq. (3.19) can be expressed in terms of the reference current, as shown in Eq. (3.20),

$$I_{ref} = I_{ref\_ideal} - I_{ref\_loss} \quad (3.20)$$

Where the current I_{ref_ideal} may be expressed by Eqs. (3.21) and (3.22).

$$I_{ref\_ideal} = \frac{P_{dc_{ideal}}}{V} = \frac{I_1 V_1}{V} \quad (3.21)$$

$$I_{ref\_ideal} = \frac{P_{dc_{ideal}}}{V} = \frac{I_{PV}V_{PV}}{V} \tag{3.22}$$

To control the DC-link voltage, the ideal reference current $I_{\text{ref\_ideal}}$ must be expressed by the actual voltage V_1 and the reference voltage V_{ref}. So, from Eqs. (3.21) and (3.22), the ideal reference current is expressed as Eq. (3.23),

$$I_1 = \frac{I_{PV}V_{PV}}{V_{ref}} \tag{3.23}$$

By substituting Eq. (3.23) in Eq. (3.21), I_{ref_ideal} can be expressed using Eq. (3.24):

$$I_{ref\_ideal} = \frac{I_{PV}V_{PV}V_1}{V_{ref}V} \tag{3.24}$$

Similarly, using Eq. (3.20), the current I_{ref_loss} can be expressed as Eq. (3.25)

$$I_{ref\_loss} = I_{ref\_ideal} - I^* \tag{3.25}$$

Where I^* is the RMS value of reference grid current.

By substituting Eq. (3.22) in Eq. (3.25), the expression for the current I_{ref_loss} is obtained using Eq. (3.26):

$$I_{ref\_loss} = \frac{I_{PV}V_{PV}}{V} - I^* \tag{3.26}$$

By substituting Eqs. (3.25), (3.24), (3.26) and (3.22) in Eq. (3.20), the final expression for the reference current is given by Eq. (3.27) as follows:

$$I_{ref} = (V_1 - V_{ref})\frac{I_{PV}V_{PV}}{V_{ref}V} + I^* \tag{3.27}$$

Eq. (3.27) is valid for the steady state, making it possible to guarantee the estimation of the current injected into the grid, as well as the balance of voltage V_1 with the reference voltage V_{ref} and zero stability error. With regard to the transient state, in this paper, a method is proposed to reduce the response time and overshoot of the voltage V_1 for the required V_{ref} value, which is achieved by determining the minimum and maximum RMS values of the reference current from the variation of the capacitor C_1 voltage as proposed in [11], which is as follows.

$$C_1 = \frac{P}{2\pi f V_1 \Delta V_1} \tag{3.28}$$

Where ΔV_1 is the peak-to-peak capacitor voltage variation and f is the grid frequency. The amplitude of ΔV_1 is given by:

$$\Delta V_{1\_peak} = \frac{I_{PV} V_{PV}}{4\pi f V_1 C_1} \tag{3.29}$$

Considering the amplitude of the reference current variation ΔI_{ref_peak}, from Eqs. (3.11), (3.18) and (3.29), we get its expression which is given by Eq. (3.30):

$$\Delta I_{ref\_peak} = \frac{(I_{PV} V_{PV})^2}{4\pi f V {V_1}^2 C_1} \tag{3.30}$$

By Eqs. (3.27) and (3.30), the final expression for the maximum and minimum values of the RMS reference current are given by Eq. (3.31) as follows:

$$\begin{cases} I_{MAX} = \left| I_{ref} + \Delta I_{ref\_peak} \right| \\ I_{MIN} = \left| I_{ref} - \Delta I_{ref\_peak} \right| \end{cases} \tag{3.31}$$

Figure 3.4 represents the adaptive reference current estimator proposed to reduce the response time and overshoot of the DC-link voltage.

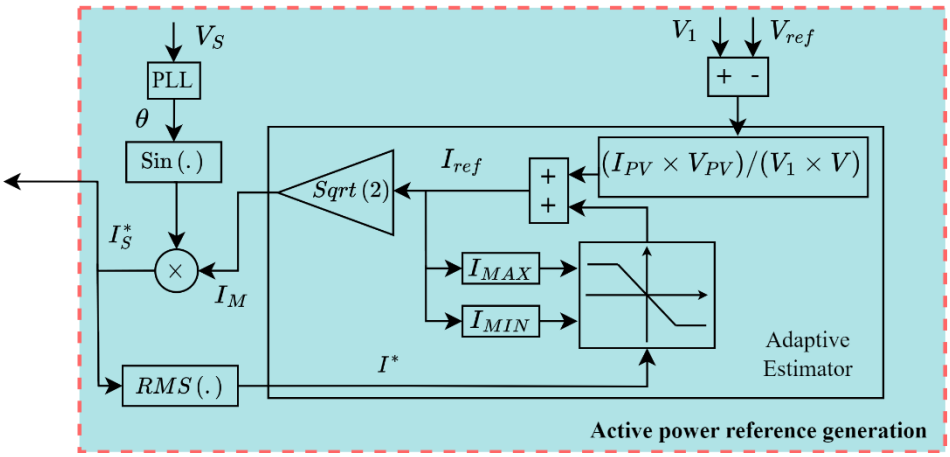

Figure 3.4: Adaptive estimator block.

3.4 Simulation outcomes and discussion

The MATLAB/Simulink offers a flexible platform to validate the entire and underlying performances of the designed systems. The proposed design inverter, composed of a BP SX120 photovoltaic module to create a photovoltaic array by connecting three panels in parallel and two in series, a boost converter and single-phase 7L-PUC inverter connected to the grid with FCS-MPC control, was simulated on the MATLAB/Simulink platform to verify its robustness and effectiveness. Table 3.2 lists the system parameters used in this study. It should be noted that $T_s = 15\ \mu s$ was the sampling time.

The simulation results of the steady state operation are presented in Figure 3.5. In Figure 3.5 (a), (b) and (c), the effectiveness of the MPC-MPPT algorithm that controls the converter to operate at the MPP has been shown to be incorporated into reference current generation. Where we note the accuracy and speed of reaching the maximum value of voltage V_{MP} and current I_{MP} , thus reaching the maximum power of photovoltaic panels P_{MPP} with high efficiency and excellent quality. The fully conditioned voltage balancing is also demonstrated in Figure 3.5 (d) by the proposed DC-link controller.

Table 3.2: Test parameters.

Parameters	Values
Voltage ($\boldsymbol{V_{MP}}$)	67.4 V
Current ($\boldsymbol{I_{MP}}$)	10.68 A
STC Power ($\boldsymbol{P_{MPP}}$)	720 W
Grid Frequency ($\boldsymbol{f_S}$)	50 Hz
DC Capacitors ($\boldsymbol{C_1}$&$\boldsymbol{C_2}$)	2000 µF
Parasitic Resistor (**r**)	0.1 Ω
Line Inductor (**l**)	2.5 mH
AC Grid Voltage ($\boldsymbol{V_S}$)	120 V
Converter Inductors ($\boldsymbol{L_1}$&$\boldsymbol{L_2}$)	3 mH
DC Voltage Reference ($\boldsymbol{V_{ref}}$)	150 V

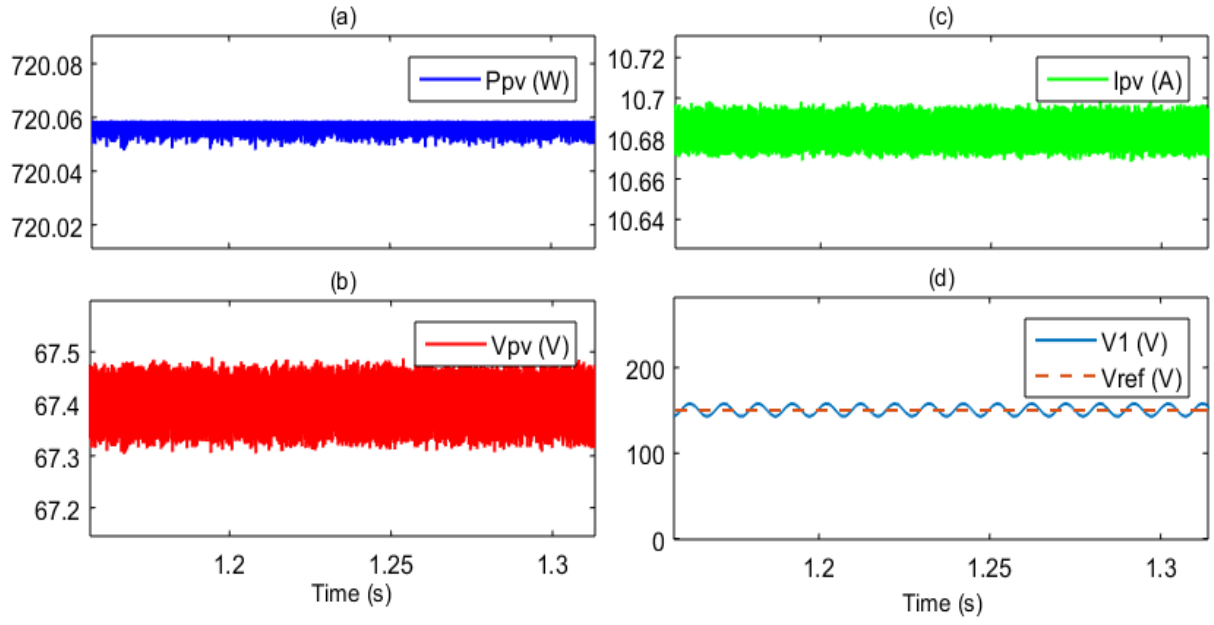

Figure 3.5: Simulation results of MPC-MPPT and active power controller proposed.

Figure 3.6 shows the starting conditions of the grid voltage and current, inverter voltage and capacitor C_2 voltage. Because the capacitor voltage increases from zero to stabilize at the required value, which is 1/3 of V_1, a start circuit is not required. 7-level output voltage is successfully produced at the PUC inverter output, and the current waveform clearly demonstrates the rapid dynamic response of the proposed controller.

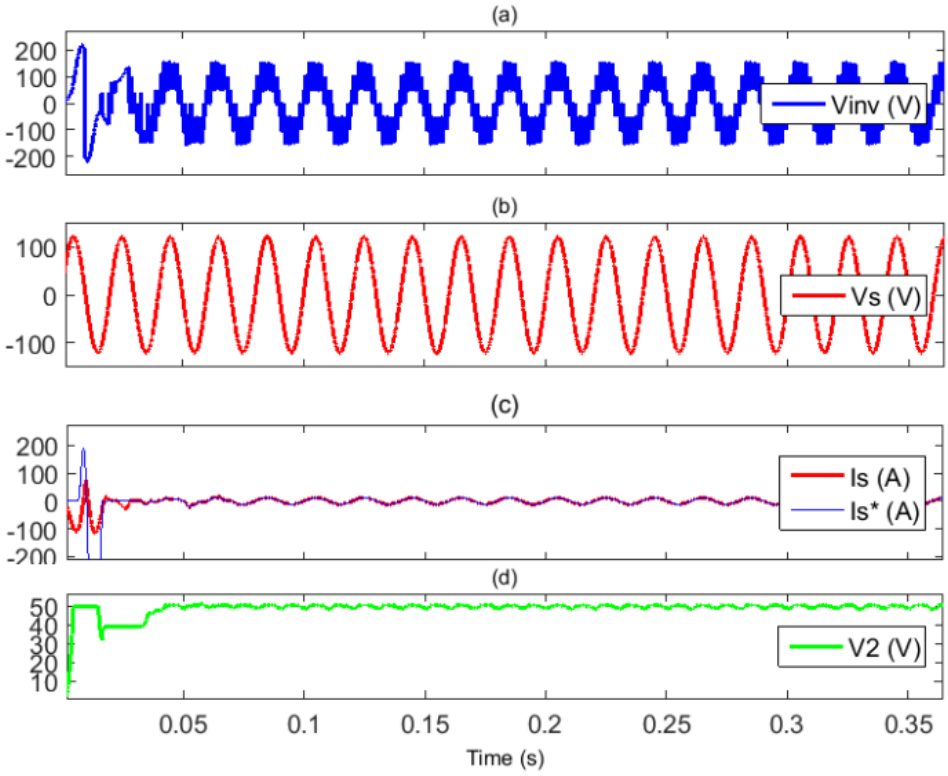

Figure 3.6: Simulation results of the grid voltage, grid current, capacitor (C_2) voltage and inverter voltage.

Figure 3.7 shows the reaction of the proposed system with an abrupt change in solar radiation from 700 W/m^2 to 1000 W/m^2 and then to 800 W/m^2. The abrupt change in radiation corresponds to a fast response and low overshoot, where the maximum overshoot is 3.76 V and the voltage V_1 reaches a steady state within 100 ms, with the perfect equilibrium voltage of capacitor V_1 as shown in Figure 3.7 (b). Consequently, the grid current changes with the change in the reference current, and quickly stabilizes at the desired value as shown in Figure 3.7 (a). The effect of an abrupt change in solar radiation for capacitor C_2 voltage and inverter voltage V_{inv} is almost insignificant, due to the accuracy and speed of response of the proposed controller, as shown by the simulation results in Figure 3.7(c) and (d).

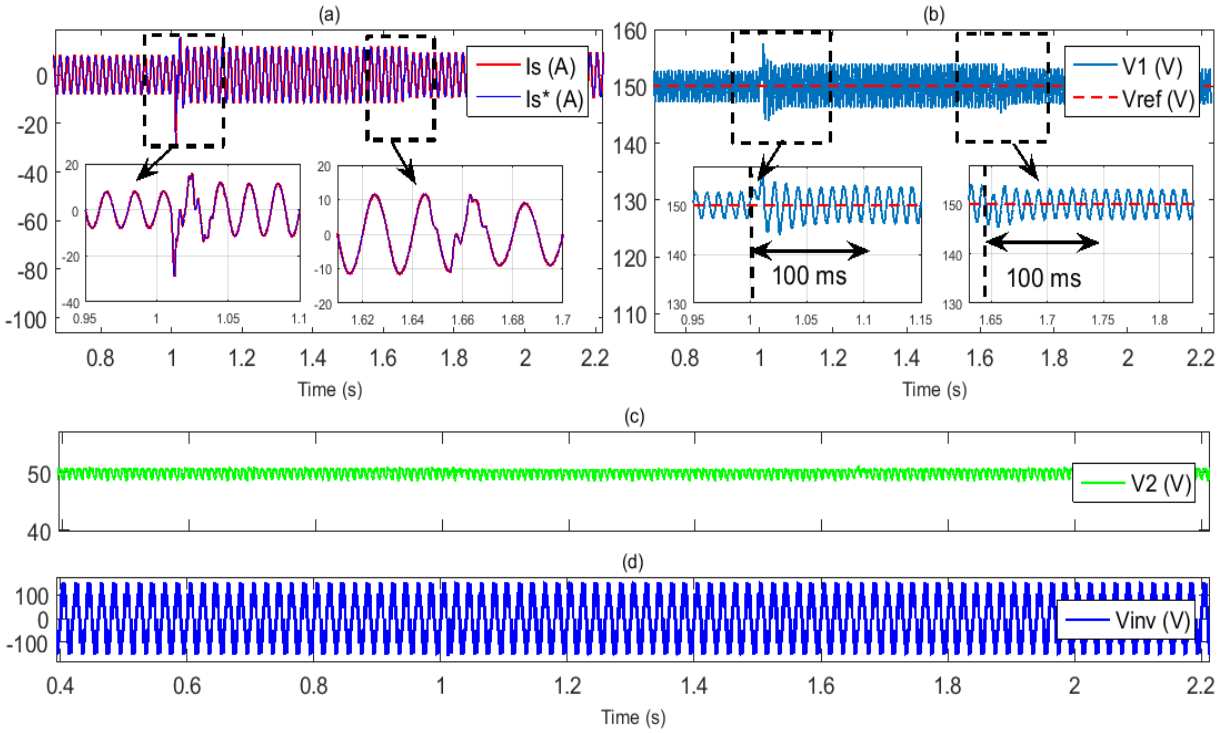

Figure 3.7: Simulation results of the proposed control for an abrupt change in solar radiation from 700 W/m^2 to 1000 W/m^2 and then to 800 W/m^2.

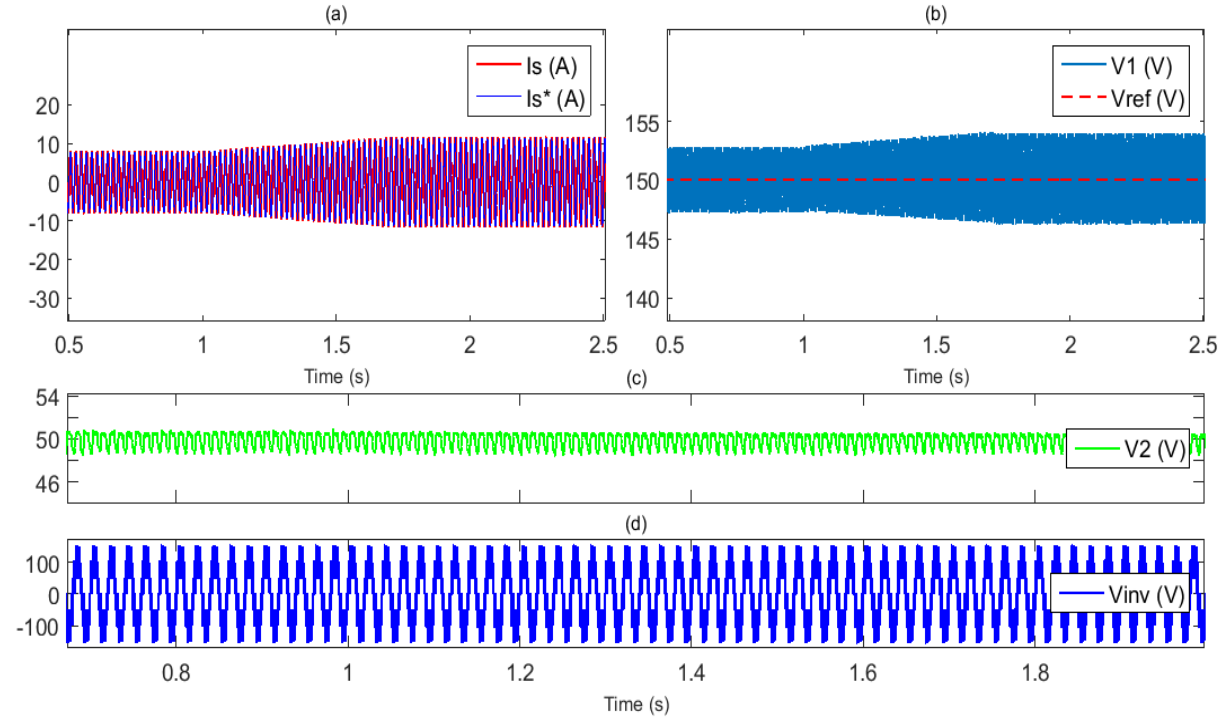

Figure 3.8: Simulation results of the proposed control for a gradual change in solar radiation from 700 W/m^2 to 1000 W/m^2.

Figure 3.8 shows the reaction of the proposed system with a gradual change in solar irradiation from 700 W/m^2 to 1000 W/m^2. The gradual change in irradiation was followed by

a gradual change in ΔV_1, and good tracking of the reference voltage V_{ref}, as shown in Figure 3.8 (b). As a result, the grid current changes with the change in the reference current and stabilizes smoothly at the desired value, as shown in Figure 3.8 (a). However, the capacitor C_2 voltage and inverter voltage V_{inv} remained almost constant, because of the good tracking accuracy of the proposed controller, as shown in Figure 3.8 (c) and (d).

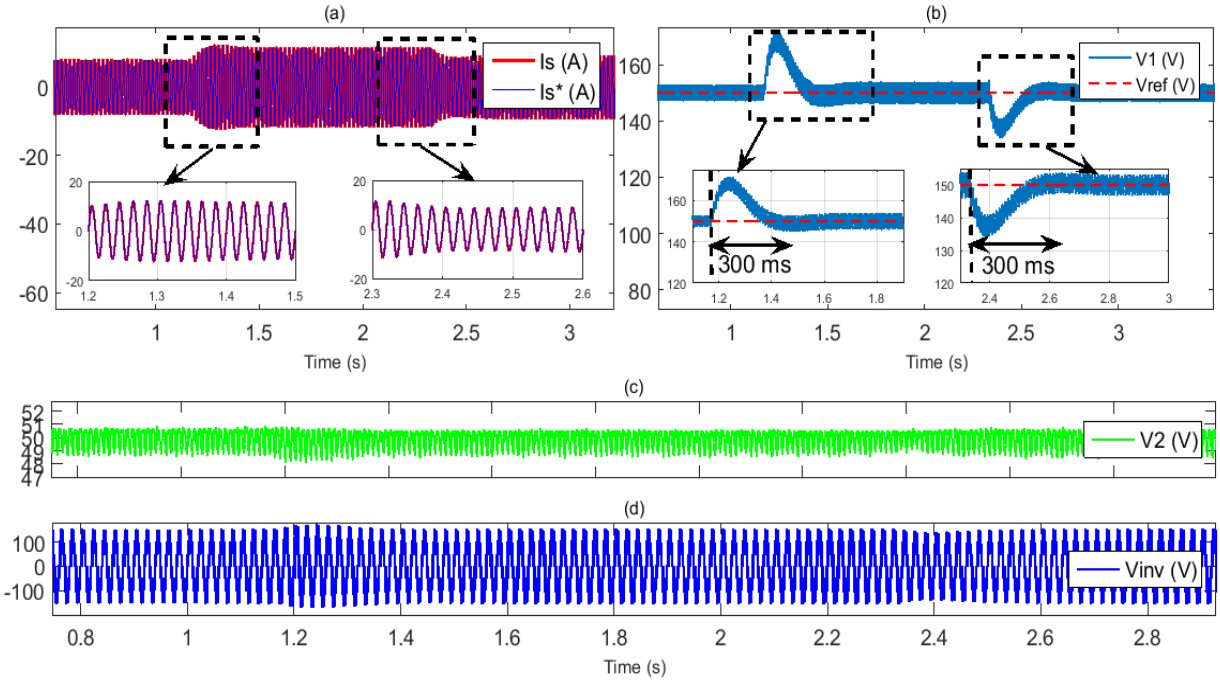

Figure 3.9: Simulation results of a PI controller for an abrupt change in solar radiation from 700 W/m^2 to 1000 W/m^2 and then to 800 W/m^2.

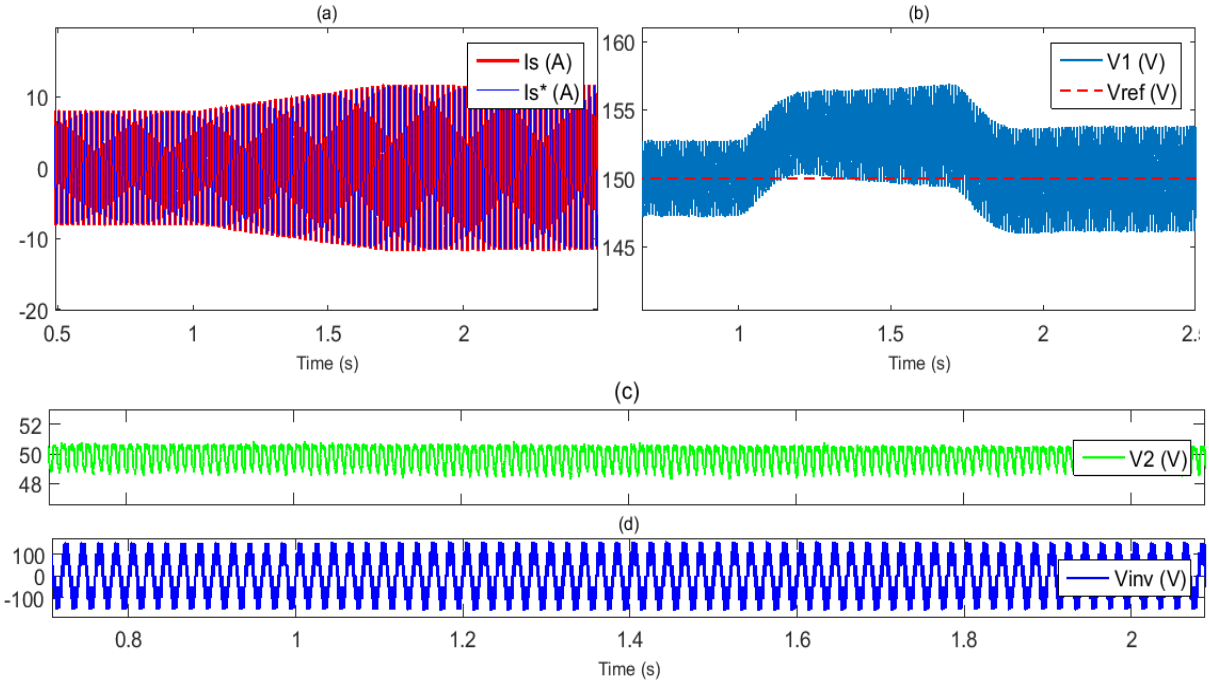

Figure 3.10: Simulation results of a PI controller for a gradual change in solar radiation from 700 W/m^2 to 1000 W/m^2.

Figure 3.9 and Figure 3.10 represent the simulation results for an abrupt and gradual change in solar irradiation respectively, by using a PI controller to regulate V_1 and estimate the reference grid current, where the parameters K_P and K_I are set experimentally and depicted in Table 3.3. In Figure 3.9 (b), we note that the maximum overshoot voltage of the capacitor C_1 is 17.43 V, with a slow response of V_1 which reaches the steady state within 300 ms. This is followed by a rise in the grid current and inverter voltage V_{inv}, as shown in Figure 3.9 (a) and (d). In Figure 3.10 (b), the capacitor voltage rises gradually with a fluctuation in tracking the reference voltage V_{ref}, and this fluctuation in the capacitor voltage negatively affects the inverter voltage and grid current, as shown in Figure 3.10 (a) and (d).

Table 3.3: Controller parameters.

Parameters	**Values**
Proportional factor $\boldsymbol{K_P}$	-0.12
Integral factor $\boldsymbol{K_I}$	-1.6
Weight factor $\boldsymbol{k_1}$	2.5
Weight factor $\boldsymbol{k_2}$	1.75

3.5 Experimental results

Experimental testing was conducted to verify the simulation results. Hardware in the loop (HIL) was used to implement the proposed system, as illustrated in Figure 3.1 utilizing a test bench based on a dSPACE 1104 control board. In the experimental stage, the parameters used in the simulation are preserved, as listed in Table 3.2, with a sampling time of 50 µs.

Figure 3.11 represents the waveforms of the grid current, grid voltage, capacitor C_1 voltage and inverter voltage, respectively. It is important to note that the sinusoidal grid current and output voltage of the seven-level inverter are in phase with the grid voltage as they are perfectly generated.

Figure 3.12 illustrates the experimental results of the proposed system for an abrupt change in solar irradiation form 700 W/m^2 to 1000 W/m^2 and then to 800 W/m^2. While Figure 3.13 depicts the results of the system for a gradual change in solar irradiation from 700 W/m^2 to 1000 W/m^2. The abrupt and gradual changes in the solar irradiation correspond to a rapid response and ideal balancing of the capacitor C_1 voltage.

Figure 3.14 and Figure 3.15 represent the experimental results of the proposed system for abrupt and gradual changes in solar irradiation, respectively, using the PI controller to regulate V_1 and estimate the reference grid current. These figures show a slow response, which

negatively affects the system in terms of capacitor C_1 voltage and grid current. This reverses the proposed controller which has proven to be highly efficient.

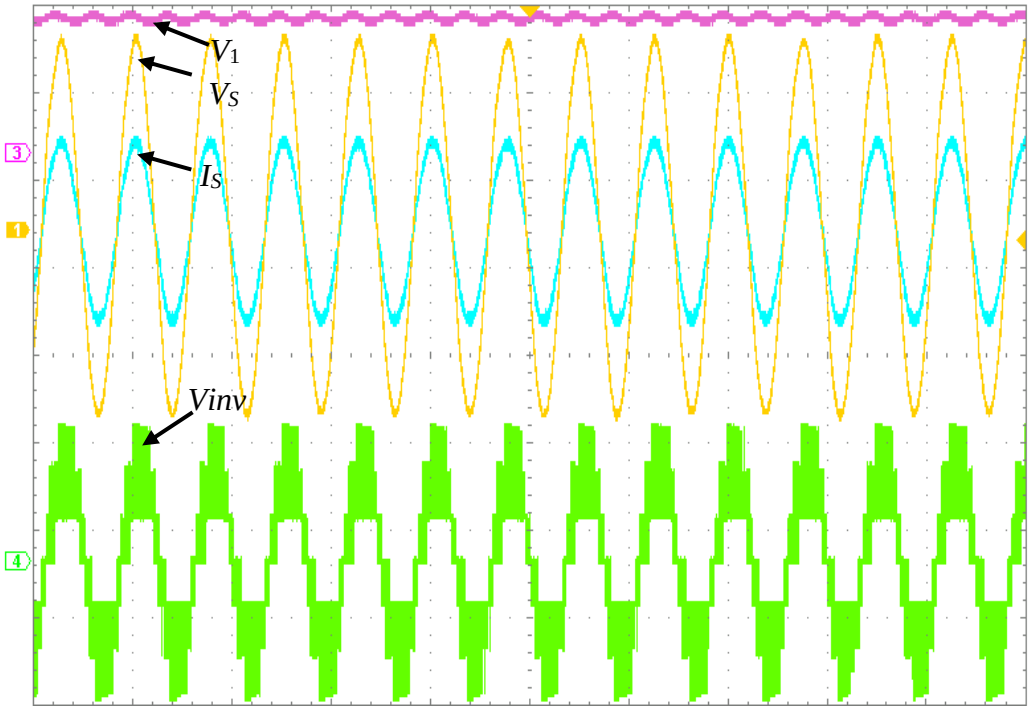

Figure 3.11: Experimental waveforms of the grid voltage, grid current, capacitor (C_2) voltage and inverter voltage.

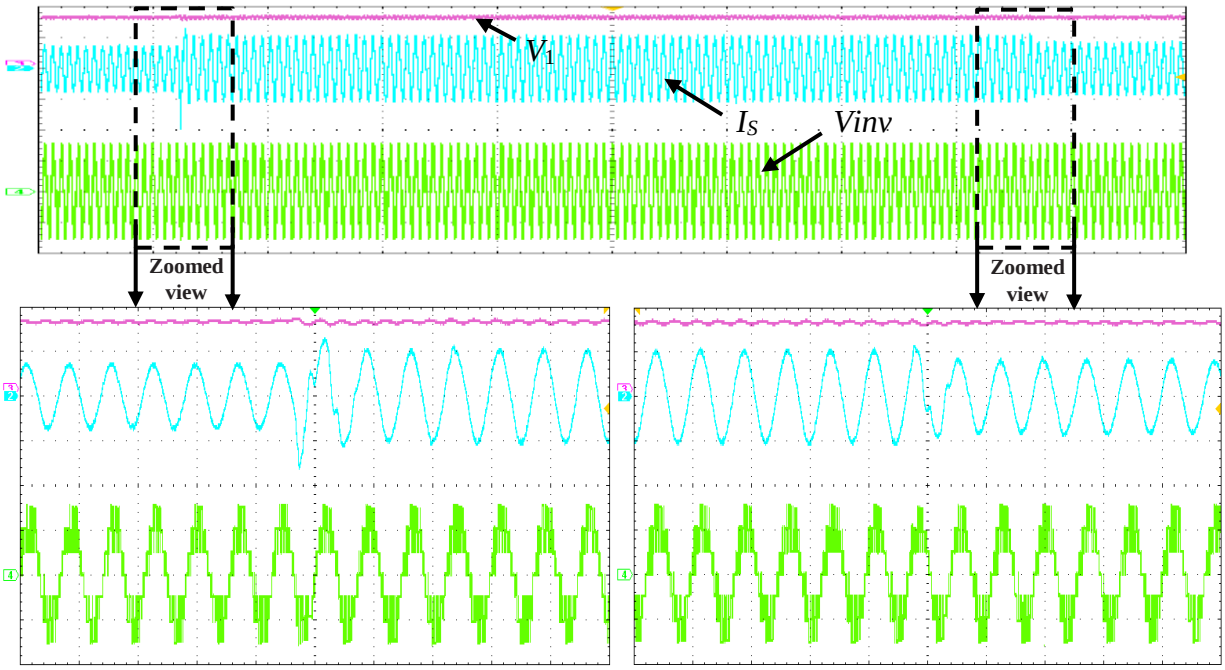

Figure 3.12: Experimental waveforms of the proposed system for an abrupt change in solar radiation from 700 W/m^2 to 1000 W/m^2 and then to 800 W/m^2.

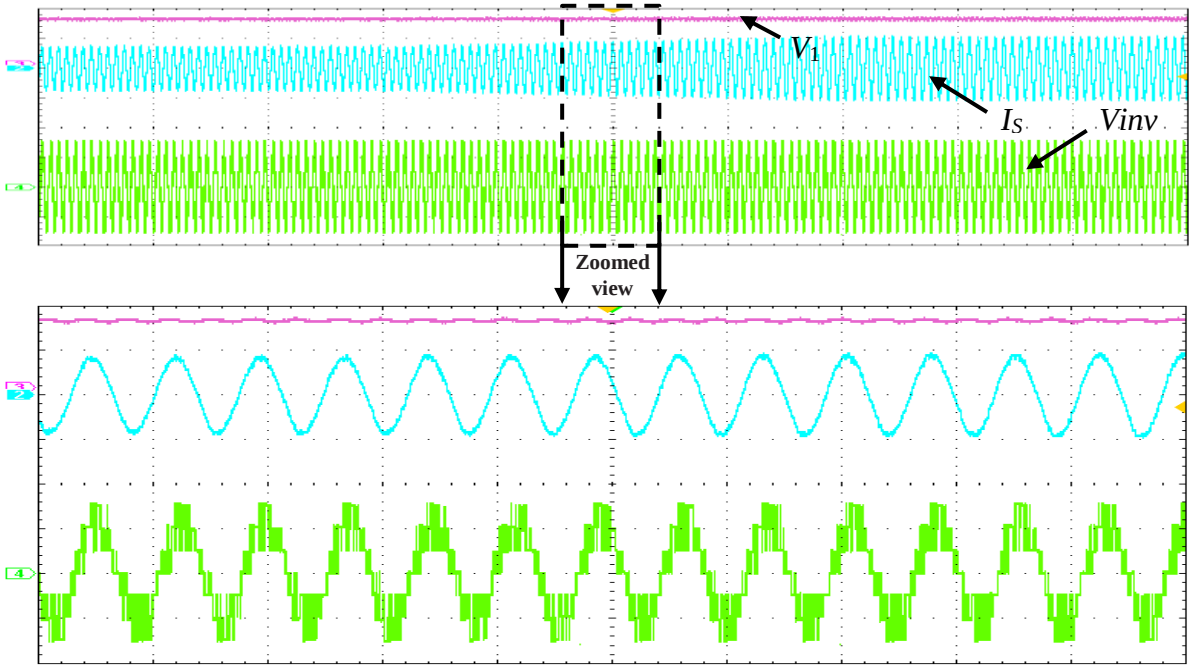

Figure 3.13: Experimental waveforms of the proposed system for a gradual change in solar radiation from 700 W/m^2 to 1000 W/m^2.

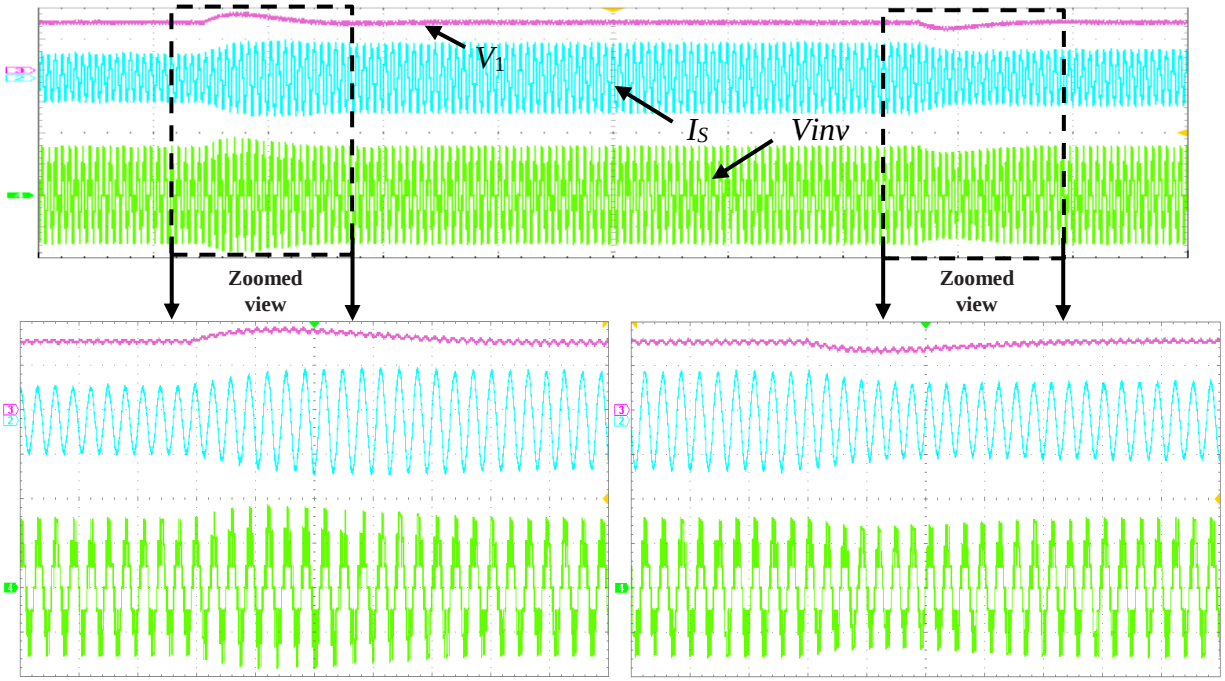

Figure 3.14: Experimental waveforms of the proposed system with PI controller for an abrupt change in solar radiation from 700W/m^2 to 1000 W/m^2 and then to 800 W/m^2.

These tests show the efficiency of the proposed active power controller on the PI controller, as it showed speed and dynamic three times larger from the PI controller in tracking the reference voltage and estimating the reference current to the grid. Achieving a low overshoot of the required value six times less, and a low content of harmonic distortion at

maximum power given by PV, as shown in Table 3.4. This proves that the injected current conforms to the IEEE standards and requirements of grid connectivity (THD less than 5%) [12].

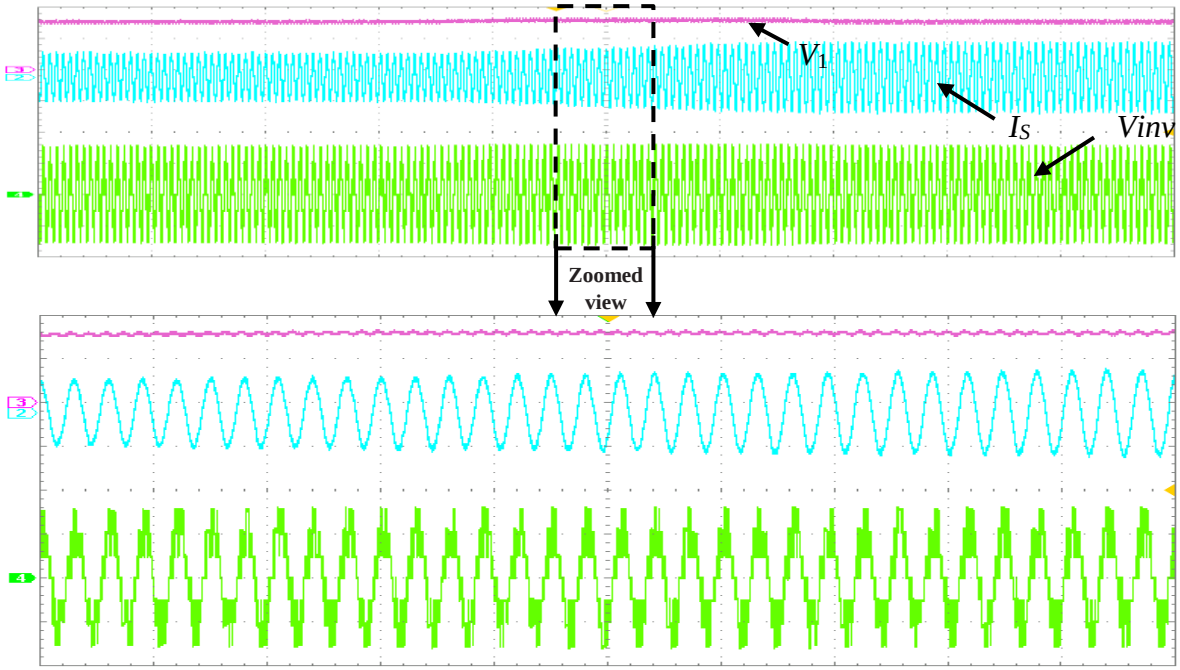

Figure 3.15: Experimental waveforms of the proposed system with PI controller for a gradual change in solar radiation from 700W/m^2 to 1000 W/m^2.

In Table 3.4, the static performance, in term of the grid current THD, and the dynamic performance, in term of the DC-link voltage overshoot, regarding the proposed predictive control and the PI control. The obtained results clearly demonstrate that the proposed controller outperforms a traditional PI controller.

Table 3.4: Static and dynamic performances.

			Maximum overshoot					
			an abrupt change				**a gradual change**	
			700 to 1000 W/m^2		**1000 to 800 W/m^2**		**700 to 1000 W/m^2**	
	Simulation THD%	**Experimental THD%**	**(V)**	**(%)**	**(V)**	**(%)**	**(V)**	**(%)**
Proposed controller	1.41	3.33	03.765	02.510	01.935	01.290	00.547	00.365
PI controller	2.02	3.75	17.430	11.620	12.84	08.560	03.270	02.180

3.6 Conclusion

In this chapter, a novel design of a two-stage grid-connected PV was proposed, using a high-gain DC-DC converter and a 7-level PUC inverter that are controlled by the MPC-MPPT and FCS-MPC, respectively. In addition, a novel DC-link voltage controller was proposed which provides an estimation of the reference current injected into the grid by the direct control of the PUC inverter power. A comparison was made between the designed controller and PI control by simulation and experimental results using a dSPACE 1104 board, where the results demonstrate good operation of the proposed design with fast response and provision of quasi sinusoidal grid current with a low THD.

References

[1] O. Abdel-Rahim and H. Wang, "A new high gain DC-DC converter with model-predictive-control based MPPT technique for photovoltaic systems," *CPSS Transactions on Power Electronics and Applications,* vol. 5, no. 2, pp. 191-200, 2020.

[2] M. Tariq, M. Meraj, A. Azeem, A. I. Maswood, A. Iqbal, and B. Chokkalingam, "Evaluation of level-shifted and phase-shifted PWM schemes for seven level single-phase packed U cell inverter," *CPSS Transactions on Power Electronics and Applications,* vol. 3, no. 3, pp. 232-242, 2018.

[3] M. Babaie, M. Sharifzadeh, H. Y. Kanaan, and K. Al-Haddad, "Switching-based optimized sliding-mode control for capacitor self-voltage balancing operation of seven-level PUC inverter," *IEEE Transactions on Industrial Electronics,* vol. 68, no. 4, pp. 3044-3057, 2020.

[4] H. Vahedi, P.-A. Labbé, and K. Al-Haddad, "Sensor-less five-level packed U-cell (PUC5) inverter operating in stand-alone and grid-connected modes," *IEEE Transactions on Industrial Informatics,* vol. 12, no. 1, pp. 361-370, 2015.

[5] M. Metry, M. B. Shadmand, R. S. Balog, and H. Abu-Rub, "MPPT of photovoltaic systems using sensorless current-based model predictive control," *IEEE Transactions on Industry Applications,* vol. 53, no. 2, pp. 1157-1167, 2016.

[6] R. Khawaja, F. Sebaaly, and H. Y. Kanaan, "Design of a 7-Level Single-Stage/Phase PUC Grid-Connected PV Inverter with FS-MPC Control," in *2020 IEEE International Conference on Industrial Technology (ICIT)*, 2020: IEEE, pp. 751-756.

[7] J. I. Metri, H. Vahedi, H. Y. Kanaan, and K. Al-Haddad, "Real-time implementation of model-predictive control on seven-level packed U-cell inverter," *IEEE Transactions on Industrial Electronics,* vol. 63, no. 7, pp. 4180-4186, 2016.

[8] A. Sahli, F. Krim, A. Laib, and B. Talbi, "Model predictive control for single phase active power filter using modified packed U-cell (MPUC5) converter," *Electric Power Systems Research,* vol. 180, p. 106139, 2020.

[9] X. Fang, X. Ding, S. Zhong, and Y. Tian, "Improved quasi-Y-source DC-DC converter for renewable energy," *CPSS transactions on Power Electronics and Applications,* vol. 4, no. 2, pp. 163-170, 2019.

[10] H. Makhamreh, M. Sleiman, O. Kükrer, and K. Al-Haddad, "Lyapunov-based model predictive control of a PUC7 grid-connected multilevel inverter," *IEEE Transactions on Industrial Electronics,* vol. 66, no. 9, pp. 7012-7021, 2018.

[11] P. T. Krein, R. S. Balog, and M. Mirjafari, "Minimum energy and capacitance requirements for single-phase inverters and rectifiers using a ripple port," *IEEE Transactions on Power Electronics,* vol. 27, no. 11, pp. 4690-4698, 2012.

[12] A. Iqbal, M. Meraj, M. Tariq, K. A. Lodi, A. I. Maswood, and S. Rahman, "Experimental investigation and comparative evaluation of standard level shifted multi-carrier modulation schemes with a constraint GA based SHE techniques for a seven-level PUC inverter," *IEEE Access,* vol. 7, pp. 100605-100617, 2019.

Chapter 4: Single-Stage Grid-Connected Photovoltaic-Based qZSI

4.1 Introduction

This chapter introduces a novel approach that combines Modulated Model Predictive Control (M^2PC) [1-3] with Fuzzy Logic Control (FLC) [4-6] to enhance the management of the qZSI duty-cycle. By integrating these techniques, we aim to leverage their respective advantages in controlling both DC and AC variables of the qZSI, thereby improving system performance and grid integration capabilities. Specifically, the DC variables are regulated using an FL control unit to enhance speed and accuracy, while the AC variables are managed by an M^2PC control unit to stabilize switching and enhance grid current quality.

What sets this approach apart is its simplicity and effectiveness. Despite the complexity of qZSI control, our method employs a reduced number of rules, making it easily implementable while maintaining high system accuracy and speed. By combining FLC and M^2PC, we exploit the complementary strengths of both techniques to achieve superior control performance in qZSI-based systems.

To validate the effectiveness of our proposed approach, extensive experimental testing has been conducted, comparing the results with those obtained using Conventional Modulated Model Predictive Control (CM^2PC) [7, 8]. The evaluation criteria include factors such as current oscillations, control speed, and grid current quality. Through rigorous testing and analysis, we aim to demonstrate the superiority of our approach in managing the qZSI duty-cycle and enhancing overall system performance.

The findings presented in this chapter not only contribute to advancing the state-of-the-art in qZSI control but also have significant implications for the broader field of power

electronics and renewable energy integration. By improving the efficiency and reliability of qZSI-based systems, our approach has the potential to accelerate the adoption of renewable energy technologies and contribute to the development of a more sustainable energy future.

4.2 Quasi-Z-Source Inverter Structure

Figure 4.1 illustrates a photovoltaic system consisting of solar panels and a qZSI converter connected to the grid. A qZSI is a type of power electronic converter that plays a crucial role in energy conversion and control systems. This innovative inverter topology is designed to overcome the limitations of traditional VSI [9] and CSI [10]. The qZSI operates by utilizing an impedance network, typically implemented using a coupled inductor and a capacitor, to provide a unique feature of voltage buck-boost capability. The qZSI consists of several key components that work together to enable its functionality. These components include two capacitors C_2 and C_1, and two inductors L_2 and L_1, where L_2=L_1=L, C_2=C_1=C.

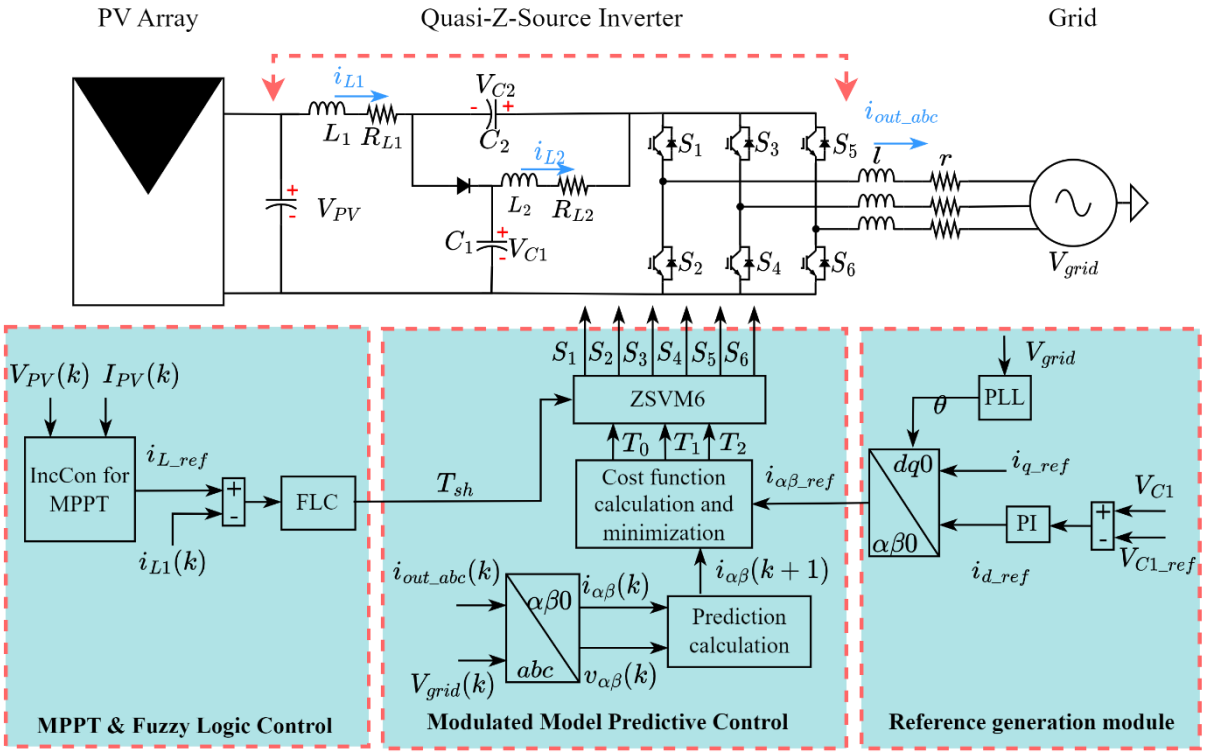

Figure 4.1: Structure and the proposed control for PV grid-connected qZSI.

The shoot-through state (ST) and the non-shoot-through state (NST) are the two operating states of the qZSI, as illustrated in Figure 4.2. When in active mode, the inverter functions similarly to a VSI, as shown in Figure 4.3 (b). In ST mode, the two switches within the same circuit leg are turned on simultaneously.

Assuming that during one switching cycle T, the interval of the shoot-through state is T_0, then the interval of the non-shoot-through state is T_1; thus, T=T_0+T_1 and the shoot-through

duty ratio $D=T_0/T$. From Figure 4.2 (a), during the interval of the non-shoot-through state T_1, we have:

$$\begin{cases} v_{L1} = L\dfrac{di_{L1}}{dt} = V_{PV} - v_{C1} \\ v_{L2} = -v_{C2} \\ V_{DC} = v_{C1} - v_{L1} = v_{C1} + v_{C2} \\ v_{diode} = 0 \end{cases} \tag{4.1}$$

where i_{L1}, v_{C1}, and V_{PV} stand for the inductor L_1 current, capacitor C_1 voltage, input voltage and, respectively. L represents the inductor's inductance.

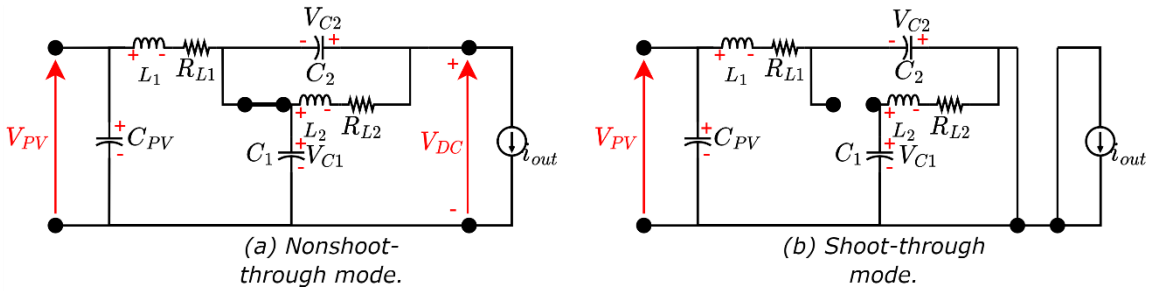

Figure 4.2: qZSI equivalent circuit.

From Figure 4.2 (b), during the interval of the shoot-through state T_0, one can get:

$$\begin{cases} v_{L1} = L\dfrac{di_{L1}}{dt} = v_{C2} + V_{PV} \\ v_{L2} = v_{C1} \\ V_{DC} = 0 \\ v_{diode} = \left(v_{C1} + v_{C2}\right) \end{cases} \tag{4.2}$$

At steady state, the average voltage of the inductors over one switching cycle is zero. From Eqs (4.1) and (4.2), we have

$$\begin{cases} v_{L1} = \overline{v}_{L1} = \dfrac{T_0\left(v_{C2} + V_{PV}\right) + T_1\left(V_{PV} - v_{C1}\right)}{T} = 0 \\ v_{L2} = \overline{v}_{L2} = \dfrac{T_0\left(v_{C1}\right) + T_1\left(-v_{C2}\right)}{T} = 0 \end{cases} \tag{4.3}$$

Thus,

$$\begin{cases} v_{C1} = \dfrac{1-D}{1-2D}V_{PV} \\ v_{C2} = \dfrac{D}{1-2D}V_{PV} \end{cases} \tag{4.4}$$

From Eq (4.4), the peak dc-link voltage across the inverter bridge is

$$V_{DC} = v_{C1} + v_{C2} = \frac{T}{T_1 - T_0} V_{PV} = \frac{1}{1-2D} V_{PV} = BV_{PV} \quad (4.5)$$

B represents the boost factor and *D* stands for the ST duty-cycle.

4.3 Proposed Controller

Considering the distinctive characteristics of qZSI, an appropriate control technique must be implemented to ensure maximum utilization of these features. This paper proposes M^{2}PC with an FLC of the ST. This combination of controls has been proposed to enhance the control quality of the Direct Current (DC) and reduce the harmonic distortion of the injected current into the grid. The suggested system's general controller concept is shown in Figure 4.1.

4.3.1 Modulated Model Predictive Control

M^{2}PC integrates an appropriate modulation scheme into minimizing the Cost Function within the MPC algorithm. In this study, a modulation scheme designed explicitly for qZSI control is implemented within the framework of M^{2}PC with SVM for the qZSI, called the ZSVM6. The ZSVM6 controller concept is shown in Figure 4.3 (a). To achieve the concept of ZSVM6, the firing times were derived by proposing an FLC, as explained in the following section. In this section, we present the method of extracting traditional time intervals for SVM by controlling the output current of the converter with an M^{2}PC.

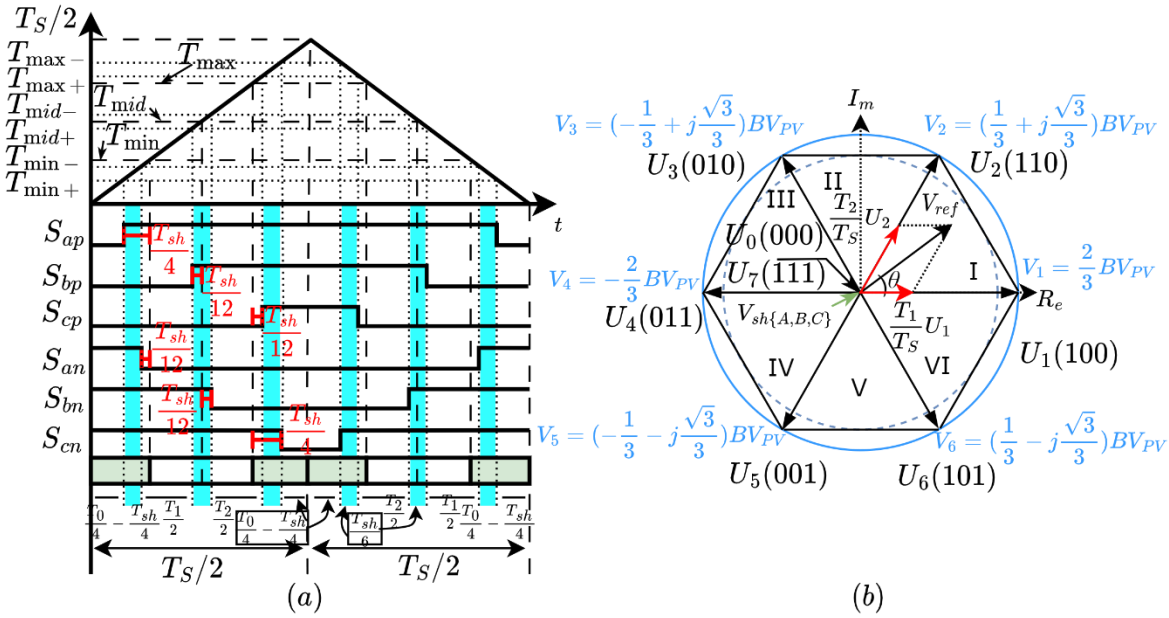

Figure 4.3: (a) ZSVM6, (b) Switching states of the qZSI.

The mathematical model utilized in this study employs the voltage vector generated by the inverter, denoted as *V*, to inject power into the grid voltage $V_{grid\_\alpha\beta}$ through an RL filter, resulting in the predictive equation for the output current. The continuous-time equation for the

inverter grid interface is represented by Eq (4.6). To make the computation more tractable, the equation is then transformed into its equivalent discrete-time expression using the forward Euler method, as provided by Eq (4.7). To further streamline the computation process, each three-phase parameter is defined within a complex frame of reference represented by ($\alpha\beta$). This approach effectively reduces the number of equations from three to one complex equation, significantly reducing the critical computation time for algorithms such as MPC.

$$V = ri + l\frac{di}{dt}V_{grid\_\alpha\beta} \tag{4.6}$$

$$i_{\alpha\beta}(k+1) = i_{\alpha\beta}(k)\left[1-\frac{r}{l}T_S\right] + \frac{T_S}{l}\left[V(k) - V_{grid\_\alpha\beta}(k)\right] \tag{4.7}$$

A cost function is formulated to achieve the control objective, which incorporates the output current of the qZSI.

$$J = \left\| i_{\alpha\beta}(k+1) - i_{\alpha\beta}(k+1)^* \right\| \tag{4.8}$$

$i_{\alpha\beta}(k+1)$ and $i_{\alpha\beta}(k+1)^*$ stands for the output and reference current of the qZSI.

The cost function is assessed for every prediction in M^{2}PC, taking into account the ST and the optimal two vectors, to determine the duty-cycles. Three dues, J_1, J_2, and J_0, are the outcome of this examination, where T_S stands for the sampling time. The following defines the corresponding duty-cycles:

$$\begin{cases} d_1 = T_S J_2 J_0 / (J_2 J_0 + J_1 J_0 + J_2 J_1) \\ d_2 = T_S J_1 J_0 / (J_2 J_0 + J_1 J_0 + J_2 J_1) \\ d_0 = T_S J_2 J_1 / (J_2 J_0 + J_1 J_0 + J_2 J_1) \end{cases} \tag{4.9}$$

Where J_1, J_2, and J_0 are the cost function of vectors (U_0, U_1 and U_2).

4.3.2 Fuzzy Logic Duty Ratio Control

In this work, a new strategy for controlling the shoot-through time of qZSI has been developed using FLC, and this is without the need for a detailed mathematical model of the system. Fuzzification, a fuzzy rule base, and defuzzification are the three components that make up the fuzzy controller. FLC has emerged as one of the best practical applications of fuzzy sets. The use of linguistic factors as opposed to numerical factors is one of its main features [11, 12]. The FLC approach is based on quality control regulations and depends on the human ability to understand the behavior of the system. This approach allows for a more intuitive and human-like control strategy, making it particularly suitable for systems with complex dynamics or uncertain environments.

The physical variables input's translation into fuzzy sets is possible through fuzzification. The variation of the error "ΔE" and the error "E" are our two inputs in this instance, and they are defined as follows:

$$E = i_{L\_ref}(n) - i_L(n) \tag{4.10}$$

$$\Delta E = E(n) - E(n-1) \tag{4.11}$$

In the elicitation step, logical connections are established between the inputs and the output, represented by their respective membership functions as depicted in Figure 4.4. These membership functions are utilized to determine the inference rules. Subsequently, a table of inference rules is constructed. Table 4.1 lists the 25 rules that make up the fuzzy D.

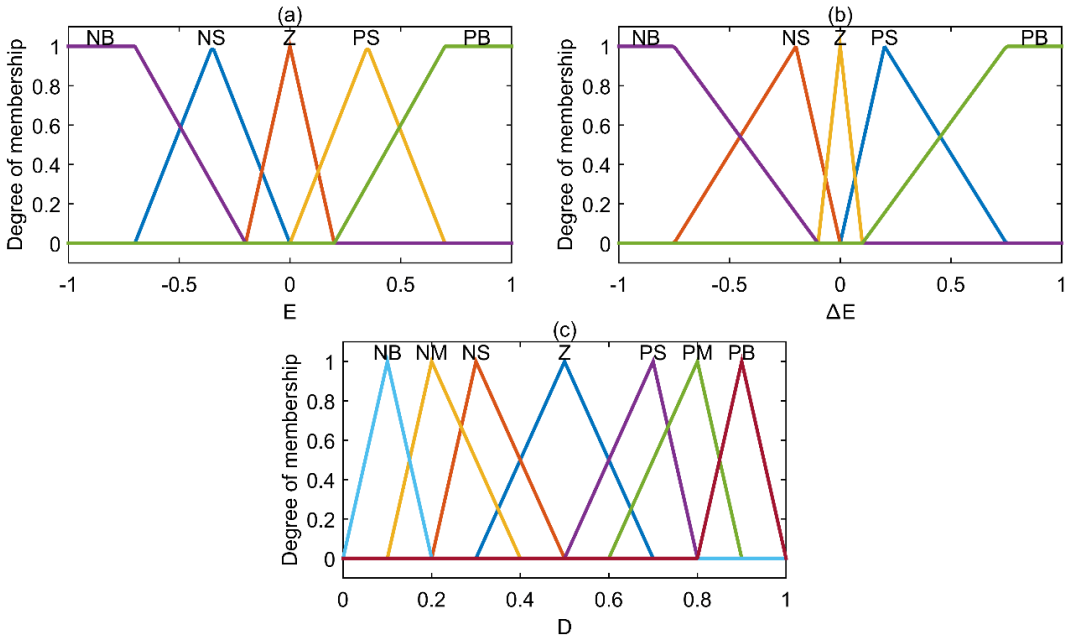

Figure 4.4: Membership function: (a) The error, (b) The variation of the error, (c) ST duty-cycle.

Table 4.1: Fuzzy Rule Base.

ΔE/E	NB	NS	Z	PS	PB
NB	Z	NM	NB	PS	PB
NS	NS	NS	NM	PS	PM
Z	NB	NS	Z	PS	PB
PS	NM	NS	PM	PS	PS
PB	NB	NS	PB	PM	Z

4.4 Simulation

The proposed control technique for the studied system has been validated and compared with CM^2PC based on the PI controller through computer simulation using "Simpower Systems" in MATLAB/Simulink®. Table 4.2 presents the main system parameters. The system is analyzed separately to monitor the MPP while also independently managing the active power injection into the grid and observing the dynamic behavior of the controlled parameters.

Table 4.2: Test parameters.

Parameters	Values
($\boldsymbol{P_{MPP}}$) STC Power	2519W
($\boldsymbol{I_{MP}}$) Current	24.90A
($\boldsymbol{V_{MP}}$) Voltage	101.16V
($\boldsymbol{V_{grid}}$) AC Grid Voltage(RMS)	60V
($\boldsymbol{f}$) Grid Frequency	50Hz
($\boldsymbol{C_1}$&$\boldsymbol{C_2}$) qZS Capacitors	4700µF
(**l**) Line Inductor	10mH
(**r**) Parasitic Resistor	0.1Ω
($\boldsymbol{L_1}$&$\boldsymbol{L_2}$) qZS Inductors	5mH
($\boldsymbol{f_s}$) Sampling Frequency	20kHz

The simulation results for the PV-side and AC-side steady-state operations are displayed in Figure 4.5 and Figure 4.6. In Figure 4.5, we observe the precision and speed at which the voltage V_{MP} and current I_{MP} reach their peak values, consequently achieving the maximum power output of PV panels P_{MPP} with remarkable quality and efficiency. As for Figure 4.6 (a), (b), and (c), they depict the steady-state

behavior of capacitor C_2 voltage, DC voltage, and grid current, respectively. The pulsating DC-link indicates the boosting operation, with the system smoothly adhering to the given instructions and exhibiting no abrupt voltage spikes in the DC-Link. This guarantees the dynamic performance of the system and adheres to the current limits of the system.

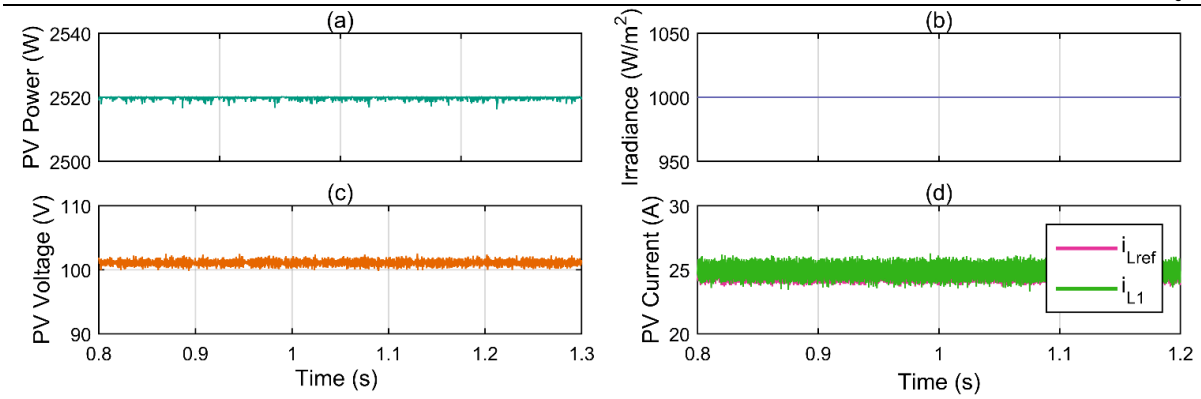

Figure 4.5: The results pertaining to the PV-side of the proposed control: (a) PV power, (b) Solar irradiance levels, (c) PV Voltage, (d) Inductance current and inductance reference current.

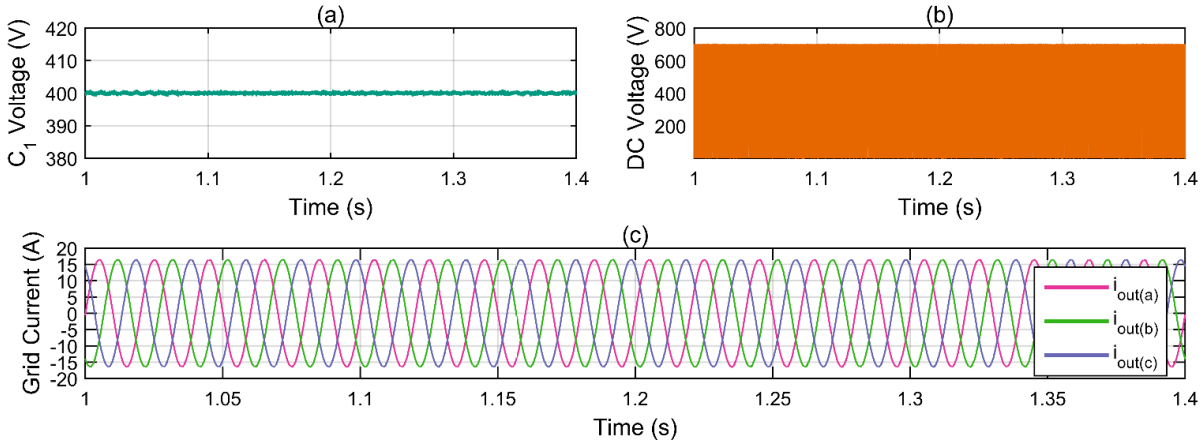

Figure 4.6: The results pertaining to the DC and AC-side of the proposed control: (a) Capacitor C_2 voltage, (b) DC voltage, (c) Three-phase grid currents.

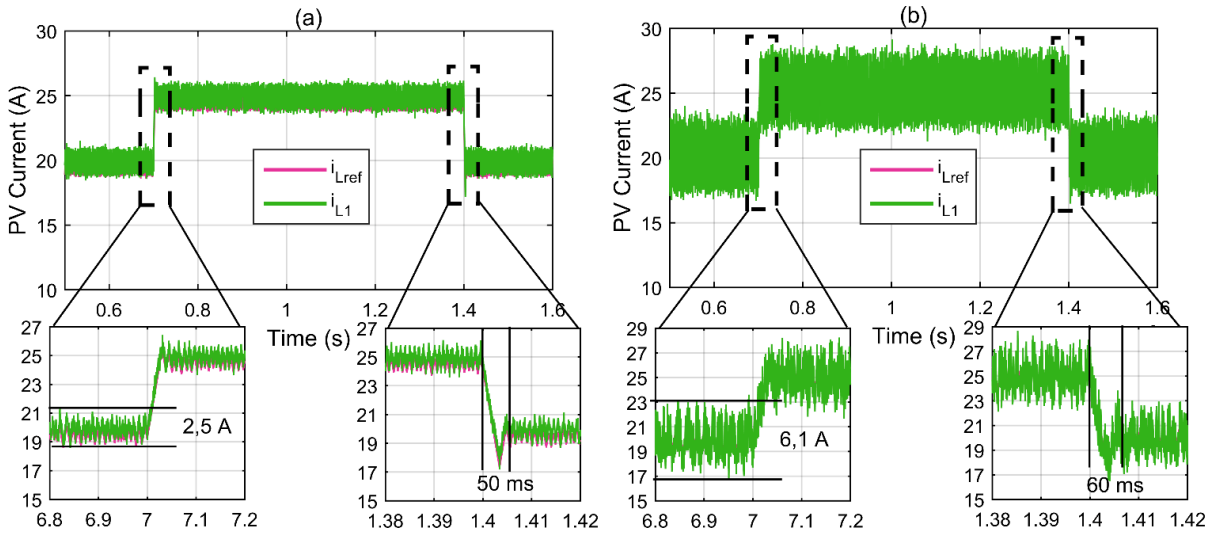

Figure 4.7: Inductance L_1 current waveforms for the change in abrupt solar radiation: (a) proposed control, (b) CM^{2}PC.

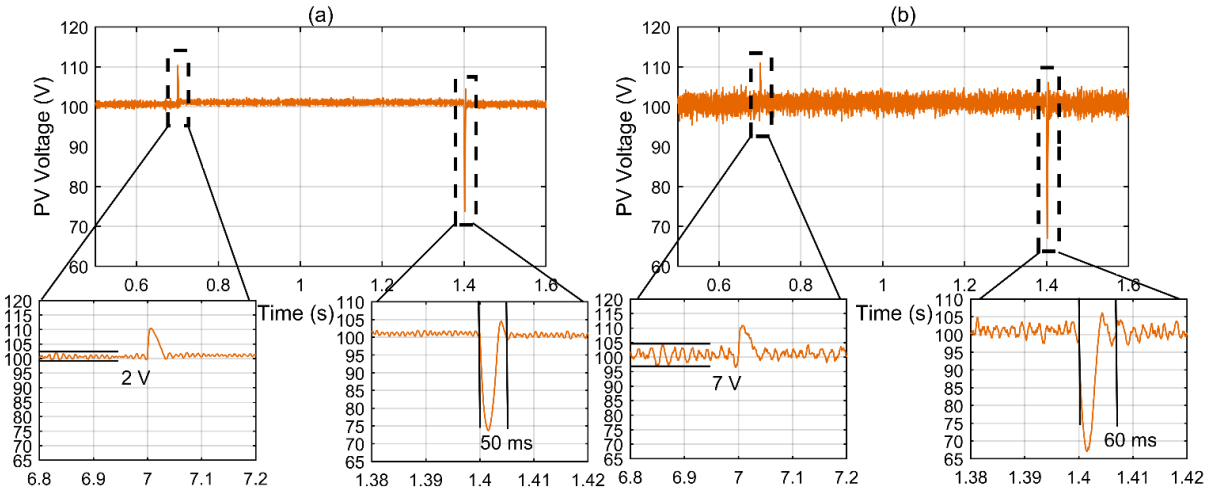

Figure 4.8: PV Voltage waveforms for the change in abrupt solar radiation: (a) proposed control, (b) CM^{2}PC.

In Figure 4.7, and Figure 4.8, we can observe the response of the proposed system and CM^{2}PC when exposed to a sudden shift in solar radiation levels, transitioning from 800 W/m^2 to 1000 W/m^2 and then to 800 W/m^2. This rapid change in radiation induces a swift system reaction with minimal overshooting. As visually depicted in Figure 4.7 (a), and Figure 4.8 (a), current L_1, and PV voltage achieve a stable state within just 50 *m*s, and the maximum change of current L_1, and PV voltage is ΔI=2.5A and ΔV=2V, respectively. As for the CM^{2}PC, the current L_1, and PV voltage reach a steady state within 60 *m*s, and the maximum change in current, and PV voltage is ΔI = 6.1A and ΔV = 7V, respectively. As illustrated in Figure 4.7 (b), and Figure 4.8 (b).

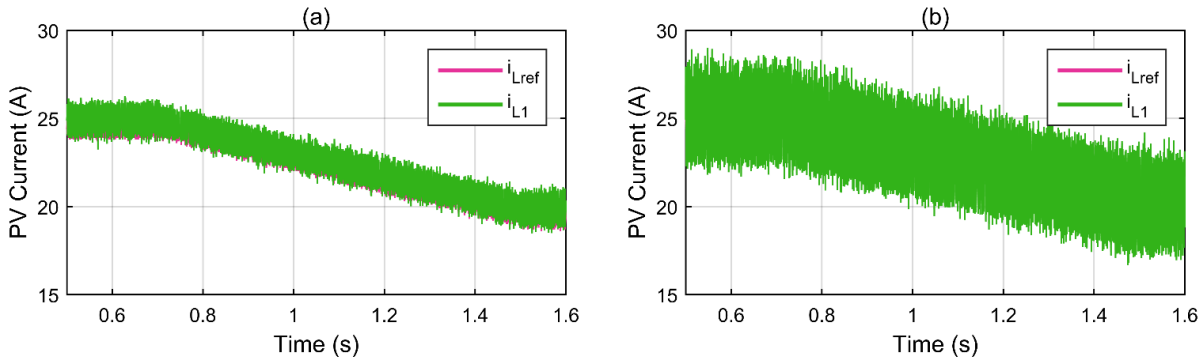

Figure 4.9: Inductance L_1 current waveforms for the change in progressive solar radiation: (a) proposed control, (b) CM^{2}PC.

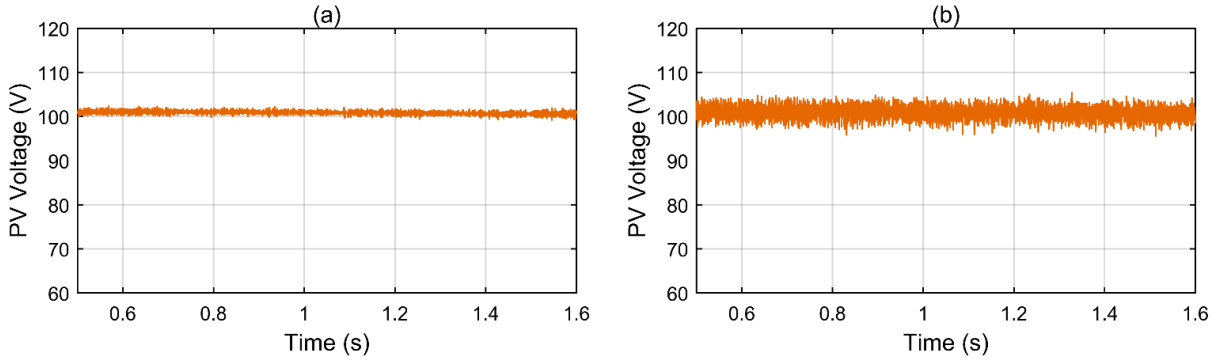

Figure 4.10: PV voltage waveforms for the change in progressive solar radiation: (a) proposed control, (b) CM^{2}PC.

Figure 4.9, and Figure 4.10, we can observe the response of the proposed system and CM^{2}PC when exposed to a gradual in solar radiation levels, transitioning from 1000 W/m^2 to 800 W/m^2. As shown in Figure 4.9, and Figure 4.10, the maximum change of current L_1, and PV voltage for the proposed method is much smaller than CM^{2}PC.

The proposed system has proven to excel in response speed, surpassing the CM^{2}PC by 16.67%. One of the key strengths of the proposed system lies in its significant superiority over the CM^{2}PC in terms of the maximum change in L_1 current and photovoltaic voltage. The percentage difference between them amounted to 59.01% and 71.43%, respectively, as shown in Table 4.3 .This advantage on the PV-side positively impacts the AC-side. As illustrated in Figure 4.11, the comparison is conducted of the THD ratio of the proposed system's grid current and the CM^{2}PC, where the difference between them is 69.21%.

Table 4.3: Comparative analysis of the suggested and CM^{2}PC methods.

	Time to steady-state (T)		**The maximum change (Δ)**		
	Current (*ms*)	**Voltage (*ms*)**	**Current (A)**	**Voltage (V)**	**THD%**
CM^{2}PC	60	60	6.1	7	2.89
Proposed method	50	50	2.5	2	0.89
The percentage difference (%)	16.67	16.67	59.01	71.43	69.21

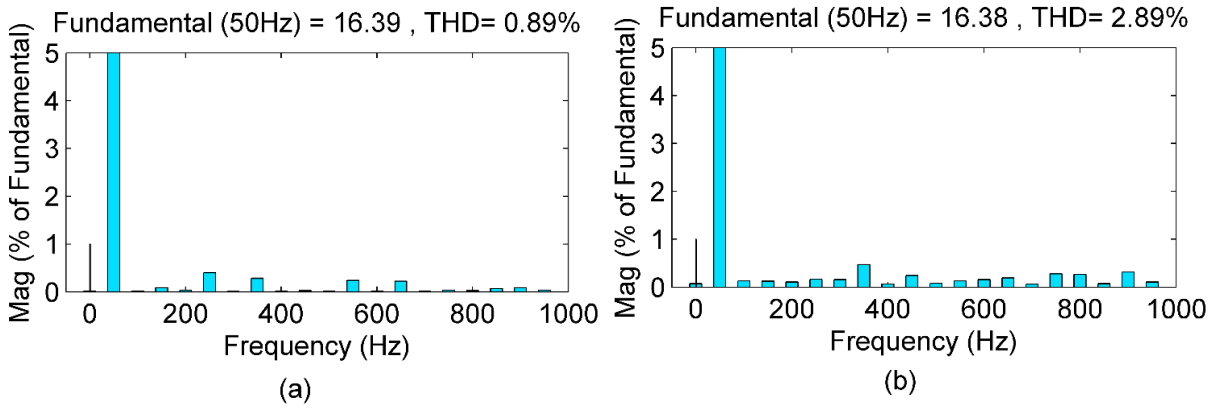

Figure 4.11: THD: (a) proposed control, (b) CM^{2}PC.

4.5 Conclusion

In this chapter, we proposed a novel grid-connected qZSI control system, leveraging a combination of M^{2}PC and FLC. This approach was compared with CM^{2}PC to evaluate its performance in regulating a grid-connected PV system. To ensure continuous operation of the PV system at its MPP, a simple yet effective current-based IncCon-MPPT algorithm was employed to generate the reference current for the FL controller. This approach facilitated rapid and efficient tracking dynamics, allowing the system to effectively extract maximum power from the PV source. The proposed system exhibited exceptional capabilities in both power extraction and grid integration. It demonstrated the ability to independently inject current into the grid while maintaining stable operation. Simulation and comparison results confirmed the robust performance of the implemented control techniques and the efficacy of the proposed system. Through comprehensive testing and analysis, we have shown that the combined M^{2}PC-FLC approach offers significant advantages over traditional control methods, such as CM^{2}PC. Notably, our system achieved superior tracking accuracy, faster response times, and enhanced grid current quality, thereby improving the overall performance of the grid-connected PV system. The findings presented in this chapter underscore the importance of advanced control strategies in optimizing the operation of renewable energy systems. By harnessing the synergistic benefits of M^{2}PC and FLC, we have demonstrated a promising approach for enhancing the efficiency, reliability, and grid integration capabilities of qZSI-based PV systems.

References

[1] A. A. Ahmed, A. Bakeer, H. H. Alhelou, P. Siano, and M. A. Mossa, "A new modulated finite control set-model predictive control of quasi-Z-source inverter for PMSM drives," *Electronics,* vol. 10, no. 22, p. 2814, 2021.

[2] O. Romero *et al.*, "Finite states-modulated model predictive control of a quasi-z-source inverter with lcl filter," in *2017 IEEE Southern Power Electronics Conference (SPEC)*, 2017: IEEE, pp. 1-6.

[3] A. Ayad, P. Karamanakos, and R. Kennel, "Variable switching point predictive current control of quasi-Z-source inverters," in *2017 IEEE Applied Power Electronics Conference and Exposition (APEC)*, 2017: IEEE, pp. 2773-2780.

[4] D. Himabindui, G. Sreenivasan, and R. Kiranmayi, "Fuzzy logic controlled QuasiZ Source Inverter Fed Induction Motor-Drive System with fast response," in *2021 7th International Conference on Electrical Energy Systems (ICEES)*, 2021: IEEE, pp. 45-50.

[5] B. Hamed and N. A. Qaoud, "Fuzzy control design for quasi-Z-source three phase inverter," in *2019 IEEE 7th Palestinian International Conference on Electrical and Computer Engineering (PICECE)*, 2019: IEEE, pp. 1-6.

[6] U. Devaraj, S. Ramalingam, and D. Sambasivan, "Comparative evaluation of PI and fuzzy logic controller for PV grid-tie quasi Z-source multilevel inverter," *Mehran University Research Journal Of Engineering & Technology,* vol. 40, no. 3, pp. 465-473, 2021.

[7] D. Xiao, K. S. Alam, M. Norambuena, M. F. Rahman, and J. Rodriguez, "Modified modulated model predictive control strategy for a grid-connected converter," *IEEE Transactions on Industrial Electronics,* vol. 68, no. 1, pp. 575-585, 2020.

[8] J. Wang, X. Liu, Q. Xiao, D. Zhou, H. Qiu, and Y. Tang, "Modulated model predictive control for modular multilevel converters with easy implementation and enhanced steady-state performance," *IEEE Transactions on Power Electronics,* vol. 35, no. 9, pp. 9107-9118, 2020.

[9] A. A. Estévez-Bén, A. Alvarez-Diazcomas, and J. Rodríguez-Reséndiz, "Transformerless multilevel voltage-source inverter topology comparative study for PV systems," *Energies,* vol. 13, no. 12, p. 3261, 2020.

[10] G. Migliazza *et al.*, "DC current control for a single-stage current source inverter in motor drive application," *IEEE Transactions on Power Electronics,* vol. 36, no. 3, pp. 3367-3376, 2020.

[11] M. Ranjani and P. Murugesan, "Optimal fuzzy controller parameters using PSO for speed control of Quasi-Z Source DC/DC converter fed drive," *Applied soft computing,* vol. 27, pp. 332-356, 2015.

[12] M. Zangeneh, E. Aghajari, and M. Forouzanfar, "A survey: Fuzzify parameters and membership function in electrical applications," *International Journal of Dynamics and Control,* vol. 8, pp. 1040-1051, 2020.

General conclusion and Future works

Following the energy crisis and environmental problems including pollution and global warming, research interest has shifted to the development of renewable energy sources. Renewable energy from sources like solar and wind power is now considerably more prevalent in the electrical system. Because of their flexibility for distributed production, photovoltaic systems (PV) are regarded as one of the most popular and efficient renewable energy sources for local and large-scale power generation.

Making significant advances in the field of power electronic interfaces for grid-connected photovoltaic systems is the primary goal of this thesis. The new inverters topology—PUC and qZSI—was selected for this reason. To make sure about the originality of the work and to avoid repetition of the past work, an extensive literature survey was carried out first. The literature survey covers a range of topologies employed for interfacing PVs. A part of literature survey focusses on existing control strategies and modulation techniques. Whereas the last part addresses grid connected PV systems, that incorporate PUC and qZSI as their power conditioning unit. The survey was a useful way to determine the research gap in the field of VSI and qZSI for PV applications.

In chapter three, a novel design of a two-stage grid-connected PV was proposed, using a high-gain DC-DC converter and a 7-level PUC inverter that are controlled by the MPC-MPPT and FCS-MPC, respectively. In addition, a novel DC-link voltage controller was proposed which provides an estimation of the reference current injected into the grid by the direct control of the PUC inverter power. A comparison was made between the designed controller and PI control by simulation and experimental results using a dSPACE 1104 board.

Chapter four focused on the design of controllers for a three-phase single-stage grid-connected PV-fed qZSI. The design involved developing a DC-link current controller, which allowed MPPT. The MPPT is based on the widely-used IncCond algorithm and can track the MPP in the order of milliseconds. Control techniques were proposed in this chapter as well. has been introduce a novel approach that combines FLC with M^2PC to managing the duty-cycle of the qZSI. It has been proposed to integrate these techniques to leverage the benefits they offer to controlling the qZSI. The DC variables are controlled by proposing an FL control unit to enhance speed and accuracy. Meanwhile, the AC variables are managed by an M^2PC control unit to stabilize the switching and improve the quality of the grid current. What makes this approach apart is its simple design, a reduced number of rules, while maintaining high system accuracy and speed. The effectiveness of this technique has been rigorously tested, and the results have been compared to the CM^2PC regarding its ability to control the qZSI duty-cycle.

Future works

The knowledge presented in this thesis can be expanded through the following proposed future research projects:

- Creation of enhanced MPPT algorithms that have the potential to increase the amount of energy gathered from photovoltaic sources, hence raising system efficiency. The MPPT methods based on artificial intelligence, such as fuzzy logic, neural networks, and others, offer an excellent avenue for further research.
- Investigation of the effect of partial shading of PV arrays and the effect of reactive power on the proposed techniques in this thesis.
- Improve the performance of the predictive strategy by suggesting a method to determine the weighting factors for MPC.
- Implementation of the proposed control scheme for two-stage grid-connected PV using a Field Programmable Gate Array (FPGA) control board instead of the dSPACE platform. Verify the efficiency of the proposed control scheme for single-phase grid-connected PV experimentally using an FPGA board or a dSPACE platform.

List of Publications

❖ Journal papers

[1] **A. May**, F. Krim, H. Feroura, and A. Belaout, "Power Quality Enhancement of Grid-Tied 7L-PUC Inverter-Based PV System Using a Novel DC-Link Controller," *Arabian Journal for Science and Engineering*, vol. 48, no. 11, pp. 15305-15319, 2023. https://doi.org/10.1007/s13369-023-08074-3

❖ Conference Papers

[1] **A. May**, F. Krim, H. Feroura, "Model predictive control with two-step horizon for the Packed U Cells 7-Level Grid Connected Inverter," **In: Proc. IC3E'2022, Bouira, Algeria, Dec. 2022.**

[2] H. Feroura, F. Krim, **A. May**, "PV Grid-Integration Of Single-stage Three Phase Split-Source Inverter using a predictive controller," **In: Proc. IC3E'2022, Bouira, Algeria, Dec. 2022.**

[3] A. Belaout, H. Feroura, F. Krim, M. Cheniti, A. Laib, **A. May**, "Automatic fault detection and classification in photovoltaic array using convolutional neural network" **In: Proc. NCPERE'2023, Khemis Miliana, Algeria, May. 2023.**

[4] **A. May**, F. Krim, H. Feroura, "Shoot-Through Duty Ratio in Modulated Model Predictive Control for Quasi-Z-Source Based on Fuzzy Logic," **In: Proc. IC-AIRE2023, Tipasa, Algeria, Nov. 2023.**

[5] **A. May**, F. Krim, H. Feroura, "Using Model Predictive Control-Based MPPT Technique for Control the High Gain DC-DC Converter for Photovoltaic Systems," **In: Proc. NCETEE'23, Setif, Algeria, Dec. 2023.**

[6] **A. May**, H. Bey, F. Krim, H. Feroura, M. Khitas, "An IC-MPPT Technique for Controlling the Boost Converter in Photovoltaic Systems Using Model Predictive Control," **In: Proc. ICADA'24, İzmir, Turkey, Mar. 2024.**

[7] H. Bey, **A. May**, F. Krim, M. Khitas, H. Feroura, A. Krim "Innovative implemented MPC-MPPT for FPGA-Based boost converter," **In: Proc. ICADA'24, İzmir, Turkey, Mar. 2024.**

[8] **A. May**, H. Feroura, H. Bey, A. Krim, F. Krim, A. Belaout, "Enhancement of Modulated Model Predictive Control of Grid-Tied PV Z-Source Inverter by Fuzzy Logic," **In: Proc. ATECE'24, Khenchela, Algeria, May. 2024.**

❖ Others

[1] **A. May**, F. Krim, "Contribution à la commande prédictive d'onduleurs de type quasi-Zsource dédiés à la gestion d'énergie d'une installation photovoltaïque connectée au réseau," **Participation in the UFAS1 Doctoriales dedicated to innovation, Sétif, Algérie, May. 2022.**

[2] **A. May**, F. Krim, H. Feroura, "Contribution to the predictive control of quasi-Z-source type inverters dedicated to the energy management of a photovoltaic installation connected to the grid," **Participation in the UFAS1 Doctoriales dedicated to innovation, Sétif, Algérie, May. 2023.**

ABSTRACT
This research work deals with the integration of photovoltaic (PV) energy to the electrical grid by the design of the power electronic interface. In this context, two topologies are considered, the dual-stage topology based on a grid-tied multi-level inverter and the single-stage topology based on quasi Z-source inverter. A two-stage grid-tied PV design based on a high-gain DC-DC converter and a 7-level Packed U Cells (7L-PUC) inverter, controlled by Finite-Control-Set Model Predictive Control (FCS-MPC) is presented, with the proposal of a novel model for controlling the DC-link voltage by considering system losses. The simulation and experimental results demonstrate the high effectiveness of the proposed control strategy in terms of response time under changes in weather conditions and demonstrate the feasibility of the proposed strategy. This thesis also introduces a novel grid-tied PV quasi-Z-Source Inverter (qZSI) control system, which combines the Modulated Model Predictive Control (M^2PC) and Fuzzy Logic Control (FLC) techniques. The proposed control is compared to the Conventional M^2PC (CM^2PC) to assess its performance. The proposed control system exhibits rapid and accurate tracking of the MPP. Additionally, it can autonomously inject current into the grid. Through comprehensive simulation and comparative analysis, the effectiveness of the proposed system is verified, demonstrating the high performance of the implemented control techniques. The results underscore the robust performance of the system in regulating grid-connected PV systems.

Keywords : *Photovoltaic; Inverter; Multi-level; PUC; MPC; qZSI; FLC*

RESUME
Ce travail de recherche porte sur l'intégration de l'énergie photovoltaïque (PV) au réseau électrique par la conception de l'interface électronique de puissance. Dans ce contexte, deux topologies sont considérées, la topologie à deux étages basée sur un onduleur multi-niveaux connecté au réseau et la topologie à un étage basée sur un onduleur quasi Z source. Une topologie à deux étages connectée au réseau, basée sur un convertisseur DC-DC à gain élevé et un onduleur à cellules U à 7 niveaux (7L-PUC), commandée par une commande de type FSC-MPC est proposée. Une nouvelle commande du bus continu est introduite, en considérant les pertes du système. Les résultats de simulation et expérimentaux démontrent la grande efficacité de la stratégie de commande proposée en termes de temps de réponse aux changements de conditions météorologiques et démontrent la faisabilité de la stratégie proposée. Cette thèse présente également un nouveau système de commande d'onduleur PV quasi-Z (qZSI) connecté au réseau, qui combine les techniques de commande prédictive modulé (M^2PC) et de commande à logique floue (FLC). La commande proposée est comparée à la M^2PC conventionnelle (CM^2PC) pour évaluer ses performances. Le système de commande proposé présente un suivi rapide et précis du point de puissance maximale. De plus, il peut injecter du courant de manière autonome dans le réseau. Grâce à une simulation complète et à une analyse comparative, l'efficacité du système proposé est vérifiée, démontrant la haute performance des techniques de commande mises en œuvre. Les résultats soulignent les performances robustes du système dans la régulation des systèmes PV connectés au réseau.

Mots clés : *Photovoltaïque ; Onduleur ; Multiniveaux ; PUC ; MPC ; qZSI ; FLC*

الملخص
يتناول هذا العمل البحثي دمج الطاقة الكهروضوئية في الشبكة الكهربائية من خلال تصميم الواجهة الإلكترونية للطاقة. في هذا السياق، تم النظر في طوبولوجيتين، طوبولوجيا ذات مرحلتين تعتمد على عاكس متعدد المستويات مرتبط بالشبكة وطوبولوجيا أحادية المرحلة تعتمد على عاكس شبه Z المصدر. يتم تقديم تصميم كهروضوئي مرتبط بالشبكة على مرحلتين يعتمد على محول DC-DC عالي الكسب وعاكس خلايا U معبأة بـ 7 مستويات (7L-PUC7)، يتم التحكم فيه بواسطة التحكم التنبئي لنموذج مجموعة التحكم المحدودة (FCS-MPC). مع اقتراح نموذج جديد للتحكم في جهد وصلة التيار المستمر من خلال النظر في خسائر النظام. أظهرت نتائج المحاكاة والتجريب الفعالية العالية لاستراتيجية المكافحة المقترحة من حيث زمن الاستجابة في ظل التغيرات في الظروف الجوية وإثبات جدوى الاستراتيجية المقترحة. تقدم هذه الأطروحة أيضًا نظام تحكم جديد في العاكس الكهروضوئي (qZSI) المرتبط بالشبكة، والذي يجمع بين تقنيات التحكم التنبئي للنموذج المعدل (M^2PC) والتحكم المنطقي الضبابي (FLC). تتم مقارنة التحكم المقترح بـ M^2PC التقليدي (CM^2PC) لتقييم أدائه. يُظهر نظام التحكم المقترح تتبعًا سريعًا ودقيقًا لـ MP. بالإضافة إلى ذلك، يمكنها حقن التيار بشكل مستقل في الشبكة. ومن خلال المحاكاة الشاملة والتحليل المقارن، تم التحقق من فعالية النظام المقترح، مما يدل على الأداء العالي لتقنيات التحكم المطبقة. تؤكد النتائج على الأداء القوي للنظام في تنظيم الأنظمة الكهروضوئية المتصلة بالشبكة.

الكلمات الدالة : *الطاقة الكهروضوئية ; عاكس ; متعدد المستويات PUC ; MPC ; qZSI ; FLC*